Advanced Energy Materials

ADVANCED ENERGY MATERIALS
www.advenergymat.de

REVIEW

Multiscale Interfacial Regulation for Stable Zinc Anodes: From Fundamental Mechanisms to Practical Applications

Yuexin Liu[1] | Tianyu Zhang[1] | Zian Li[1] | Zhongqing Ma[2] | Yong Hu[1]

[1]Institute of Nanocatalysis and Energy Conversion, College of Chemistry and Materials Engineering, Zhejiang A&F University, Hangzhou, China | [2]Bamboo Industry Institute, Zhejiang A & F University, Hangzhou, Zhejiang, China

Correspondence: Yuexin Liu (20240113@zafu.edu.cn) | Zhongqing Ma (mazq@zafu.edu.cn) | Yong Hu (yonghu@zafu.edu.cn)

Received: 27 November 2025 | **Revised:** 7 January 2026 | **Accepted:** 20 January 2026

Keywords: aqueous zinc ion batteries | gradient interface | Janus | multiscale interfacial regulation | zinc anode

ABSTRACT

Aqueous zinc-ion batteries (AZIBs) are promising candidates for large-scale energy storage due to their intrinsic safety and low cost. However, their commercialization is hampered by notorious zinc anode issues, including uncontrolled dendrite growth and parasitic side reactions. Multiscale interfacial regulation has recently emerged as a transformative strategy to address these challenges. This approach overcomes the limitations of single-interface modulation by constructing multilayer structures and optimizing interface coupling, thereby providing effective anode protection. To promote uniform zinc plating and suppress side reactions, this review comprehensively summarizes multiscale strategies that span the optimization of multi-physical fields, zinc deposition orientation, and electrolyte solvation structures. We systematically present recent advances in applying these multiscale strategies to zinc foil, zinc powder, and host-based anodes, as well as separators and hydrogel electrolytes, with a focus on their design principles, underlying mechanisms, and scenario-specific applicability. Furthermore, we elucidate how this technology achieves synergistic optimization of ion transport, deposition behavior, and the interfacial environment through functionally complementary multilayer, Janus, or gradient interfaces, thereby systematically mitigating zinc anode failure. Finally, future research directions and challenges are discussed, emphasizing that a profound mechanistic understanding coupled with rational design is pivotal for unlocking the full potential of next-generation AZIBs.

1 | Introduction

The development of safe and efficient energy storage systems presents a promising strategy to overcome the inherent intermittency and geographical constraints of renewable sources like solar, wind, and tidal energy [1–5]. In the realm of electrochemical energy storage, lithium-ion batteries (LIBs) dominate the market with ~89% share, owing to their high energy density, wide operating voltage, and long cycle life [6]. However, the scarcity of lithium resources and the flammability of electrolytes restrict their broader application [7]. Presently, many applications supplementary to LIBs still rely on the more economical and safer lead-acid batteries (LABs). Nevertheless, the low energy density, short cycle life, and prolonged charging times of LABs severely limit their viability [8]. Consequently, there is a pressing need to develop economical, environmentally benign, and high-performance energy storage devices that can better complement LIBs.

Aqueous zinc ion batteries (AZIBs) have attracted significant attention in academic research due to their high energy density, excellent safety performance, low cost, and minimal environmental requirements (Scheme 1a) [9–10]. As shown in Scheme 1b, the conventional AZIBs consist of a cathode, a zinc metal anode, a separator, and an aqueous electrolyte, in which Zn^{2+} ions shuttle back and forth between the cathode and the anode

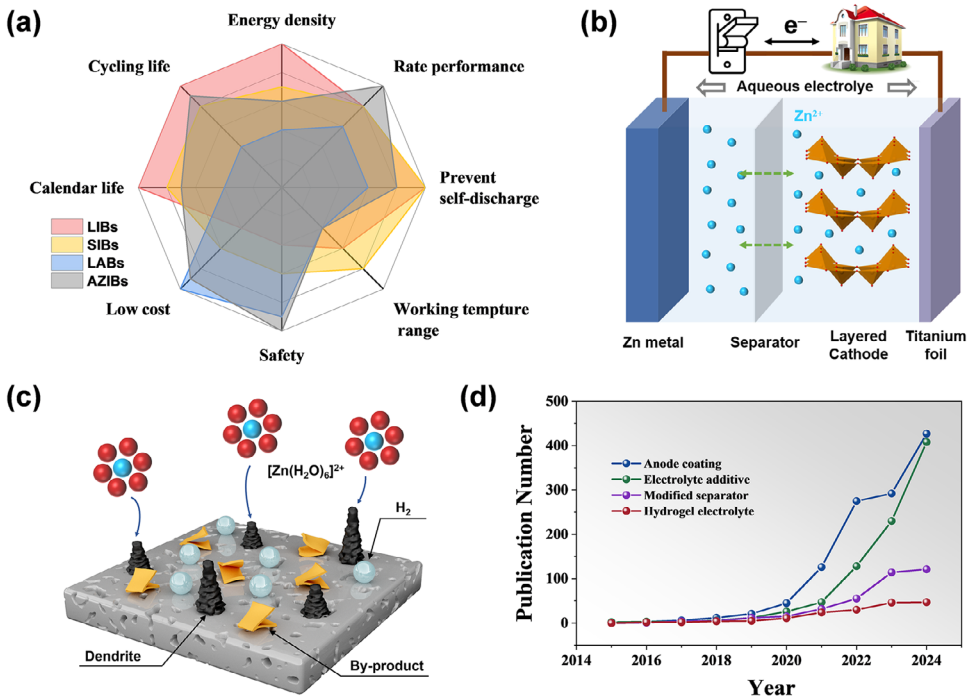

SCHEME 1 | (a) Statistics on the advantages and disadvantages of different types of batteries. (b) The working mechanism of AZIBs. (c) The challenges faced by zinc metal anodes. (d) Annual publication volume of different zinc metal anode protection methods.

to enable energy conversion and storage. In comparison to organic electrolytes, aqueous electrolytes have the advantages of enhanced safety, reduced cost, and improved ion transport kinetics. Meanwhile, the weakly acidic nature of this electrolyte is less corrosive to zinc metal anodes than strongly alkaline electrolytes, reducing side reactions such as hydrogen evolution and passivation [11–12]. The cathode materials of AZIBs comprise manganese-based oxides, vanadium-based oxides, conductive polymers, and Prussian blue analogs, among other categories [13–14]. These materials typically achieve zinc ion insertion chemical reactions through various specific structures [15–16]. However, due to thermodynamic mismatch, dynamic hysteresis, and uneven interface electric field, cathode materials face problems such as structural collapse, dissolution of active ingredients, and accumulation of by-products [17–18]. Researchers have greatly improved the electrochemical performance of cathode materials through methods such as guest ion pre-intercalation, defect engineering, construction of conductive networks, and three-dimensional structural design [19–20].

The anode material used for zinc batteries is still mainly zinc metal, although zinc-free or zinc-host anodes such as carbon-based materials, transition metal sulfides, and organic polymers have also been developed [21–23]. This is because zinc metal has a high theoretical specific capacity (5855 mAh cm^{-3} and 820 mAh g^{-1}), a low electrochemical equilibrium potential (−0.76 V vs. SHE), and cost-effectiveness (22.5 ¥ kg^{-1}) [24–25]. However, zinc metal anodes used in aqueous solutions also face some challenges that hinder the reversibility of Zn^{2+} ion deposition/stripping (Scheme 1c). For example, Zn^{2+} ions tend to deposit unevenly on the anode surface due to an uneven electric field distribution and restricted ion diffusion, leading to dendrite formation. The growth of zinc dendrites with a high Young's modulus will eventually puncture the separator and cause a short circuit in the battery [26]. Meanwhile, this brittle zinc dendrite is prone to fracture and form dead zinc, resulting in a loss of battery capacity and an increase in internal resistance [27]. In addition, the hydrogen evolution reaction (HER) occurring at the zinc metal anode not only increases the internal pressure of the battery but also leads to a local rise in pH due to the consumption of hydrogen ions [28–29]. The elevated pH promotes the reaction between metallic zinc and water, resulting in the formation of a zinc oxide/zinc hydroxide passivation layer, which further depletes the active zinc. Unfortunately, the solid electrolyte interphase (SEI) is typically absent in AZIBs, making the suppression of water-induced side reactions and dendritic growth on zinc metal anodes particularly challenging [30–31].

Recently, researchers have proposed various strategies to regulate the deposition behavior of Zn^{2+} ions on the surface of zinc metal anodes, and the number of related publications has shown a rapid upward trend every year (Scheme 1d). The improvement method contains building an artificial SEI interface [32], alloying zinc anode [33], constructing a three-dimensional (3D) collector [34], multifunctional separator design [35], electrolyte modification [36–37], and employing hydrogel electrolyte [38], etc. These methods follow several adjustment principles: [39–41] (1) reducing the desolvation energy barrier of hydrated zinc ions ($[Zn(H_2O)_6]^{2+}$) to minimize energy loss; (2) optimizing the electric field distribution to achieve uniform transmission of zinc ions; (3) preventing active water molecules from directly contacting the zinc anode, thereby suppressing the hydrogen evolution reaction and reducing the formation of by-products; (4) guiding the zinc metal to preferentially grow along the low-energy (002) crystal plane to inhibit dendrite formation; (5) optimizing the migration path of zinc ions to alleviate concentration

polarization. Among these improvement strategies, interface engineering is widely used in AZIBs due to its strong economic and practical value [11]. Specifically, interfacial engineering achieves effective regulation of zinc ion deposition behavior and water molecule interaction by constructing interfaces with specific functions on the surface of zinc anodes, separators, or hydrogel electrolyte [42]. These strategies can significantly suppress the growth of zinc dendrites and reduce the occurrence of side reactions at zinc anodes, making it an effective approach to enhance the stability of zinc metal anodes [43]. There are various methods to construct the interface layer, including typical approaches such as physical coating, in-situ conversion, and electrochemical deposition [11]. However, the selection of interface materials should fully consider their intrinsic characteristics and adaptability to the target technology, including but not limited to key parameters such as electrochemical stability, mechanical strength, and interface compatibility, to ensure the synergistic optimization of the material technology system [44].

Moreover, existing research indicates that a single interfacial protection strategy typically only offers limited mitigation for a specific failure mechanism of zinc metal anodes (such as dendrite growth or HER), and it is difficult to achieve coordinated inhibition of multiple failure behaviors [45, 46]. In other words, single interface protection struggles to reconcile the inherent trade-off between "rapid ion transport" and "effective blocking of harmful species". The densely engineered barrier layer, intended to mitigate side reactions, typically elevates the energy barrier for ion migration, resulting in heightened polarization and diminished rate capability of the battery. Therefore, research efforts have increasingly focused on the development of multilayer interface cooperative regulation systems. By designing multiscale interfacial regulation layers with complementary functions, the excellent properties of different materials can be effectively integrated, and multiple problems, such as dendrite formation, parasitic reactions, and interface passivation, can be solved simultaneously through functional zoning, collaborative coupling, and structural gradient design. For example, an inner layer enriched with zincophilic sites can promote uniform zinc nucleation, while an outer layer exhibiting high ionic conductivity and hydrophobicity can inhibit water-induced degradation and facilitate efficient ion transport. Such a hierarchical and multifunctional multiscale interfacial architecture not only substantially improves the cycling stability of zinc metal anodes but also enables the realization of higher capacity and extended cycle life in AZIBs.

While numerous reviews have covered interfacial regulation strategies for AZIBs, most focus on listing materials or preparation methods, often limited to a single strategy. This narrow focus fails to coordinate the suppression of multiple failure modes like dendrite growth, hydrogen evolution, and corrosion [47–50]. Recently, multiscale interfacial regulation methods have gained popularity for hierarchically controlling zinc ion diffusion and deposition. However, a comprehensive review that systematically summarizes these emerging strategies and outlines future research directions is still lacking. This review systematically correlates the construction mechanisms of multiscale interfaces in AZIBs with their control over zinc anode behavior. The insights provided herein are intended to offer essential theoretical guidance and viable technical pathways for advancing high-performance, long-life, zinc-based energy storage. Specifically, this review covers the following types of interface strategies: construction of a multiscale interfacial protection layer for zinc foil anode and zinc powder anode, internal/external interface control in zinc-host anode system, collaborative design of functional coatings on both sides of the separator, and interface control in hydrogel electrolyte (Scheme 2). These strategies enhance the overall performance of the battery by optimizing ion transport, suppressing side reactions, and guiding uniform deposition. Finally, this review also provides an outlook on the future research directions and development prospects of zinc anodes. With the increasing demand for large-scale energy storage, it is particularly crucial to develop zinc anodes that combine high capacity, high stability, and good economy. We expect this review to inspire researchers to further explore new interface materials and multi-level structure designs, pushing the performance boundaries of AZIBs in practical applications, and ultimately meeting the stringent requirements for electrode material lifespan and safety in large-scale energy storage systems.

2 | Regulatory Mechanism of Interface Engineering

Eliminating zinc dendrites and suppressing side reactions are key to improving the anode electrochemical performance of AZIBs. It is an effective strategy to obtain high reversibility and utilization of zinc anode to regulate the deposition behavior of Zn^{2+} ions by surface coating protection, electrolyte modification, and construction of hydrogel polymer electrolyte. The core mechanism of these strategies lies in achieving multi-scale regulation through interface engineering, and their common features are reflected in the precise modification and functional design of electrode/electrolyte interfaces. Multiscale interfacial regulation technology achieves collaborative coupling and complementary advantages of multiple protection mechanisms by constructing a composite interface system with functional gradient characteristics. To further reveal its mechanism of action, this section will focus on the research of single interface systems in advance, with a particular emphasis on analyzing their dual mechanisms of inhibiting dendritic nucleation/growth through interface energy barrier regulation and suppressing side reactions through interface chemical reaction kinetics optimization. The collaborative regulation mechanism of multiscale interfaces will be introduced in subsequent sections.

2.1 | Inhibiting Dendrite Growth

According to the Nernst–Planck equation [51–52] and Butler–Volmer equation [26, 53], the nucleation and growth rate of crystals during electrochemical deposition are significantly influenced by multiple parameters such as ion concentration, electric field strength, convection conditions, and temperature. These factors are positively correlated with the nucleation rate, and a fluctuation in any of these parameters will change the nucleation energy barrier for zinc metal deposition, thereby affecting the nucleation overpotential. When the above parameters are unevenly distributed at the electrode interface, zinc metal tends to preferentially nucleate in local areas and grow rapidly, leading

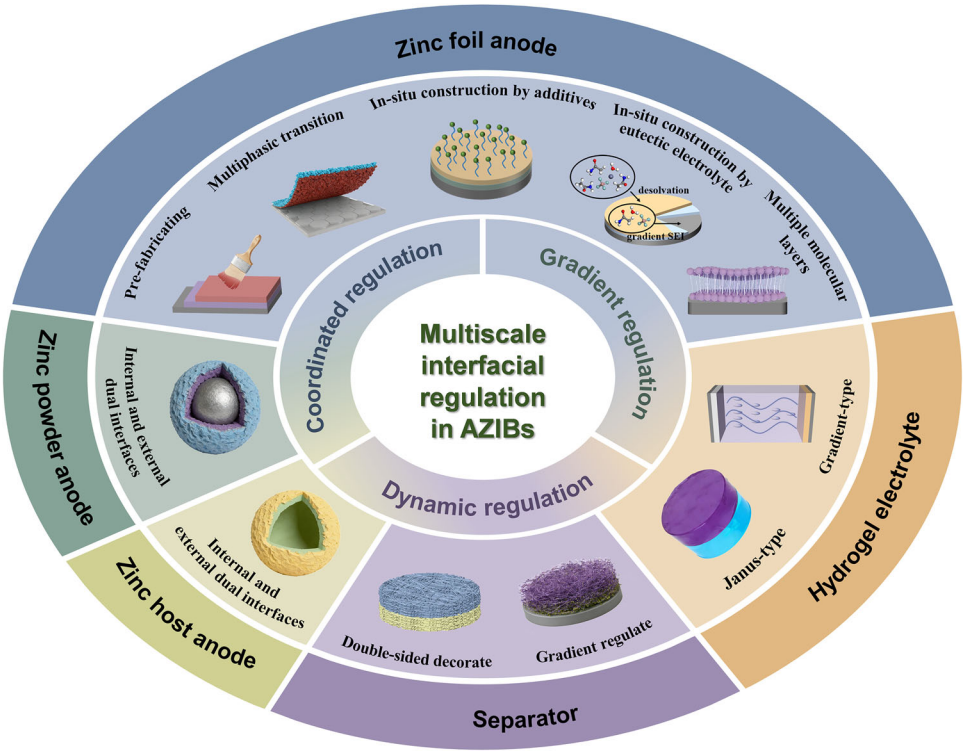

SCHEME 2 | Schematic diagram of multiscale interfacial regulation technologies in AZIBs.

to a decrease in interface stability and causing instability in crystal growth morphology [54]. Ultimately, under sustained non-equilibrium growth conditions, zinc metal tends to form dendritic structures, which in turn affect the cycling and safety performance of the electrode. Unfortunately, the rough surface and impurities inside the zinc metal anode will cause uneven distribution of local electric fields or differences in ion flux on its surface, ultimately leading to the preferential nucleation and growth of zinc ions in specific regions, forming protrusions [55–56]. Even worse, this tip effect significantly enhances the electric field strength around these protrusions, resulting in a serious mismatch between the diffusion rate and deposition rate of zinc ions near the tip, which in turn triggers a sharp increase in local concentration gradient and uncontrolled two-dimensional (2D) diffusion [24]. This positive feedback further facilitates preferential deposition at the tip, eventually evolving into dendritic growth. When zinc dendrites grow to a certain extent, they will puncture the separator and cause a short circuit in the battery. And due to their brittle nature, dendrites easily detach from the zinc anode surface, forming "dead zinc" and greatly reducing the utilization rate of zinc metal [57].

There are two main ways to eliminate zinc dendrites: one is to "block," and the other is to "guide." For the first method, a physical protective layer can be formed between the metal Zn anode and the electrolyte to directly block the growth of dendrites, such as through the use of $CaCO_3$ [58], TiO_2 [59], and so on. Although this method is the most direct, microscopic defects or inadequate edge protection in the mechanical barrier may allow zinc dendrites to grow from weak points, causing short circuits. In the process of zinc deposition, due to its high volume expansion rate of about 88%, if the mechanical barrier lacks sufficient elasticity and a deformable structure, it is prone to stress concentration, which induces crack formation and provides a priority path for the growth of zinc dendrites [60]. Therefore, researchers are more committed to developing interface layers that can induce uniform deposition of zinc ions. In terms of regulating zinc deposition behavior, four main strategies have been used to guide the uniform deposition of zinc ions: ensuring a uniform zinc ion concentration field, achieving a uniform distribution of electric field strength, optimizing zinc ion migration pathways, and inducing preferred growth of zinc along specific crystallographic directions.

2.1.1 | Homogenizing the Concentration of Zinc Ions

The differences in the dynamics of exfoliation and deposition, along with variations in the gravitational field, can result in an uneven ion concentration distribution. The mismatch between the diffusion rate and deposition rate of zinc ions in high-concentration areas leads to a sharp increase in local current density, exacerbating the formation of dendrites [61]. In addition, the supersaturation of zinc ions in high-concentration areas can trigger instantaneous nucleation, resulting in the formation of a large number of small crystal nuclei and rapid growth to form dendrites [62]. Therefore, a uniform zinc ion concentration will eliminate the concentration gradient on the electrode surface, reduce concentration overpotential, and prevent dendrite deposition caused by local electric field variations [63]. Pre-setting the migration trajectory of zinc ions is an effective method to promote the orderly deposition of zinc ions along the channel from bottom to top, thus avoiding local concentration polarization of zinc ions [48]. There are two main methods to restrict the diffusion path of zinc ions: one is a high ion conduction network constraint, and the other is pore limitation.

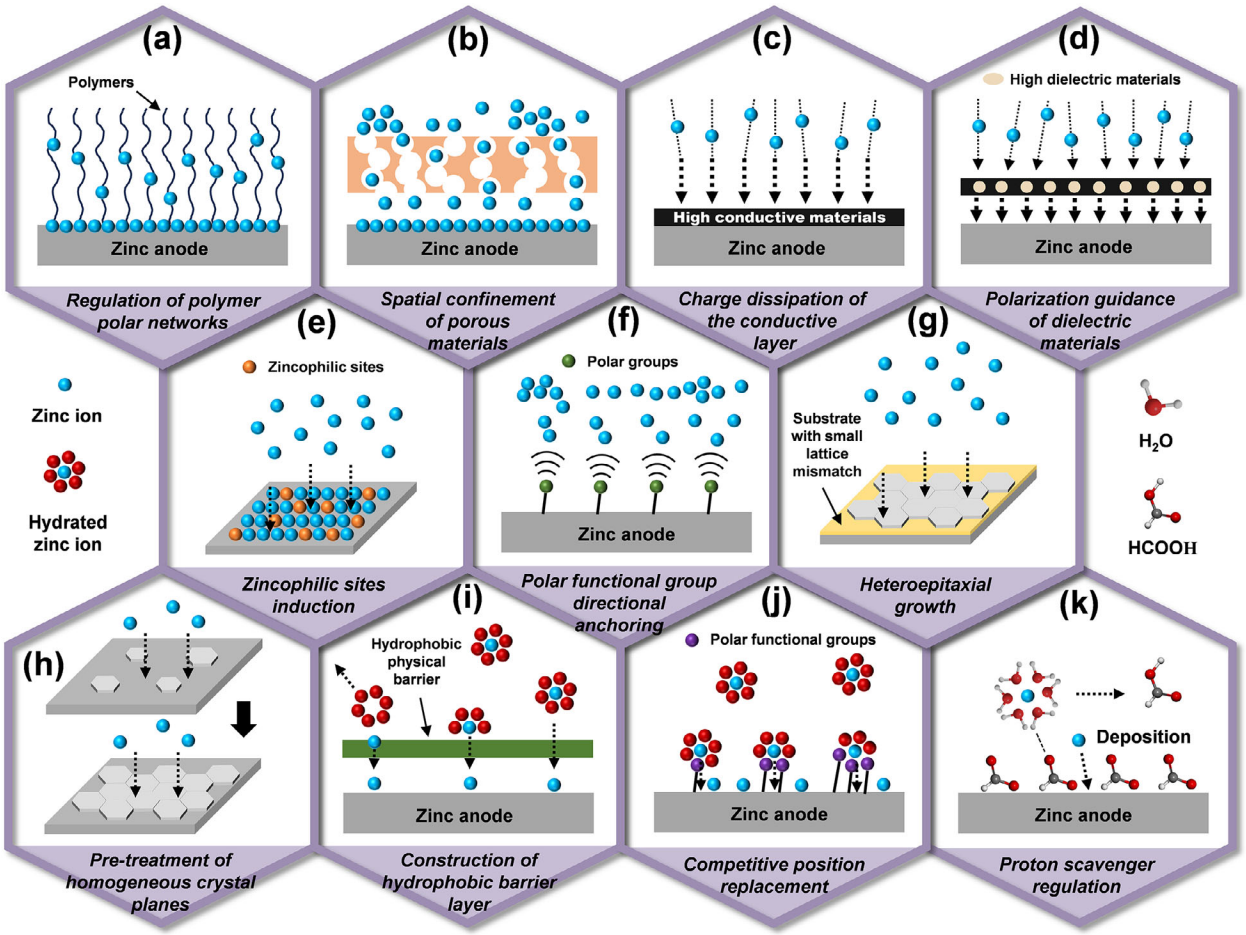

SCHEME 3 | Interface engineering in the protection mechanism of the zinc metal anode.

1. Polymer coatings with polar functional groups such as carbonyl (C═O) [64–65], hydroxyl (–OH) [66], sulfonate ($–SO_3^-$) [67–68], cyano group (C≡N) [69], and amino ($–NH_2$) [70] have been found to form high-speed ion transfer networks to alleviate the non-uniformity of ion flux. This is attributed to the highly polar and dipolar characteristics of these functional groups, which facilitate the uniform migration and nucleation of Zn^{2+} through the formation of coordination bonds with Zn^{2+}, thereby playing a critical role in enhancing the cycling stability of zinc anodes [71]. In addition, certain hydrophilic polymers can be further extended to the application of hydrogel electrolytes. The resulting 3D network exhibits high ionic conductivity, which facilitates uniform zinc ion flux and enables effective regulation of global ion distribution (Scheme 3a) [72].
2. The interface coating containing porous materials (such as porous SiO_2 [73], mesoporous hollow carbon spheres [74], 3D graphene [75], metal organic frameworks (MOFs) [76] and covalent organic frameworks (COFs) [77]) effectively reduce the zinc ion flux density per unit projected area through the spatial confinement effect formed by its three-dimensional network, thereby achieving precise control of zinc deposition kinetics (Scheme 3b) [78]. Further research has shown that the surface of such porous materials is often modified with abundant polar functional groups, and these active sites can be directionally coupled with solvated zinc ions through coordination, significantly reducing the ion desolvation energy barrier and promoting rapid diffusion and migration of zinc ions [79–80]. This collaborative mechanism not only optimizes the uniformity of zinc deposition but also provides a dual guarantee for suppressing dendrite growth.

2.1.2 | Homogenizing the Electric Field Strength

According to the Poisson equation ($\nabla \cdot E = \rho/\varepsilon$, where ∇ is the Laplace operator, E is the potential, ρ is the electric charge volume density, and ε is the permittivity of free space), the electric field strength on the surface of the zinc metal anode is often positively correlated with the ion concentration [81]. Uneven concentration of zinc ions alters the potential distribution of the electron-conducting layer and leads to differences in the electric field strength in different regions of the interface, especially at higher current densities [82]. In addition, the inherent roughness of the zinc anode surface (such as grain boundaries and defects) can cause local electric field distortion, forming a tip effect, which in turn triggers the preferential growth of zinc dendrites [83]. Therefore, it is necessary to regulate the electric field distribution on the surface of the zinc metal anode to promote uniform deposition of zinc ions. There are two main methods to regulate the distribution of electric fields, including the following:

1. Enhancing the overall electric field strength on the surface of zinc metal to weaken the difference in electric field distribution. The common method is to attach materials with high electronic conductivity to the surface of the zinc anode, such as MXene [84], metallic silver [85], and poly(3,4-ethylenedioxythiophene) (PEDOT) [86], which helps minimize charge accumulation and form a uniform electric field on the zinc anode surface (Scheme 3c).
2. Using high dielectric materials such as Si_3N_4 [87], $PbTiO_3$ [88], $ZnTiO_3$ [89] as "electric field pumps", which generate polarization effects under the action of external electric fields. These materials not only significantly increase the vertical electric field strength on the electrode surface but also suppress the horizontal electric field component and eliminate the local growth of zinc dendrites caused by tip effects (Scheme 3d) [90].

2.1.3 | Reducing the Energy Barrier for Nucleation

According to classical nucleation theory, reducing the nucleation energy barrier can simultaneously increase nucleation density and reduce crystal nucleus size, providing a thermodynamic basis for suppressing dendrites [91]. The common method is to introduce zincophilic sites in the interface layer, which promote uniform ion flux through strong ion adsorption ability and synergistically regulate the nucleation and growth behavior of metallic zinc. Zincophilic sites are divided into two types: zincophilic metal sites and polymers with a large number of polar functional groups.

1. The 3d/4d electron orbitals of some low electronegative elements (such as Bi [92], In [93], Sn [94]) are prone to form covalent bonds with the 3d orbitals of Zn^{2+}, reducing the nucleation overpotential. In addition, the d-band centers of these zincophilic metals are close to the Fermi level, further enhancing the electronic coupling with Zn^{2+} [95]. According to the classical heterogeneous nucleation theory, enhancing the absorption/binding ability of Zn^{2+} at the interface reduces the nucleation energy barrier, leading to denser and more uniform zinc deposition, which enhances the stability of the zinc metal anode (Scheme 3e) [96].
2. In addition, some polar groups, such as O–H, C═O, and N–H, present in polymer coatings form local low-energy potential wells through the coordination of electronegative atoms with Zn^{2+}, which can reduce the difference in Zn^{2+} concentration and guide the uniform deposition of Zn^{2+} [65, 70, 97]. This directional ion transport can reduce nucleation overpotential and suppress random dendrite growth (Scheme 3f).

2.1.4 | Inducing the Crystal Growth Direction of Zinc Metal

The lattice structure of zinc metal belongs to the P63/mmc space group, exhibiting a hexagonal close-packed (hcp) structure [98]. In the process of electrodeposition, the typical crystal surface characteristics of zinc metal are mainly defined by three Miller indices: (100), (002), and (101) planes, each with a unique atomic arrangement [99]. Among them, when deposited along the (100) and (101) crystal planes, zinc atoms are inclined at a large angle of 70°–90°, making it easy to form dendrites. In contrast, when deposited along the (002) crystal plane, zinc atoms tend to deposit parallel to the substrate at a small angle of 0°–30°, which effectively suppresses the growth of zinc dendrites and the occurrence of corrosion reactions [100]. However, the atomic arrangement of the (100) and (101) crystal planes is relatively loose and has a higher surface energy, while the (002) crystal plane has the lowest surface energy [101]. This energy difference promotes the preferential deposition of zinc ions on the crystal plane with higher surface energy, and repeated cycling exacerbates this heterogeneity, leading to surface roughness or dendrite formation. Therefore, maintaining a parallel orientation between the zinc (002) crystal plane and the current collector can guide the deposition of zinc to form a smooth morphology, which helps to achieve stable zinc stripping and deposition processes in mild electrolytes. In interface engineering technology, there are two main methods for inducing zinc growth along the (002) crystal plane: the first method is to use a heterogeneous substrate with less lattice mismatch with the zinc (002) crystal plane to orient zinc ion deposition, and the second method is to use physical or chemical methods to expose more (002) crystal planes on the zinc metal substrate, allowing it to grow along the (002) texture and ultimately develop into a continuous plane.

1. According to the lattice distortion theory, when the interface between the zinc coating and the substrate has a small lattice mismatch (<15%), epitaxial deposition of zinc can occur in the direction parallel to the substrate [102]. Some materials with less lattice mismatch to zinc (002) crystal planes, such as graphene [103], MXene [104–105], metallic Cu [106–108], ZnSe [109], nitinol alloy [110], etc., are often used to construct interfacial layers to guide the preferential orientation deposition of zinc ions. The construction position of the interface layer can be selected from the zinc metal surface, the current collector surface, and the separator surface, all of which play a good regulatory role (Scheme 3 g) [35].
2. The second method, also known as homoepitaxial deposition, exposes more zinc (002) crystal planes through pretreatment. The mechanism of the physical pretreatment method is to rearrange zinc atoms through rolling or heat treatment [111]. During the recrystallization process of grains, the (002) crystal plane with the lowest surface energy gradually dominates the grain orientation due to its energy advantage [112–114]. The mechanism of the chemical pretreatment method is to selectively etch the high surface energy crystal planes on the zinc metal anode surface using chemical reagents and acids, such as sodium hexametaphosphate [115], glutamic acid [116], terephthalic/zirconium chloride [117], to expose specific (002) crystal planes. During the cycling process, these zinc ions will grow epitaxially along the exposed (002) crystal plane and gradually connect into a whole (Scheme 3 h).

It should be noted that the low surface energy of the (002) crystal plane implies lower electrochemical activity and higher activation energy. In contrast, other planes, such as (101) and (100), have lower activation energies and promote rapid reaction kinetics at the interface. Therefore, inducing zinc ions to uniformly deposit

along the (101) and (100) planes to form a flat surface may result in higher charge and discharge efficiency [98].

2.1.5 | Others

In addition to the mainstream strategies for regulating zinc ion deposition mentioned above, dendrite suppression can also be achieved by controlling the thermodynamic distribution on the surface of zinc metal. La et al. [118]. constructed functionalized heat transfer enhancement layers on both sides of the zinc foil, effectively preventing local heat accumulation at the electrode and successfully eliminating hot spot effects, thereby significantly reducing thermodynamically driven side reactions and dendrite growth rates.

2.2 | Inhibiting Hydrogen Evolution and By-Products

Another factor restricting the practical application of AZIBs is the decomposition of water molecules in the electrolyte. On the one hand, the water decomposition process generates a large amount of hydrogen gas, causing bubbles/expansion in the battery. On the other hand, locally generated OH^- further reacts with Zn^{2+} and acidic atomic groups in the electrolyte to produce reversible by-products that adhere to the surface of metallic zinc [119]. These low-conductivity and loosely structured by-products increase the interface impedance of the zinc anode, reducing the active nucleation sites of zinc while also increasing the concentration polarization on the electrode surface, promoting the formation of dendrites [120]. Moreover, these loose by-products do not hinder the continuous occurrence of the process, which will continuously consume active zinc substances and electrolytes, leading to a decrease in Coulombic efficiency [121].

According to different hydrogen evolution mechanisms, it can be divided into two types: self-corrosion hydrogen evolution and electrochemical corrosion hydrogen evolution. As is well known, pure zinc barely reacts with pure water under normal temperature and pressure due to its relatively low metal activity, which makes it difficult to displace hydrogen from water. However, in fact, when zinc metal is immersed in a weakly acidic salt solution, it spontaneously produces hydrogen gas and by-products. This is because impurities (such as Cu and Fe) in the zinc metal anode form micro batteries with the zinc metal itself. Zinc dissolves preferentially as the anode ($Zn \rightarrow Zn^{2+} + 2e^-$), while impurities act as the cathode to promote the reduction of H^+ to H_2 [122]. This process is thermodynamically spontaneous, which continuously generates H_2 and consumes active zinc, resulting in a decrease in the Coulombic efficiency of AZIBs [123]. One of the more important reasons for causing side reactions is the electrochemical corrosion process. In neutral or weakly acidic environments, the theoretical HER potential is higher than the standard electrode potential of Zn^{2+}/Zn, making HER thermodynamically spontaneous [124]. In fact, due to the high hydrogen evolution overpotential of zinc metal, this will greatly inhibit the HER to a certain extent according to the Butler-Volmer equation [125–126]. However, Zn^{2+} has strong polarization and a high charge, which strongly attracts it to the negatively charged oxygen terminals of six water molecules through ion-dipole interactions, forming a stable solvation shell [127]. This strong interaction will cause electrons to transfer from Zn^{2+} to water molecules in $[Zn(H_2O)_6]^{2+}$, thereby weakening the O–H bond in water molecules and making it easier to break. During the zinc ion deposition process, highly active water molecules in the solvation shell undergo desolvation at the electrode interface, resulting in a decrease in the O–H bond dissociation energy and easier release of H^+, leading to a decrease in hydrogen evolution overpotential and ultimately causing HER and the generation of by-products [128]. In addition, the hydrogen evolution overpotential is also affected by the roughness of the electrode surface, operating temperature, zinc concentration, and other factors. In response to the above situation, researchers in the field of interface engineering have proposed various improvement measures.

2.2.1 | Physical Isolating Water Molecules

Constructing a physical interface layer on the surface of the zinc anode to prevent H_2O molecules in the electrolyte from contacting the zinc metal surface is the most direct method to suppress the decomposition of H_2O molecules, including free water and bound water. So far, various hydrophobic materials with stable structures and chemical properties have been developed, such as Mg-Al LDH [129], polydimethylsiloxane [130], hydrophobic adiponitrile [131], and some self-assembling supermolecules [132], etc., to provide an isolation function (Scheme 3i). These hydrophobic groups strip Zn^{2+} coordinated water molecules through electrostatic repulsion, forming partially dehydrated intermediate states. However, it should be noted that the interface layer that completely isolates H_2O molecules may hinder the transport of Zn^{2+}, and porous structures or gradient coatings need to be designed to balance water resistance and ion conductivity.

2.2.2 | Reducing Coordinated Active Water Molecules

As mentioned above, the decomposition of active water molecules is the main culprit leading to HERs and by-products. Therefore, another approach is to reduce the number and reduce the activity of coordinated active water molecules of $[Zn(H_2O)_6]^{2+}$ to slow down the HER:

1. Through the competitive hydrogen bonding mechanism involving highly electronegative functional groups (such as $-COO^-$, $-SO^{3-}$, and $-O-$), water molecules in the solvation shell of zinc ions are progressively displaced, as these functional groups preferentially occupy the coordination sites [133]. This facilitates the transformation of $[Zn(H_2O)_6]^{2+}$ into a lower hydration state (e.g., $[Zn(H_2O)_5]^{2+}$), thereby reducing the degree of hydration of zinc ions at the interface and creating favorable conditions for subsequent deposition reactions (Scheme 3j).
2. Some polar functional groups (such as OH^-, $-CONH^-$, $-COO^-$, etc.) effectively anchor and bind free water molecules and bound water released during the desolvation process of $[Zn(H_2O)_6]^{2+}$ by forming a strong hydrogen bonding network [134–135]. These highly active water molecules transition from a "reactant" state where they can freely move and

easily access the electrode surface to obtain electrons, to a "bound water" state where translational and rotational degrees of freedom are limited, thereby significantly reducing their chemical activity and reaction probability at the electrode/electrolyte interface [136]. This microscopic fixation breaks the continuous hydrogen bonding channels that rely on interface H^+ transfer, fundamentally suppressing the hydrogen evolution side reaction that leads to battery failure.

3. Using the pore channels of microporous materials (such as hybrid molecular sieves [137], ultra-micropores nanospheres [138], zeolite nanoparticles [67]) to apply spatial confinement to $[Zn(H_2O)_6]^{2+}$ ions, forcing some bound water to desorb [44]. It should be noted that the diameter of hydrated zinc ions is about 0.74 nm, and the micropore size needs to be less than 2 nm to form a confinement effect, but being too small (such as < 0.8 nm) will hinder ion entry. Therefore, it is recommended to design graded pores, with micropores accounting for no more than 70%, to avoid kinetic hysteresis caused by insufficient electrolyte infiltration. In addition, introducing oxygen/nitrogen functional groups (such as carboxyl and pyridine nitrogen) can reduce the desolvation energy barrier and increase the migration number of zinc ions [1].

2.2.3 | Increasing Hydrogen Evolution Overpotential

The last protection to prevent parasitic HER and suppress side reactions is to increase the hydrogen evolution overpotential on the surface of the zinc anode, which can be regulated at multiple scales through thermodynamics, kinetics, and interface microenvironment.

1. The first principle calculations indicate that the Zn (002) crystal plane has the lowest surface energy, resulting in a significant increase in the adsorption energy barrier of H^+ on this crystal plane, thereby suppressing HER kinetics [139]. The hexagonal close-packed structure exposed on the Zn (002) crystal plane can induce the formation of a highly ordered hydrogen bonding network at the interface of water molecules, which contributes to the protons needing to overcome higher energy barriers to break through the hydrogen bonding network and reach the active site [140]. Therefore, exposing the (002) crystal plane of zinc metal as much as possible is beneficial for increasing the hydrogen evolution overpotential, thereby suppressing HER and side reactions.
2. Depositing zincophilic metals (such as Pb, Cd, Bi, In, etc.) with high HER overpotential on the surface of zinc can reduce H^+ adsorption energy through electronic structure regulation [33]. Density function theory (DFT) calculations indicate that these elements will weaken the hydrogen adsorption capacity of surrounding zinc vacancies, thereby increasing the Gibbs energy barrier for hydrogen evolution [33]. And thanks to the zincophilicity of these elements, a uniform zinc coating can be achieved. The introduction of high hydrogen potential metals can be divided into two methods: surface deposition [92, 95] and alloying treatment [93, 141].
3. By utilizing active functional groups in organic polymers to selectively coordinate with highly mobile H^+ ions and form stable hydrogen-bonded intermediates (e.g., H–COOH), the concentration of free H^+ ions is significantly reduced, thereby inhibiting the Volmer reaction [142]. The charge redistribution effect weakened the adsorption energy of H^+ on the zinc surface, increasing the hydrogen evolution overpotential (Scheme 3k).

3 | Multiscale Interface Construction Techniques in Zinc Foil Anode

Constructing an artificial interphase layer on the surface of zinc foil anodes to regulate their interaction with electrolytes has become a common method for protecting zinc foil anodes. Specifically, an artificial SEI layer can be constructed to isolate H_2O molecules, promote desolvation of hydrated zinc ions, create a uniform electric field, optimize the diffusion path of zinc ions, and induce directional deposition of zinc ions, among other methods [143]. However, the diffusion and deposition process of zinc ions is complex and variable, so relying solely on a single regulatory method has limited effectiveness. Furthermore, poor compatibility between the coating and zinc metal may lead to cracking or reduced adhesion during cycling, compromising long-term electrode stability [99]. Therefore, constructing double-layer or even multi-layer protective layers on the surface of zinc metal anodes to synergistically regulate the deposition of zinc ions and suppress side reactions has become a novel and effective approach [144]. There are three methods for constructing multiscale interfaces on zinc foil anodes: pre-fabricating multilayer interface coating, in-situ multiphasic transition, and in-situ construction by electrolyte additives or eutectic electrolyte. According to the different types of interfaces, they can be divided into the SEI layer, the molecular layer, and the SEI-molecular composite layer. The multiscale interfacial regulation technologies for zinc anodes reported in the literature are summarized in Table 1. The majority of these studies demonstrate excellent durability of zinc anodes. This chapter will provide a comprehensive explanation and examples of five different methods from the perspective of construction principles and methods, with a focus on the construction principles and control mechanisms of multiscale interfaces.

3.1 | Pre-Fabricating Multiscale Interface Layers

The simplest and most effective method to obtain a multiscale interface layer is to directly construct it on the surface of the zinc metal anode through physical or chemical means in multiple steps. This method has a highly controllable preparation process, enabling precise design of coating structure, thickness, and functional layering, and facilitating the realization of multi-functional synergy, such as a zincophilic layer and a hydrophobic layer. Its interface has been stably formed before the cycle, and its structure is predictable and independent of electrochemical reactions, avoiding capacity loss and efficiency decline caused by additive consumption. In addition, this strategy features flexible material selection and mature technology, making it easy to integrate with existing battery manufacturing processes. It has great potential for large-scale application and is an efficient,

TABLE 1 | Summary of artificial layers based on multiscale interface construction techniques, including construction methods, types of interphase, symmetry cell performance, and asymmetrical cell performance.

Constructing methods	Types of interphase	Artificial interphase materials	Symmetric cells (cycling time, cycling condition)	Asymmetric cells (Coulombic efficiency, cycling condition, cycling number)	Reference
Pre-fabricating	SEI	Cu@graphene oxide	2000 h, 0.5 mA cm^{-2}/0.5 mAh cm^{-2}	—	[145]
Pre-fabricating	SEI	SA@Cu	2000 h, 1 mA cm^{-2}/1 mAh cm^{-2}	99.83%, 1 mA cm^{-2}/1 mAh cm^{-2}, 900 cycles	[146]
Pre-fabricating	SEI	Cu@NMP	>2000 h, 1 mA cm^{-2}/1 mAh cm^{-2}	99.6%, 1 mA cm^{-2}/1 mAh cm^{-2}, 1600 cycles	[147]
Pre-fabricating	SEI	Nafion@$Zn_3(PO_4)_2$	2800 h, 0.5 mA cm^{-2}/0.25 mAh cm^{-2}	—	[148]
Pre-fabricating	SEI	OH-mSiO_2@F-mSiO_2	>8000 h, 2 mA cm^{-2}/4 mAh cm^{-2}	99.84%, 2 mA cm^{-2}/1 mAh cm^{-2}, >3000 cycles	[149]
Pre-fabricating	SEI	La_2O_3@Sn	3000 h, 1 mA cm^{-2}/0.5 mAh cm^{-2}	~100%, 4 mA cm^{-2}/1 mAh cm^{-2}, >2500 cycles	[150]
Pre-fabricating	SEI	MXene@Ag	4000 h, 1 mA cm^{-2}/1 mAh cm^{-2}	99.6%, 2 mA cm^{-2}/1 mAh cm^{-2}, 670 cycles	[151]
Pre-fabricating	SEI	TPA@PEDOT	3200 h, 1 mA cm^{-2}/1 mAh cm^{-2}	99.78%, 2 mA cm^{-2}/1 mAh cm^{-2}, 3000 cycles	[152]
Pre-fabricating	SEI	OSA/PAM@Sn	5000 h, 1 mA cm^{-2}/1 mAh cm^{-2}	99.8%, 1 mA cm^{-2}/1 mAh cm^{-2}, 2000 cycles	[153]
Pre-fabricating	SEI	Gelatinized-starch@C	3000 h, 1 mA cm^{-2}/1 mAh cm^{-2}	—	[154]
Pre-fabricating	SEI	In_4Te_3/PVDF@In_2Te_3/PVDF	3330 h, 1 mA cm^{-2}/1 mAh cm^{-2}	99.2%, 1 mA cm^{-2}/1 mAh cm^{-2}, >700 cycles	[155]
Pre-fabricating	SEI	Sn@PVDF	1200 h, 1 mA cm^{-2}/1 mAh cm^{-2}	>99%, 5 mA cm^{-2}/1 mAh cm^{-2}, 500 cycles	[156]
Pre-fabricating	SEI	LLP@Treated Zn	>1500 h, 3 mA cm^{-2}/0.5 mAh cm^{-2}	99.37%, 5 mA cm^{-2}/1 mAh cm^{-2}, 1200 cycles	[157]
Pre-fabricating	SEI	Four double layers of CS@SA	>6500 h, 1 mA cm^{-2}/1 mAh cm^{-2}	~100%, 1 mA cm^{-2}/1 mAh cm^{-2}, >1000 cycles	[158]
Pre-fabricating	SEI + molecular layer	Cu@Fluoroalkylsilane	2400 h, 1 mA cm^{-2}/1 mAh cm^{-2}	99.7%, 5 mA cm^{-2}/1 mAh cm^{-2}, 7500 cycles	[159]

(Continues)

TABLE 1 | (Continued)

Constructing methods	Types of interphase	Artificial interphase materials	Symmetric cells (cycling time, cycling condition)	Asymmetric cells (Coulombic efficiency, cycling condition, cycling number)	Reference
Pre-fabricating	SEI + molecular layer	Ag@hexadecanethiol	>2600 h, 1 mA cm^{-2}/1 mAh cm^{-2}	99.71%, 1 mA cm^{-2}/1 mAh cm^{-2}, >1300 cycles	[160]
Pre-fabricating	Molecular layers	APTES@POTES	1000 h, 1 mA cm^{-2}/1 mAh cm^{-2}	99.89%, 1 mA cm^{-2}/1 mAh cm^{-2}, 1000 cycles	[133]
Multiphasic transition	SEI	Organic component@Cu	3300 h, 3 mA cm^{-2}/3 mAh cm^{-2}	99.7%, 1 mA cm^{-2}/1 mAh cm^{-2}, 1800 cycles	[161]
Multiphasic transition	SEI	ZnF_2@In	6000 h, 0.5 mA cm^{-2}/0.5 mAh cm^{-2}	99.6%, 0.5 mA cm^{-2}/0.5 mAh cm^{-2}, 700 cycles	[162]
Multiphasic transition	SEI	ZnF_2@FAG	4000 h, 1 mA cm^{-2}/0.5 mAh cm^{-2}	~100%, 1 mA cm^{-2}/1 mAh cm^{-2}, 160 cycles	[163]
Multiphasic transition	SEI	VSe_2/ZnSe@V	2200 h, 1 mA cm^{-2}/1 mAh cm^{-2}	—	[164]
Multiphasic transition	SEI	ZnSe@Ag	500 h, 1 mA cm^{-2}/1 mAh cm^{-2}	>95%, 1 mA cm^{-2}/1 mAh cm^{-2}, 100 cycles	[165]
Multiphasic transition	SEI	$CuZn_5$@Cu	1800 h, 1 mA cm^{-2}/1 mAh cm^{-2}	~100%, 1 mA cm^{-2}/1 mAh cm^{-2}, 150 cycles	[166]
Multiphasic transition	SEI	ZnF_2@In	4200 h, 1 mA cm^{-2}/1 mAh cm^{-2}	99.8%, 5 mA cm^{-2}/1 mAh cm^{-2}, 500 cycles	[167]
Multiphasic transition	SEI	ZEA@ZnF_2	500 h, 0.5 mA cm^{-2}/0.5 mAh cm^{-2}	98.1%, 0.5 mA cm^{-2}/0.5 mAh cm^{-2}, 300 cycles	[168]
In-situ fabricating	SEI	Crystalline $ZnCO_3$@amorphous ZnS	1600 h, 2 mA cm^{-2}/1 mAh cm^{-2}	99.95%, 2 mA cm^{-2}/1 mAh cm^{-2}, 4800 cycles	[169]
In-situ fabricating	SEI	Poly(zinc thioctate)@ZnS/organic	1300 h, 3 mA cm^{-2}/1 mAh cm^{-2}	99.5%, 5 mA cm^{-2}/20 mAh cm^{-2}, 100 cycles	[170]

(Continues)

TABLE 1 | (Continued)

Constructing methods	Types of interphase	Artificial interphase materials	Symmetric cells (cycling time, cycling condition)	Asymmetric cells (Coulombic efficiency, cycling condition, cycling number)	Reference
In-situ fabricating	SEI	ZnF_2@$Zn_5(CO_3)_2(OH)_6$/organic	1200 h, 0.5 mA cm^{-2}/0.5 mAh cm^{-2}	99.8%, 1 mA cm^{-2}/0.5 mAh cm^{-2}, 200 cycles	[171]
In-situ fabricating	SEI	$Zn(PO_3)_2$@organic	1700 h, 10 mA cm^{-2}/1 mAh cm^{-2}	99.6%, 2 mA cm^{-2}/1 mAh cm^{-2}, 900 cycles	[172]
In-situ fabricating	SEI	$ZnCO_3$@organic	5500 h, 1 mA cm^{-2}/1 mAh cm^{-2}	99.73%, 8 mA cm^{-2}/1 mAh cm^{-2}, 700 cycles	[173]
In-situ fabricating	SEI	(PDDA-TFSI)@$Zn_5(OH)_8Cl_2{\cdot}H_2O$@Sn(PT-ZHC-Sn)	6500 h, 0.5 mA cm^{-2}/0.5 mAh cm^{-2}	99.1%, 1 mA cm^{-2}/1 mAh cm^{-2}, 950 cycles	[174]
In-situ fabricating	SEI	C-rich organic@Cl-rich inorganic	2000 h, 1 mA cm^{-2}/1 mAh cm^{-2}	—	[175]
In-situ fabricating	SEI	ZnF_2@organic	1600 h, 1 mA cm^{-2}/2 mAh cm^{-2}	99.47%, 0.5 mA cm^{-2}/0.5 mAh cm^{-2}, 200 cycles	[176]
In-situ fabricating	SEI	ZnF_2@organic	4000 h, 0.5 mA cm^{-2}/0.5 mAh cm^{-2}	99.5%, 0.5 mA cm^{-2}/0.5 mAh cm^{-2}, 1200 cycles	[177]
In-situ fabricating	SEI	ZnF_2@organic	2500 h, 1 mA cm^{-2}/1 mAh cm^{-2}	99.95%, 1 mA cm^{-2}/1 mAh cm^{-2}, 5000 cycles	[178]
In-situ fabricating	SEI	ZnS/$ZnCO_3$@organic	1750 h, 1 mA cm^{-2}/1 mAh cm^{-2}	99.0%, 1 mA cm^{-2}/0.5 mAh cm^{-2}, 800 cycles	[179]
In-situ fabricating	SEI	ZnF_2@PANI	1200 h, 5 mA cm^{-2}/5 mAh cm^{-2}	95%, 0.2 mA cm^{-2}/0.2 mAh cm^{-2}, 300 cycles	[180]
In-situ fabricating	SEI	ZnS, Zn_3N_2, and $Zn_3(PO_4)_2$	2200 h, 1 mA cm^{-2}/1 mAh cm^{-2}	99.7%, 1 mA cm^{-2}/0.5 mAh cm^{-2}, >800 cycles	[181]
In-situ fabricating	SEI	ZnF_2-ZnO-ZnS-$ZnCO_3$@amorphous phase	4350 h, 1 mA cm^{-2}/1 mAh cm^{-2}	99.0%, 5 mA cm^{-2}/1 mAh cm^{-2}, 1100 cycles	[182]
In-situ fabricating	SEI	ZnS@organic	3000 h, 1 mA cm^{-2}/1 mAh cm^{-2}	99.7%, 10 mA cm^{-2}/5 mAh cm^{-2}, 300 cycles	[183]
In-situ fabricating	SEI	Sn@I^- rich adsorption layer	3100 h, 1 mA cm^{-2}/1 mAh cm^{-2}	~100%, 1 mA cm^{-2}/0.5 mAh cm^{-2}, 600 cycles	[184]

(Continues)

TABLE 1 | (Continued)

Constructing methods	Types of interphase	Artificial interphase materials	Symmetric cells (cycling time, cycling condition)	Asymmetric cells (Coulombic efficiency, cycling condition, cycling number)	Reference
In-situ fabricating	SEI	$Sn@Zn_5(OH)_8Cl_2{\cdot}H_2O$	500 h, 3 mA cm^{-2}/3 mAh cm^{-2}	99.7%, 1 mA cm^{-2}/0.5 mAh cm^{-2}, 200 cycles	[185]
In-situ fabricating	SEI	$In@Zn_5(OH)_8Cl_2{\cdot}H_2O/ZnCO_3$@organic	3000 h, 1 mA cm^{-2}/0.5 mAh cm^{-2}	99.3%, 1 mA cm^{-2}/0.5 mAh cm^{-2}, 2000 cycles	[186]
In-situ fabricating	SEI	B,O-inner layer@F,O-exterior layer	4400 h, 0.5 mA cm^{-2}/0.25 mAh cm^{-2}	99.53%, 2 mA cm^{-2}/0.5 mAh cm^{-2}, 1600 cycles	[187]
In-situ fabricating	SEI	B-O and C species	1200 h, 1 mA cm^{-2}/1 mAh cm^{-2}	99.5%, 1 mA cm^{-2}/1 mAh cm^{-2}, 1500 cycles	[188]
In-situ fabricating	SEI	B, O-rich, S-rich, and F-rich SEI	1650 h, 2 mA cm^{-2}/1 mAh cm^{-2}	99.5%, 1 mA cm^{-2}/1 mAh cm^{-2}, 1050 cycles	[189]
In-situ fabricating	SEI	ZnF_2@organic	3200 h, 1 mA cm^{-2}/1 mAh cm^{-2}	99.83%, 5 mA cm^{-2}/2 mAh cm^{-2}, >1200 cycles	[190]
In-situ fabricating	Molecular layers	Amphiphilic acetylcholine cation	3700 h, 1 mA cm^{-2}/1 mAh cm^{-2}	99.75%, 1 mA cm^{-2}/0.5 mAh cm^{-2}, >2200 cycles	[191]
In-situ fabricating	Molecular layers	Bovine serum albumin	2400 h, 10 mA cm^{-2}/1 mAh cm^{-2}	>99%, 2 mA cm^{-2}/0.5 mAh cm^{-2}, 4800 cycles	[192]
In-situ fabricating	Molecular layers	Lipopeptides and di-tryptophan	3000 h, 1 mA cm^{-2}/1 mAh cm^{-2}	99.6%, 1 mA cm^{-2}/1 mAh cm^{-2}, 1000 cycles	[193]
In-situ fabricating	Molecular layers	KH590 silane@TFPS silane	4300 h, 1 mA cm^{-2}/0.5 mAh cm^{-2}	99.1%, 1 mA cm^{-2}/0.5 mAh cm^{-2}, 2740 cycles	[194]
In-situ fabricating	Molecular layers	PC lipid analogues	>3600 h, 1 mA cm^{-2}/1 mAh cm^{-2}	99.25%, 1 mA cm^{-2}/0.5 mAh cm^{-2}, 400 cycles	[195]
In-situ fabricating	Molecular layers	Lithium nonafluorobutanesulfonate	2460 h, 5 mA cm^{-2}/5 mAh cm^{-2}	99.9%, 5 mA cm^{-2}/5 mAh cm^{-2}, >400 cycles	[196]

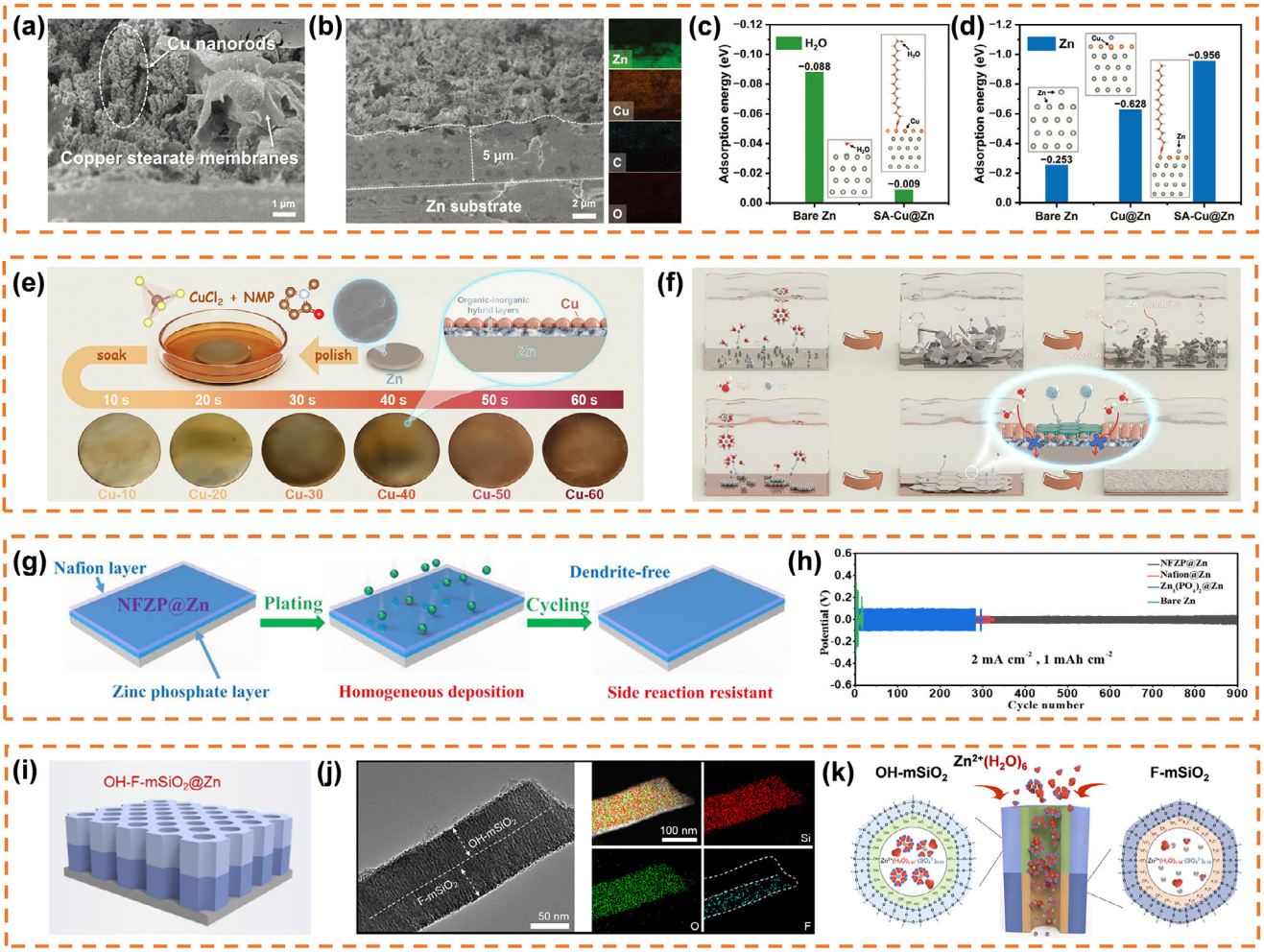

FIGURE 1 | (a) Cross-sectional SEM images of SA-Cu@Zn and (b) corresponding EDS elemental mappings. Adsorption energy of (c) one H_2O molecule and (d) one Zn atom adsorbed on different surfaces [146]. Copyright 2023, Wiley-VCH. (e) Schematic diagram and digital photos of Cu-(X) preparation process. (f) Schematic illustrations of Zn^{2+} ion deposition behavior on bare Zn and Cu-40 anodes [147]. Copyright 2025, Elsevier. (g) Schematic illustration of Zn^{2+} ion deposition behavior on the NFZP composite layer. (h) Cycling performances of NFZP@Zn, Nafion@Zn, $Zn_3(PO_4)_2$@Zn, and bare Zn symmetrical batteries [148]. Copyright 2022, Elsevier. (i) Schematic illustration and (j) TEM cross-sectional image of the Janus OH-F-mSiO_2 interphase. (k) The adsorption and desolvation mechanism of $Zn^{2+}(H_2O)_6$ in Janus OH-F-mSiO_2 interphase [149]. Copyright 2025, American Chemical Society.

stable, and engineerable interfacial regulation strategy for zinc anodes [47]. Normally, the inner interface layer regulates the uniform deposition of zinc ions by introducing zincophilicity sites or high ion conductivity materials, while the outer interface layer promotes rapid diffusion of zinc ions and acts as a barrier to water molecules. For example, inspired by the lotus effect, Han et al. [146]. developed a metal-organic bilayer structure exhibiting hydrophobic properties and zincophilic on the surface of zinc metal. The preparation process involves the in-situ growth of copper nanorod arrays on the surface of zinc (Cu@Zn) via chemical displacement reactions. During the immersion of Cu@Zn in a stearic acid ethanol solution, dissolved oxygen in the solution oxidizes the copper nanorod surface to release Cu^{2+}. These Cu^{2+} then combine with stearic acid (StA) to form a copper stearate film, creating a low surface energy hydrophobic layer on the copper nanorods (StA-Cu@Zn), similar to the wax layer on lotus leaves (Figure 1a,b). In this structure, the copper stearate film on the upper protective layer repels water molecules due to the hydrophobic nature of its long-chain alkyl groups, thereby inhibiting HER and mitigating corrosion (Figure 1c). The copper nanorod array embedded in the lower protective layer offers well-ordered Zn^{2+} transport pathways and zincophilic sites, thereby reducing the nucleation overpotential (Figure 1d). The StA-Cu@Zn symmetric battery, which incorporates a hydrophobic zinc bilayer SEI structure, exhibits long-term cycling stability over 2000 h and outstanding rate performance at a current density of 1 mA cm^{-2} and a capacity of 1 mAh cm^{-2}. In contrast, the zinc anode solely loaded with metallic copper short-circuited after only 900 h of cycling at this current density.

Similarly, Zhang and co-workers developed a Cu-based organic-inorganic hybrid protective layer on the surface of a zinc anode, with the difference being that this study penetrated metal copper nanoparticles into a hydrophobic organic layer (Figure 1e) [147]. In the process of electroless copper plating, Cu^{2+} is initially reduced to Cu^0, which subsequently nucleates and grows on the surface of zinc, ultimately forming copper nanoparticles. As

the reaction progresses, the functional groups in N-methyl-2-pyrrolidone (NMP) molecules, such as the carbonyl group (C = O), coordinate with Cu^{2+} to form complexes. These complexes subsequently decompose on the zinc surface and contribute to the formation of organic-inorganic hybrid layers. The integration of upper copper nanoparticles with a lower organic-inorganic hybrid layer constructs a synergistic bilayer architecture. The upper layer of copper nanoparticles serves to provide high electrical conductivity and facilitate the uniform deposition of zinc ions. The lower-layer organic-inorganic hybrid layer contributes to enhanced mechanical and chemical stability of the overall coating. Additionally, the organic components derived from NMP improve hydrophobicity, reduce electrolyte penetration, and help suppress HER and corrosion (Figure 1f). This dual-layer configuration demonstrates superior performance in inhibiting zinc dendrite formation, enhancing cycling stability, and promoting uniform zinc ion deposition.

In addition to copper, highly electronegative metals such as indium (In) and bismuth (Bi) can also serve as zincophilic sites. Li and colleagues constructed a novel double-layer gradient coating on the surface of zinc anodes, which consists of a zincophilic Sn inner layer and an outer layer of organic polymer (noted as OSA/PAM@Sn) [153]. The organic outer layer is prepared by scraping cross-linked sodium alginate and polyacrylamide (OSA/PAM), which not only isolates active water but also promotes the desolvation process of $[Zn(H_2O)_6]^{2+}$ with its rich polar functional groups, accelerating the diffusion of zinc ions and effectively suppressing harmful HER and zinc self-corrosion phenomena. The inner layer of metallic stannum (Sn) is obtained through an in-situ displacement reaction on the surface of zinc foil. The loosely structured Sn inner layer can provide abundant nucleation sites, which promote uniform zinc deposition in a "bottom-up" manner and result in low overpotential. The synergistic effect of the double-layer gradient coating facilitates the maintenance of a smooth surface on the zinc anode during cycling, while effectively suppressing side reactions, thereby contributing to superior electrochemical performance.

Besides incorporating zincophilic metals, favorable outcomes can also be achieved through the synergistic interaction between a Zn^{2+} ion conductive layer and a hydrophobic layer. Wang et al. [148]. developed an organic-inorganic bilayer interface, Nafion/$Zn_3(PO_4)_2$ (NFZP), to enhance the stability of zinc anodes (Figure 1g). This method forms a thin $Zn_3(PO_4)_2$ layer on the zinc metal surface through an in-situ reaction, followed by coating it with a Nafion film via impregnation. Among these, the hydrophobic region of the Nafion membrane is capable of blocking certain small anions, such as SO_4^{2-}, as well as free water molecules, whereas the $Zn_3(PO_4)_2$ layer exhibits selective conductivity for zinc ions. This synergistic protective layer can effectively suppress the uncontrolled growth of zinc dendrites and HER, thereby enabling an ultra-low overpotential of 45 mV at 0.5 mA cm^{-2} during zinc deposition and dissolution. The NFZP@Zn electrode demonstrates excellent cycling stability for over 900 h. In comparison, Zn metal electrodes modified with only a Nafion or $Zn_3(PO_4)_2$ layer exhibit lifetimes of 280 and 320 h, respectively (Figure 1h).

Constructing coatings with hydrophilic-hydrophobic dual interfaces can also asynchronously regulate the deposition of zinc ions from the perspective of desolvation. For example, Wang et al. [149]. proposed a tandem chemical strategy and constructed an SEI layer featuring Janus mesoporous channels via electrochemical-assisted self-assembly (Figure 1i). The Janus mesoporous layer enables asynchronous acceleration of cascade chemical reactions by decoupling the adsorption and desolvation processes of Zn^{2+}. In the preparation process, fluorosilane (PFOTMS) is first induced to preferentially self-polymerize and condense on the zinc surface, forming fluorinated mesoporous SiO_2 nanochannels (F-mSiO_2 layer). Subsequently, under the influence of an electric field, tetraethyl orthosilicate (TEOS) and cetyltrimethylammonium bromide (CTAB) micelles undergo secondary self-assembly on the F-mSiO_2 layer, leading to the formation of a hydrophilic, OH-enriched layer (OH-mSiO_2 layer), ultimately resulting in a Janus structure with distinct upper and lower functional regions (OH-F-mSiO_2@Zn). Energy dispersive X-ray spectroscopy (EDX) shows that silicon and oxygen are uniformly distributed, while fluorine (F) is enriched in the bottom layer (Figure 1j). In this structure, the hydrophilic upper layer with –OH groups captures $[Zn(H_2O)_6]^{2+}$ clusters via electrostatic interactions, creating the local high Zn^{2+} concentrations. This significantly shortens the diffusion path of Zn^{2+}, reduces ion transport resistance, and thereby mitigates concentration polarization. Meanwhile, the solvation structure of Zn^{2+} is transformed from $Zn^{2+}(H_2O)_{5.97}(SO_4^{2-})_{0.03}$ to $Zn^{2+}(H_2O)_{5.83}(SO_4^{2-})_{0.14}$, which reduces the number of coordinated water molecules and lowers the desolvation energy barrier. The hydrophobic –F groups in the lower layer repel the solvation of H_2O molecules, thereby reducing the activation energy of Zn^{2+} desolvation to 7.66 kJ/mol (only 20% of that on bare zinc) and increasing the diffusion coefficient to 1.09×10^{-7} cm^2/s (Figure 1k). Additionally, the ordered mesoporous channel structure features vertically aligned nanochannels, which significantly reduce the tortuosity of the Zn^{2+} transport pathway and enhance the diffusion efficiency. On the other hand, it guides the 3D uniform diffusion of Zn^{2+}, avoids local ion depletion or accumulation, and achieves dynamic equilibrium in the sedimentation/dissolution process. The obtained symmetrical battery achieved over 8000 reversible cycles at high current densities of 4 mA cm^{-2}, which is significantly longer than that of the single hydrophilic –OH interphase modified zinc anode of about 500 h.

In addition to preparing double-layer coatings, some researchers have attempted to synergistically and further regulate the deposition process of zinc ions by constructing three-layer, four-layer, or even more coatings. For example, Zhou et al. [130] fabricated a three-layer structured artificial SEI layer, denoted as SFM, on a zinc metal anode through the integration of molecular self-assembly engineering, scraper coating, and air spray techniques. During the deposition of zinc ions, the superhydrophobic interface composed of trimethoxy(octadecyl)silane (OTS)-modified nanosilicon dioxide particles in the outermost layer, together with the polydimethylsiloxane (PDMS) middle layer, effectively suppresses water-related side reactions. Meanwhile, the $–NH_2$ group located in the innermost layer, which originates from triethoxy-3-aminopropylsilane self-assembled monolayers, possesses nitrogen atoms with lone pair electrons that lower the binding energy with zinc ions, thereby facilitating their transport kinetics. Moreover, the highly elastic nature of PDMS can effectively prevent polymer failure during the dynamic evolution of Zn^{2+} ions, while also serving as a uniform diffusion layer for Zn^{2+}

during the deposition and stripping processes. Therefore, due to the synergistic effect of the three coatings, the SFM/Zn||SFM/Zn symmetric battery exhibits a highly reversible and stable zinc plating/stripping behavior. Cai et al. [158] developed a simple and controllable layer-by-layer self-assembly technique based on spin coating to construct an ion-conductive and mechanically robust electrolyte/electrode interface, thereby stabilizing the zinc electrode. This layer-by-layer film is composed of chitosan (CS) and sodium alginate (SA). Among them, CS, as a positively charged polyelectrolyte, interacts with the surface of the Zn anode through electrostatic forces to form the first layer of a protective film. Its abundant amino (—NH_2) and hydroxyl (—OH) groups can strongly adsorb onto the surface of metallic Zn via hydrogen bonding, thereby enhancing mechanical strength and suppressing dendrite growth. Moreover, the —OH of CS removes water molecules from the Zn^{2+} solvation sheath via hydrogen bonding, thereby suppressing side reactions caused by reactive water species and reducing the desolvation energy barrier. As a negatively charged polyelectrolyte, SA forms a stable, gel-like double interface layer through electrostatic interactions between its carboxyl groups (—COO^-) and the amino groups of CS. Its flexible chain structure can adapt to the volume change of Zn deposition/stripping. Additionally, Na^+ in SA forms an electrostatic shielding layer on the Zn surface, which suppresses dendritic tip growth by preventing localized enrichment of Zn^{2+}. A symmetrical battery composed of four CS/SA bilayers (CS/SA_4-Zn) exhibits stable performance over 6500 h of cycling.

Overall, constructing multiscale interface coatings on the surface of zinc metal anodes through pre-construction methods is convenient and widely applicable. However, its inherent static characteristics and limited interface stability represent the primary limitations for commercial applications. This is because the bonding between multi-layer coatings formed on the surface of zinc foil through physical methods (such as scraping, spin coating, sputtering) or chemical methods (such as chemical vapor deposition, liquid-phase reaction) typically involves physical adsorption or weak chemical interactions. During the AZIBs cycling process, the zinc anode undergoes repeated exfoliation and deposition, with inevitable volume changes causing stress between protective layers, leading to coating cracking and delamination. Moreover, poor compatibility between the two coatings will significantly increase zinc anode interface impedance, raising battery polarization voltage and reducing operating voltage and energy efficiency.

3.2 | Inducing Multiphasic Transition of A Single Interface Layer

As mentioned above, the pre-fabricated SEI layers featuring a multi-layer structure may undergo delamination under prolonged cycling conditions due to mechanical stress or chemical corrosion, thereby compromising their protective function. In contrast, in-situ inducing a multi-layer interface spontaneously from a single-layer SEI interface enables real-time adaptation to electrode deformation and electrolyte changes, preventing interface delamination due to mismatched pre-coating and electrode expansion. Additionally, the dynamically formed interface better conforms to the surface morphology of the electrode, thereby avoiding potential issues of poor contact that may arise with pre-coating methods. There are two commonly used conversion methods: one is about the displacement reaction, and the other is about the decomposition reaction.

The core of the displacement reaction strategy lies in the spontaneous redox process driven by the difference in metal activity in the electrochemical system. This strategy first performs a monolayer functional coating containing specific inert metal components (such as Cu, Sn, In, etc.) on the substrate surface. Then, when the coating comes into contact with a zinc metal anode or a zinc-containing electrolyte, due to zinc's lower electrode potential (–0.76 V vs. SHE), it spontaneously undergoes a displacement reaction with the inert metals in the coating. During this process, zinc atoms are oxidized to zinc ions and enter the solution, while the inert metal ions in the coating are reduced to metallic simple substances, thereby forming a dense inert metal protective layer beneath or on the surface of the original coating, and even further transforming into corresponding metal oxide/sulfide interphases. This in-situ formed multi-layer structure is not simply stacked but naturally constructed into a multiscale interface system with gradually changing composition, density, or function from the inside to the outside through the control of reaction kinetics and thermodynamics. This multiscale interfacial structure can not only effectively regulate the distribution of zinc ion flow, inhibit dendrite growth, but also enhance the mechanical stability and corrosion resistance of the interface, achieving an upgrade from simple physical isolation to chemical-mechanical synergistic protection. For example, Luo et al. [161]. used spin coating technology to load PVDF and CuI mixed slurry onto the surface of the zinc anode, and then constructed an organic component copper metal composite layer on the zinc anode (Org-Cu@Zn) through a one-step and in-situ spontaneous displacement reaction ($Zn + 2CuI \rightarrow 2Cu + ZnI_2$). The functional groups present in the outer organic layer can act as active sites and conductive pathways for zinc ion migration, thereby enhancing ion transport kinetics. Meanwhile, its organic components can enhance the interfacial adhesion between the copper layer and the zinc anode. The inner layer of zincophilic copper clusters reduces the interface resistance, which is beneficial for zinc ion diffusion and deposition (Figure 2a). DFT calculations show that the adsorption energy of Org-Cu@Zn is –1.06 eV, indicating that the synergistic effect of the organic layer and the metallic copper layer can further enhance the affinity for zinc (Figure 2b). This distinctive double-layer structure demonstrates enhanced zinc affinity, reduced interfacial resistance, lower nucleation energy barriers, and improved corrosion resistance, thereby effectively inhibiting zinc dendrite formation and mitigating side reactions. Thus, the Org-Cu@Zn symmetric battery achieves a remarkable lifetime of 4300 h at 1 mA cm^{-2} and 1 mAh cm^{-2}, surpassing that of bare Zn (340 h), PVDF@Zn (500 h), and Cu@Zn (1750 h) batteries.

By the same token, Zhang et al. [162] pre-prepared InF_3 coating on the surface of zinc foil using a traditional coating method, and then formed an ultra-thin ZnF_2 layer and an In layer through spontaneous electroplating displacement reaction between InF_3 and Zn. The final formation is a self-assembled multi-level solid electrolyte interface ($Zn@InF_3$) composed of InF_3, In, and ZnF_2 layers, arranged from the outside to the inside (Figure 2c). Among them, the waterproof surface of InF_3 and the high hydrogen evolution overpotential of metallic In jointly reduce electrolyte

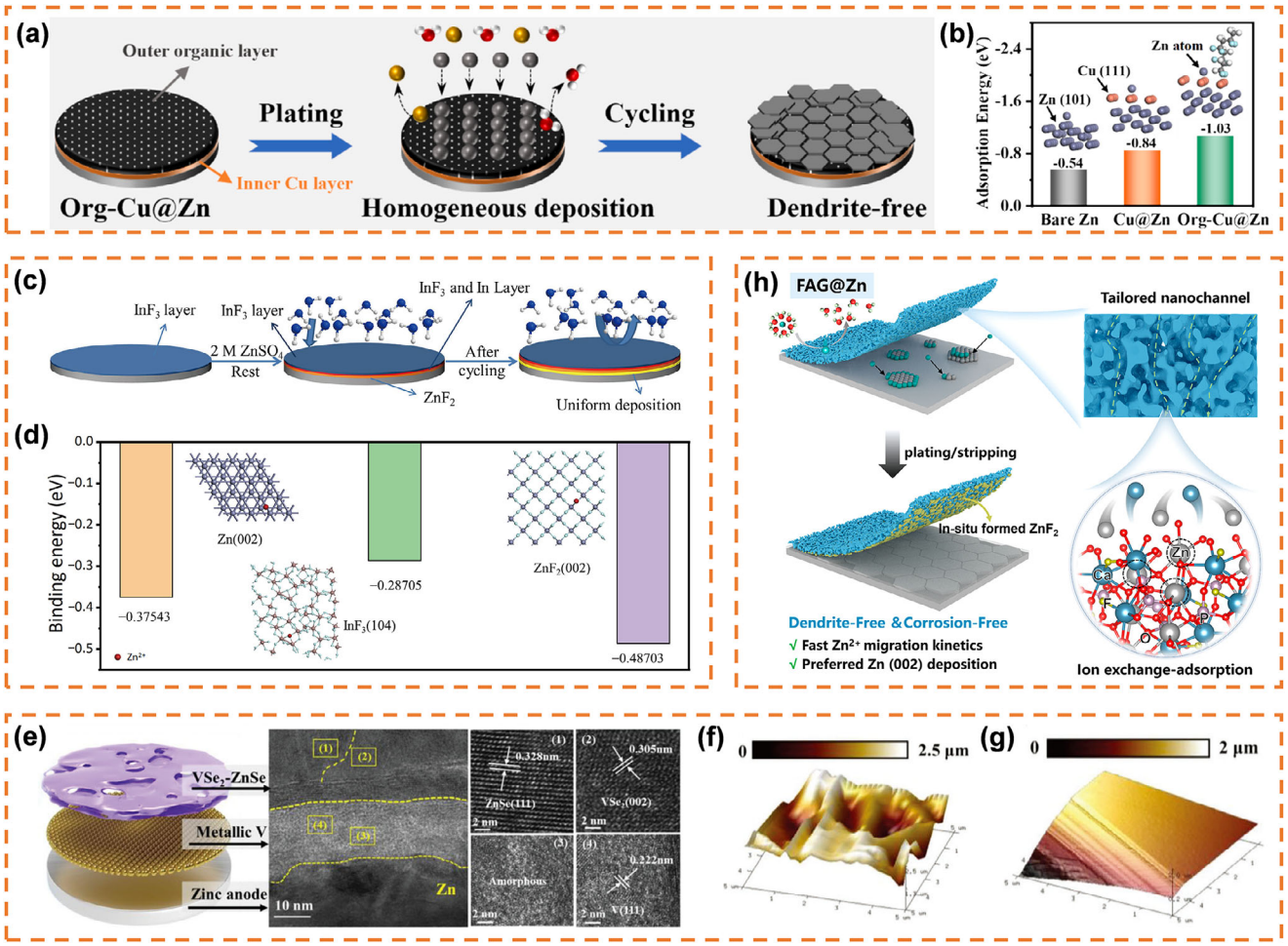

FIGURE 2 | (a) Schematic diagram of the Zn^{2+} deposition process on Org-Cu@Zn anodes. (b) The adsorption energy of a Zn atom on bare Zn, Cu@Zn, and Org-Cu@Zn anodes [161]. Copyright 2024, Elsevier. (c) Schematic illustration of the standing and circulating process of Zn@InF. (d) The binding energy of Zn^{2+} on Zn (002), InF_3 (104), and ZnF_2 (002) [162]. Copyright 2023, Springer Nature. (e) Schematic illustration of the "dual-layer" structure and the corresponding HRTEM images of the VZSe/V@Zn anode. AFM 3D reconstruction images of the (f) bare Zn anode and (g) ZEA@Zn anode after zinc plating [163]. Copyright 2024, Wiley-VCH. (h) Illustration of Zn deposition behavior on FAG@Zn Anodes [164]. Copyright 2023, American Chemical Society.

decomposition and hydrogen evolution. The inner ZnF_2 layer has a lower absorption energy barrier and higher Zn^{2+} conductivity, enabling Zn^{2+} to preferentially adsorb onto ZnF_2 and deposit uniformly (Figure 2d). Furthermore, its high resistivity hinders local current concentration, thereby suppressing zinc dendrites. The prepared zinc anode can achieve dendrite-free zinc deposition/stripping for over 6000 h at almost 100% Coulombic efficiency.

In addition to displacement reactions in the electrolyte, heat treatment represents another effective approach for constructing multiscale coating structures on zinc metal surfaces. At higher temperatures, atoms have higher kinetic energy, which is conducive to the formation of thermodynamically stable interfacial phases in electrochemical environments, which may themselves have excellent ionic conductivity and chemical stability. This technique facilitates a reaction between the initial coating and the zinc substrate, enabling the in situ formation of multiple protective layers. Zhang et al. [163]. proposed an in-situ transformation strategy for the construction of a protective bilayer structure (VZSe/V@Zn) on the surface of metallic zinc (Figure 2e). In this process, 1T-VSe_2 nanosheets were uniformly deposited onto the zinc anode via spray coating, after which the 1T-VSe_2 reacts with metallic zinc in an Ar atmosphere at 300°C, resulting in the formation of ZnSe and metallic vanadium. Among them, vanadium atoms are predominantly concentrated at the interface rather than within the zinc lattice, which contributes to superior corrosion resistance. This characteristic effectively inhibits electrolyte-induced corrosion of the zinc anode and thereby extends the operational lifespan of the battery. Moreover, the vanadium layer regulates interfacial energy during zinc deposition, thereby promoting uniform zinc deposition and suppressing the formation of zinc dendrites. The outer layer of VZSe, composed of VSe_2 and ZnSe, exhibits a lower lattice mismatch with the (002) crystal plane of zinc, thereby facilitating the ordered planar deposition of zinc ions (Figure 2f,g). Additionally, the VZSe layer possesses a high electronic conductivity of 1150 S cm^{-1}, which enhances interfacial zinc ion diffusion and improves both ion and electron transport efficiency during the deposition and stripping processes. The synergistic interaction between the inner and outer layers collectively improves the cycling stability and reversibility of the zinc anode.

For the decomposition method, elements such as F, S, Se, and Te in the single coating are released to form an electrically insulating but ion-conductive dielectric layer with zinc atoms on the surface of zinc metal [167]. This in-situ generated zinc-ion conductor layer (such as ZnF_2, ZnS, ZnSe, and ZnTe) not only optimizes the interfacial ion transport kinetics and reduces the overpotential for zinc deposition, but also guides the uniform epitaxial growth of zinc along low-energy crystal planes through its own crystal orientation and interfacial energy regulation, thereby synergistically inhibiting dendrite formation and enhancing the reversibility and stability of zinc deposition and stripping [197–198]. It is worth emphasizing that this decomposition process is selective and local, and does not completely destroy the overall structure and function of the original coating. The undecomposed parts of the original coating can still play their preset interface regulation roles (such as providing zinc affinity sites, regulating electric field distribution, and blocking water molecules), thereby forming a composite interface system with functional complementarity with the newly formed dielectric layer. This strategy of achieving functional superposition through partial decomposition not only continues the design advantages of single-layer coatings but also enhances the ion selectivity and structural stability of the interface by introducing inorganic dielectric phases, achieving multi-level coordinated regulation of zinc deposition behavior. For example, Shi et al. [164] constructed a dual-interface SEI layer on the surface of the zinc anode through an in-situ decomposition and transformation process (Figure 2h). Specifically, a multifunctional fluorapatite aerogel (FAG) protective layer was pre-constructed on the surface of the zinc metal anode. During the zinc deposition/stripping process, the F atoms in the FAG gradually released from the fluorapatite structure, and reacted with Zn^{2+} to form ZnF_2 through ion exchange adsorption and high ion electronegativity difference. The nano channels and ion exchange sites on the outer FAG layer improve the migration efficiency of Zn^{2+} and reduce their desolvation energy barrier, which helps to eliminate tip effects and suppress dendrites. In addition, due to the hydrophobic and lightweight characteristics of FAG aerogel, the FAG layer inhibits the side reactions and enhances the energy density of the battery. For the inner ZnF_2 layer, its high interface energy promotes the parallel deposition of Zn^{2+} along the (002) crystal plane, further eliminating dendrites. Based on the synergistic effect of outer and inner interfaces, the FAG@Zn symmetric battery achieves excellent cycling stability for over 4000 h at a current density of 1 mA cm^{-2}. Another design concept is to introduce highly electronegative atoms such as F, S, and Se into functionalized matrices (such as Mxene [199], graphite [200], or composite coatings) during the material synthesis stage, to construct precursor structures with ion release potential. During the battery charging and discharging process, these anions are controllably released under the drive of an electric field or chemical potential, and then react with the Zn^{2+} on the zinc metal surface or in the electrolyte to in situ generate inorganic solid electrolyte interface layers with good Zn^{2+} conduction ability. For instance, Ge et al. [201]. designed and prepared a fluorinated carbon dots (F-CDs) artificial interphase layer, which possesses three zincophilic functional groups (–C = O, –CHO, –F). DFT calculations confirmed its extremely strong Zn^{2+} adsorption capacity, which is conducive to uniform nucleation. Meanwhile, the hydrophobic property of the C–F group can block H_2O molecules, suppress hydrogen evolution, and corrosion. More importantly, the –F functional group can in situ induce the formation of a ZnF_2 layer during cycling, which acts as a solid Zn^{2+} conductor to further guide uniform deposition. The synergistic effect of these two layers enables fine control over the zinc deposition behavior, effectively suppressing dendrite growth and side reactions. As a result, the Zn@F-CDs anode achieved an ultra-long stable cycling of over 3500 h in a symmetrical cell.

In conclusion, constructing multi-layer coatings through in-situ multiphasic transition represents a highly intelligent, efficient, and advanced strategy with significant industrial potential. The key advantage of this approach lies in the formation of a robust and adaptive integrated interface. This adaptive formation ensures uniform interfacial contact and effectively mitigates dendrite growth induced by high local current density. Moreover, the mixed SEI utilizes the high hardness and strength of inorganic components, which can significantly inhibit the growth of metal dendrites. The organic components in the mixed SEI can ensure sufficient flexibility to adapt to volume changes during metal plating/stripping processes. It should be noted that the selected material must be easily coated and capable of controlled, beneficial chemical reactions within a specific electrochemical window to form an ideal multilayer structure. This demands considerable foresight and rigorous screening in material chemistry and electrochemistry, resulting in a high research and development barrier. Furthermore, the extent and kinetics of the conversion reaction, as well as the homogeneity of the final product, may be influenced by various factors, including electrolyte composition, current density, and operating temperature.

3.3 | In Situ Fabricating A Multiscale Interface Layer Using Electrolyte Additives

In the strategy of in-situ constructing the SEI layer on the zinc metal surface by using electrolyte additives, the core mechanism lies in the preferential reduction, adsorption, or coordination reactions of the additive molecules at the zinc anode interface during the electrochemical cycling process, thereby controllably generating multiscale interfacial phases with specific structures and functions [202–203]. The additive molecules typically contain highly electronegative functional groups (e.g., F, S, N, O), which migrate toward the zinc surface under an electric field and form an inorganic inner layer of zinc salts (e.g., ZnF_2, ZnS, ZnO) and an organic-rich outer layer via chemical decomposition, electrochemical reduction, or reaction with zinc ions or electrolyte components [204–205]. The in-situ construction of a multiscale interfacial layer using electrolyte additives has significant advantages over traditional coating methods: (1) The in-situ formation of a multiscale interface layer using electrolyte additives offers strong interfacial adhesion and avoids the poor physical contact issues associated with traditional coating methods. (2) Electrolyte additive molecules dynamically regulate electrolyte interface growth, adapt to electrode surface changes, and ensure uniform nanoscale coverage. (3) The in-situ formation of a multiscale interface layer usually has self-healing ability, avoiding problems such as uneven thickness or cracks caused by process influences. (4) The SEI formed by the in-situ method has high Zn^{2+} conductivity and selectivity compared to the coating method, which can greatly improve the diffusion efficiency of Zn^{2+}. (5) The construction method is simpler and can form a

double- or multi-layer structure with complementary functions in one step, making it more suitable for large-scale production.

A commonly employed approach involves utilizing organic compounds that contain highly electronegative elements as either electrolytes or electrolyte additives. These organic compounds can react with zinc anodes and electrolytes to form zinc-based semiconductor materials, such as ZnS, ZnF_2, and ZnSe, while simultaneously generating organic layers. The generated zinc-based semiconductor material, functioning as an efficient Zn^{2+} conductor, facilitates the complete desolvation of hydrated Zn^{2+} ions, ensures a uniform Zn^{2+} flux, and promotes homogeneous zinc nucleation [164–165]. In addition, the accompanying organic/inorganic layer can isolate water molecules and reduce the generation of by-products [178]. For example, Meng et al. [206] developed a robust bilayer SEI by incorporating 1,3-dimethyl-2-imidazolidinone (DMI) as an electrolyte additive. In the construction process, DMI molecules undergo electrochemically induced redox reactions through electron-driven and proton transfer mechanisms, decomposing into dimethylamine and carbon dioxide. Subsequently, dimethylamine rapidly combines with H^+ and SO_4^{2-} in the solution to form $[C_4H_{14}N_2]SO_4$. Meanwhile, the decomposed CO_2 dissolves in the electrolyte and reacts with zinc ions to form $ZnCO_3$. At the same time, a small amount of SO_4^{2-} adsorbed on the surface of the zinc electrode undergoes reduction during both electron-driven and proton-driven processes, generating S^{2-}, which subsequently reacts with zinc ions to form ZnS (Figure 3a,b). The outer layer, enriched with crystalline $ZnCO_3$, enhances mechanical stability during repeated zinc plating and stripping processes, whereas the amorphous ZnS inner layer facilitates uniform zinc ion transport, leading to homogeneous and dense zinc deposition. Moreover, the $[C_4H_{14}N_2]SO_4$ present around the double-layer SEI exhibits high viscoelasticity and can accommodate substantial volume changes during the Zn electroplating and stripping processes, thus ensuring the mechanical stability of the SEI. Therefore, this synergistic bilayer SEI can regulate the uniform transport of zinc ions, thereby enabling uniform and dendrite-free zinc deposition (Figure 3c). It simultaneously ensures homogeneous Zn^{2+} transport and sustained mechanical stability, thus enhancing the zinc electrode's high utilization rate and Coulombic efficiency.

In a similar manner, Li et al. [171] developed a low-concentration aqueous electrolyte based on $Zn(OTF)_2$ and $Zn(NO_3)_2$, and successfully constructed a stable inorganic-organic hybrid SEI composed of ZnF_2, $Zn_5(CO_3)_2(OH)_6$, and an organism on the surface of the zinc metal anode through in-situ conversion technology (Figure 3d). Simply put, when zinc metal comes into contact with this mixed electrolyte, a dense in situ passivation layer of $Zn_5(OH)_8(NO_3)_2{\cdot}2H_2O$ forms on its surface. This layer not only prevents water molecules from coming into contact with the zinc surface but also possesses self-healing properties. Subsequently, this layer will gradually transform into a more stable $Zn_5(CO_3)_2(OH)_6$ phase, accompanied by the formation of an SEI film composed of an organic outer layer derived from $CF_3SO_3^-$ and NO_3^- reaction products, as well as a ZnF_2 inner layer. The highly flexible organic outer layer effectively prevents cracking of the SEI caused by volume changes during cycling, while facilitating the migration of solvated Zn^{2+}. The hydrophobic ZnF_2 inner layer further removes solvated water molecules, thereby suppressing water decomposition and inhibiting zinc dendrite formation by preventing direct contact between the zinc anode and electrolyte, while still permitting the transport of Zn^{2+}. Owing to this double-layer gradient structure, the assembled titanium-zinc battery achieves a Coulombic efficiency as high as 99.8% over 200 h. Zhu et al. [170] introduced sodium thioctate (ST) into the zinc sulfate electrolyte and constructed a stable bilayer electrolyte-electric double layer-electrode-electrolyte interface on zinc and manganese dioxide electrodes. During this process, ST anions are selectively adsorbed onto the surface of the zinc anode via electrostatic adsorption and electrochemical interactions, leading to the formation of a densely packed coating layer. Subsequently, the ST molecules adsorbed onto the electrode surface undergo in situ polymerization at the interface, resulting in the formation of a poly(zinc thioctate) (PZT) layer. At the same time, ST molecules partially decompose on the electrode surface, combine with Zn to form ZnS, and further hybridize with organic components to construct an inorganic-organic composite inner layer. Ultimately, SEI comprises an outer layer of PZT polymer and an inner layer of ZnS organic amorphous material, thereby forming a stable bilayer structure (Figure 3e). The outer PZT layer improves the mechanical stability of the SEI, whereas the inner ZnS layer effectively regulates Zn^{2+} ion flux, promoting uniform ion deposition and dissolution. This can be observed in the morphological evolution of zinc deposited from different electrolytes (Figure 3f). In addition, this bilayer structure significantly enhances the mechanical strength and chemical stability of the SEI, effectively suppressing electrode volume expansion and structural degradation during cycling. Moreover, the dynamic disulfide bonds in ST molecules possess the capacity to break and reform, thereby endowing the SEI with self-healing properties and enabling the repair of interfacial damage during prolonged cycling.

Moreover, researchers have found that in situ constructing a layer of water-insoluble zinc-based oxygen-containing acid salts (such as $ZnCO_3$ and $Zn(PO_3)_2$) on the surface of zinc anodes can also act as physical barriers, guiding the orderly deposition of zinc ions through graded confinement and thereby extending the cycle life. On the other hand, this layer regulates the Zn^{2+} flux through electrostatic interactions, reduces nucleation overpotential, and promotes smooth deposition [24, 207]. For example, Li et al. [172]. proposed a chelating-ligand additive strategy to construct an in situ inorganic/organic hybrid bilayer interface (Figure 3g). This process employs diethylenetriaminepenta (methylenephosphonic acid) sodium salt (DS) as an additive, and its $-PO_3$ functional group, which exhibits more negative adsorption energy (−3.52 electron volts), preferentially adsorbs onto the zinc surface, forming a cross-linked network through zinc-oxygen bonding. During the reduction process, DS anions with a lower lowest unoccupied molecular orbital energy of 0.34 eV decompose preferentially, forming an inorganic SEI layer enriched with $Zn(PO_3)_2$ near the zinc surface. At the same time, the carbon skeleton crosslinks and forms an organic layer on the surface of the SEI, resulting in the formation of an inorganic/organic hybrid SEI interface (Figure 3h). The $Zn(PO_3)_2$ inner layer effectively prevents direct contact between the zinc metal and active water molecules in the electrolyte, significantly suppressing corrosion reactions and HER, while simultaneously regulating the Zn^{2+} ion flux at the interface and promoting uniform zinc deposition. Moreover, its organic outer layer further prevents harmful substances in the electrolyte from corroding the zinc metal anode, while strong

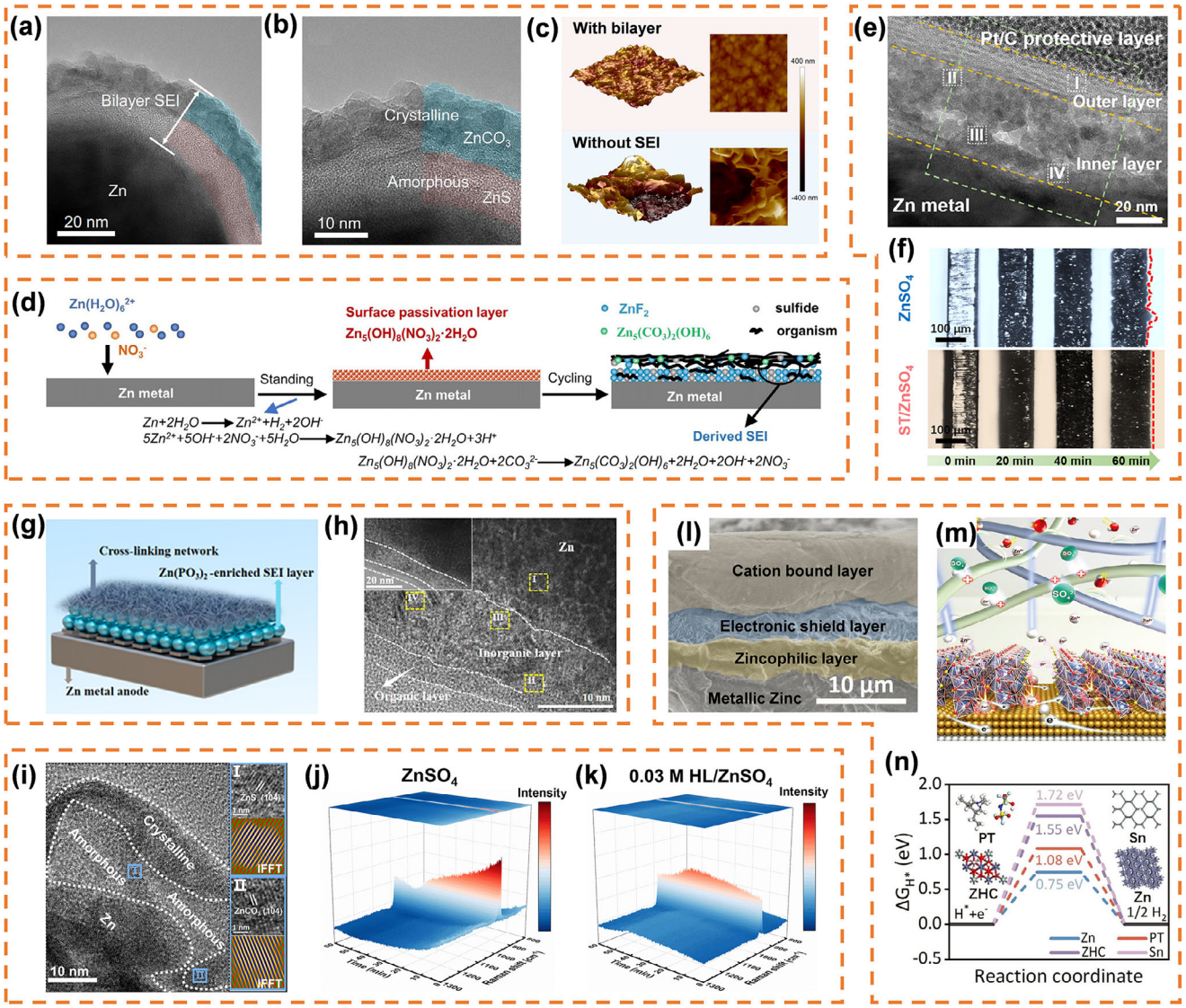

FIGURE 3 | (a,b) HRTEM images of bilayer SEI on the Zn surface in $ZnSO_4$-DMI electrolyte. (c) AFM images of Zn deposited on Cu foil with bilayer and without SEI [206]. Copyright 2024, Springer Nature. (d) Formation mechanism of ZnF_2-$Zn_5(CO_3)_2(OH)_6$-organic SEI [171]. Copyright 2021, Wiley-VCH. (e) FIB-TEM images of cycled Zn anode in ST/$ZnSO_4$ electrolyte. (f) Morphological evolution of Zn depositing in different electrolytes [170]. Copyright 2025, Wiley-VCH. (g) Schematic of the organic/inorganic hybrid SEI from the BE-DS electrolyte on the Zn anode. (h) SA-TEM images of the interphases on the Zn surface from the BE-DS electrolyte [172]. Copyright 2025, American Chemical Society. (i) HR-TEM images of the Zn anode surface in 0.03 M HL/$ZnSO_4$ electrolyte. (j-k) In situ Raman spectra of v-SO_4^{2-} band in different electrolytes [173]. Copyright 2025, Elsevier. (l) Cross-sectional SEM of PT-ZHC-Sn@Zn. (m) Hierarchical cascade modulation mechanism of Zn^{2+} deposition behavior on the PT-ZHC-Sn layer. (n) Gibbs free energy ΔGH* and adsorption configurations of an H atom on Zn, Sn, ZHC, and PT substrates [174]. Copyright 2024, Wiley-VCH.

adhesion among the organic layer, inorganic layer, and zinc metal matrix ensures the stability and durability of the SEI layer. Therefore, this symmetrical Zn||Zn battery exhibits a long cycling life exceeding 1700 h at a current density of 5 mA cm^{-2}. Moreover, the zinc-iodine battery retains 71.3% of its initial capacity after 1100 cycles.

Likewise, Sun et al. [173]. introduced L-carnitine (HL) as an electrolyte additive to form a dynamic organic-inorganic bilayer SEI, thereby enhancing the stability of the zinc anode. In a weakly acidic $ZnSO_4$ electrolyte, HL molecules tend to exist in both protonated (H_2L^+) and deprotonated (HL^-) forms. The protonated species (H_2L^+) selectively adsorbs onto the surface of the zinc anode, forming a novel organic protective layer with reduced water content. This layer effectively mitigates interfacial concentration polarization, homogenizes the Zn^{2+} ion flux, and suppresses dendrite formation. And H_2L^+ interacts with Zn^{2+} and other components in the electrolyte through its protonation, forming an amorphous organic inner layer. This inner layer is rich in C–N bonds and exhibits good flexibility. The autonomously released HL^- exhibits strong nucleophilic coordination with Zn^{2+}, disrupting the original solvation configuration and thereby lowering the desolvation energy of Zn^{2+}. Subsequently, HL^- undergoes decarboxylation to generate CO_2, which reacts with Zn^{2+} to construct a well-ordered $ZnCO_3$ crystalline layer on the outer surface of the SEI. This inorganic outer phase efficiently hinders the penetration of water molecules, mitigates HER and by-product formation, and concurrently enhances the mechanical

robustness and structural integrity of the SEI (Figure 3i). As shown in the in-situ Raman spectra presented in Figure 3j,k, the Raman signal intensity remains notably more stable in the 0.03 M HL/$ZnSO_4$ electrolyte compared to the pure $ZnSO_4$ electrolyte during the entire Zn^{2+} deposition process. This indicates that the incorporation of HL facilitates the formation of a bilayer dynamic SEI, which efficiently modulates the Zn^{2+} ion flux at the electrode/electrolyte interface, thus improving interfacial stability. Therefore, under the current density of 1 mA cm^{-2} and 1 mAh cm^{-2}, the cycle life of the Zn||Zn symmetric battery exceeds 5500 h.

There are also literature reports on using the reduction product of dimethyl carbonate to construct an outer protective layer to reduce the Hammett acidity of the electrolyte and minimize the side reactions between water molecules and the zinc anode. Constructing an inorganic inner protective layer mainly composed of Zn–Cl and Zn–O bonds to promote the rapid transport of Zn^{2+} and ensure the kinetic performance of electrochemical reactions [175]. Another work uses polyvinylidene fluoride trifluoroethylene chlorotrifluoroethylene copolymer as an ultra-thin amorphous outer layer, directly isolating the contact between the electrolyte and metallic zinc to reduce side reactions. The inner layer is rich in inorganic components such as ZnF_2, ZnS, ZnO, and $ZnCO_3$, forming gradient ion channels that promote uniform diffusion of Zn^{2+} and reduce local current density [182].

Another method is to add zincophilic metal salts (such as $SnCl_4$, $InCl_3$, and $CdCl_2$) to the electrolyte, which can generate zincophilic metal sites in situ on the surface of the zinc anode to regulate the uniform deposition of zinc ions and suppress parasitic HER. For example, Shao et al. [174] prepared a triple-gradient poly(diallyldimethylammonium) bis(trifluoromethanesulfonyl)imide (PDDA-TFSI)-$Zn_5(OH)_8Cl_2$-$\cdot H_2O$-Sn (PT-ZHC-Sn) artificial layer through in-situ self-reconstruction and solvent evaporation strategy (Figure 3l). Simply put, by coating PDDA-TFSI with an NMP solution of $SnCl_4$ on the surface of zinc metal, an in-situ reaction spontaneously occurs during vacuum drying: $SnCl_4$ reacts with Zn to form a bottom layer of metallic Sn layer, while Zn^{2+} and OH^-/Cl^- form an intermediate layer of ZHC nanosheets, and the outermost PT layer is formed by phase separation. Among them, the PT layer binds SO_4^{2-} ions through electrostatic interactions and facilitates the desolvation of Zn^{2+} ions. The ZHC layer functions as a rapid transport channel for Zn^{2+} ions, while simultaneously suppressing electrolyte decomposition and zinc nucleation at the interface. The metallic Sn layer provides abundant zinc nucleation sites, promoting the uniform deposition of Zn^{2+} ions (Figure 3m). Additionally, density functional theory calculations showed that the Gibbs free energy (ΔGH^*) values exhibited by PT, ZHC, and Sn during hydrogen adsorption were significantly higher than those of naked Zn, indicating that the PT-ZHC-Sn layer effectively suppressed the HER (Figure 3n). As a result, the PT-ZHC-Sn@Zn symmetric battery demonstrated an exceptionally long cycling stability, maintaining performance for more than 6500 h under a current density of 0.5 mA cm^{-2} and an area capacity of 0.5 mAh cm^{-2}. This lifespan is markedly superior to those of the ZHC-Sn@Zn electrode (approximately 1245 h) and the Sn@Zn electrode (around 980 h), and is nearly 46 times greater than that of the bare Zn electrode, which lasted about 255 h. Similarly, when SnI_4 is used as an electrolyte additive, it participates in a displacement reaction with the zinc metal during the electrochemical cycling process, resulting in the formation of a double-layer interface between the electrolyte and the zinc anode [184]. This interface consists of an Sn-based protective inner layer that is compatible with zinc, as well as an iodine-enriched adsorption outer layer. The zincophilicity of the Sn layer makes the diffusion energy barrier of Zn^{2+} on the Sn (200) crystal plane lower than that on the pure Zn (002) crystal plane, promoting uniform nucleation. The I^- ion rich adsorption layer repels SO_4^{2-} and reduces active H_2O contact, inhibiting the formation of $Zn_4SO_4(OH)_5\cdot H_2O$ by-products. The assembled symmetrical battery was cycled for 1660 h at 5 mA cm^{-2}/5 mAh cm^{-2}, with a cumulative galvanized capacity of 11.6 Ah cm^{-2}.

In conclusion, the in situ construction of dual- or multi-layer SEI layers using electrolytes or electrolyte additives has excellent interface compatibility and self-healing ability. The additive molecules preferentially reduce, decompose, or adsorb on the zinc anode surface under an electric field, forming an SEI interface layer that accommodates volume changes and morphological evolution during zinc deposition and dissolution. Microcracks in the interface layer during cycling can be dynamically repaired by continuous replenishment of free electrolyte additives. The interface layer is formed directly on the zinc surface via molecular-level reactions, enabling seamless atomic bonding without physical gaps. This results in a thin, uniform layer that minimizes interfacial ion transport resistance. However, SEI formation from additives during the first charge-discharge cycle is irreversible and consumes zinc ions and electrolyte permanently, reducing the battery's initial coulombic efficiency and causing capacity loss. For high-energy-density applications, this represents a drawback that must be carefully balanced.

3.4 | In Situ Fabricating A Multiscale Interface Layer Using Eutectic Electrolyte

In addition to using electrolyte additives, a dual- or multi-interface SEI layer can also be constructed through eutectic electrolytes. The eutectic electrolyte in AZIBs is a low eutectic system formed by specific salts (such as $ZnSO_4$ or $ZnCl_2$) and solvents (such as ethylene glycol, propylene glycol, and other polyols) [204]. Its core advantage lies in inhibiting dendrite growth, reducing side reactions, and improving interface stability by regulating the solvation structure of Zn^{2+} [208]. Moreover, during the electrochemical cycling process, the eutectic components at the zinc electrode interface undergo preferential reduction or decomposition and are in situ transformed into a stable SEI layer mainly composed of inorganic zinc salts such as ZnF_2 and ZnS. This SEI layer has good Zn^{2+} conductivity and can effectively prevent direct contact between water molecules and active zinc [209]. Compared with the strategy of electrolyte additives, the core advantage of using an eutectic electrolyte to construct multiscale interface layers is that it can spontaneously assemble a dense, uniform, and stable solid electrolyte interface facial mask on the zinc anode surface through strong coordination [210]. The interface layer maintains a dynamic equilibrium with the bulk electrolyte. Unlike systems that rely on sacrificial additives, this prevents the protective effect from diminishing over time, resulting in superior long-term cycling stability.

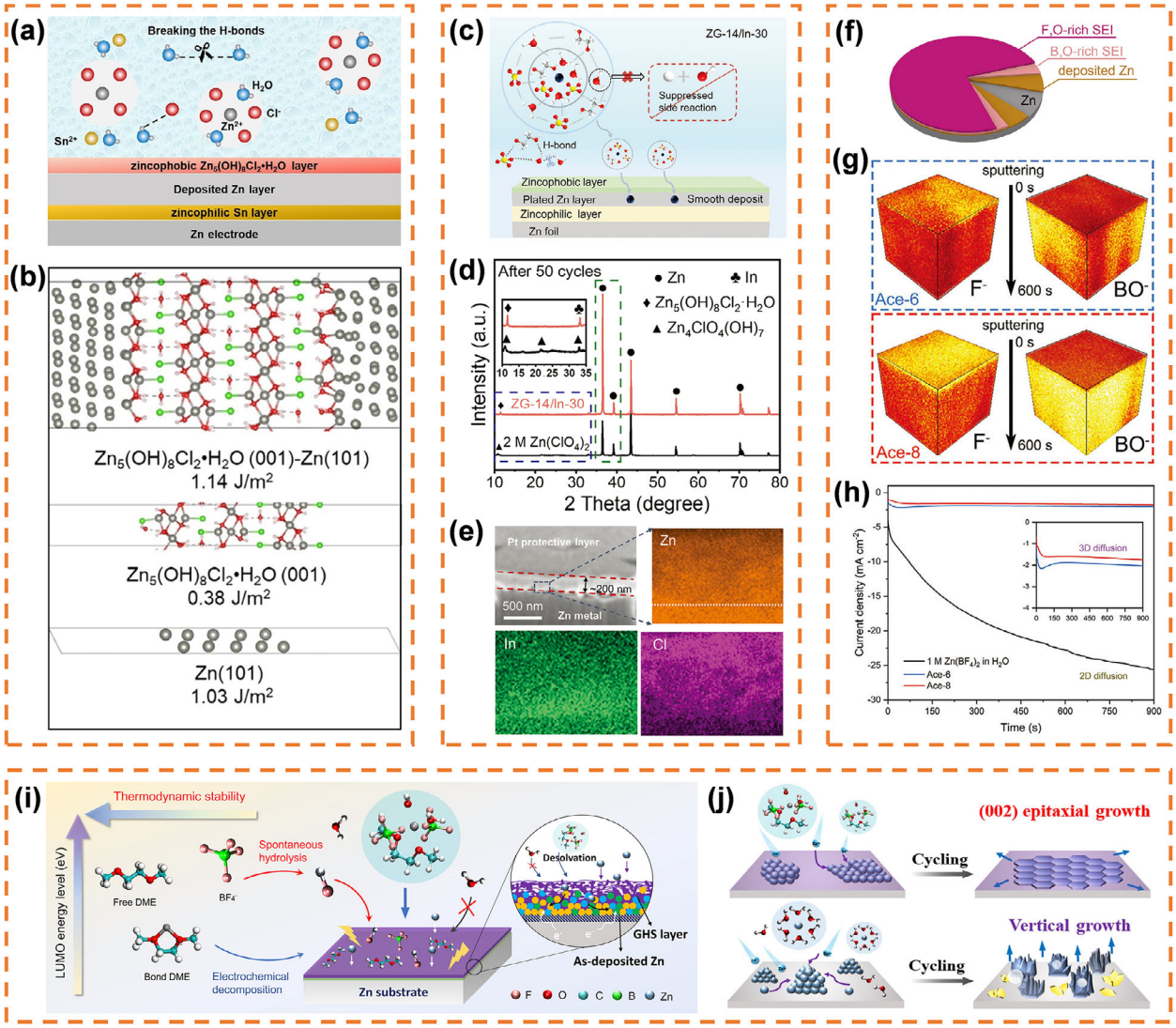

FIGURE 4 | (a) Scheme of $Sn/Zn_5(OH)_8Cl_2{\cdot}H_2O$ bilayer interface structure. (b) Atomic structures and related surface/interfacial energies of $Zn_5(OH)_8Cl_2{\cdot}H_2O$ surface, Zn surface, $Zn_5(OH)_8Cl_2{\cdot}H_2O(001)|Zn(101)$ interface [185]. Copyright 2021, Wiley-VCH. (c) Schematic illustrations depicting the Zn^{2+} solvation structure and electrochemical processes at the Zn/electrolyte interface within a hybrid hydrated eutectic electrolyte system. (d) XRD profiles of Zn anodes following cycling in 2 M $Zn(ClO_4)_2$ and the ZG-14/In-30 hydrated eutectic electrolyte. (e) Scanning electron microscopy image of the cycled zinc electrode obtained via focused ion beam, along with the associated elemental mapping [186]. Copyright 2024, Wiley-VCH. (f) Schematic representation of the interfacial characteristics within a hydrated eutectic electrolyte system. (g) 3D ToF-SIMS imaging of F^- and BO^- species on the surface of Zn electrodes after cycling in Ace-6 and Ace-8 electrolytes. (h) CA profiles of the Zn electrode in aqueous and selected eutectic electrolytes [187]. Copyright 2024, Wiley-VCH. (i) Schematic of the in-situ generated gradient organic/inorganic hybrid solid-electrolyte interphase. (j) Schematic diagrams of the Zn deposition behavior in the ZBFD electrolyte (above) and the ZnSO4 electrolyte (below) [190]. Copyright 2023, Royal Society of Chemistry.

For example, Cao et al. [185] introduced a eutectic electrolyte composed of $SnCl_2$ and $ZnCl_2$, and in situ formed a zincophilic/zincophobic bilayer interface ($Sn/Zn_5(OH)_8Cl_2{\cdot}H_2O$) on the surface of the zinc anode (Figure 4a). During construction, metallic Sn preferentially deposits on the current collector due to its higher reduction potential (0.62 V vs. Zn/Zn^{2+}) compared to Zn^{2+}. The deposited Sn is zincophilic, which reduces the overpotential of Zn deposition, promotes uniform Zn deposition, and suppresses side reactions due to its high hydrogen evolution overpotential. Based on the Sn layer, Zn^{2+} reacts with OH^-/Cl^- in the electrolyte to form a $Zn_5(OH)_8Cl_2{\cdot}H_2O$ layer. DFT calculations indicate that the surface energy of the $Zn_5(OH)_8Cl_2{\cdot}H_2O$ layer is 1.03 J m^{-2}, which is significantly higher than that of Zn (0.38 J m^{-2}), demonstrating strong zincophobicity (Figure 4b). Therefore, Zn^{2+} will deposit between the two SEI interfaces, and the $Zn_5(OH)_8Cl_2{\cdot}H_2O$ layer effectively inhibits the penetration of Zn dendrites through physical barriers and reduces interface energy. In addition, the hydrophobicity of $Zn_5(OH)_8Cl_2{\cdot}H_2O$ electrolyte interface facial mask further inhibits HER. Experiments have shown that Zn||Zn symmetric batteries can stably cycle for 500 h at 3 mA/cm^2.

In the same way, Wan et al. [186] formed a zincophobic/zincophilic bilayer interphase through in-situ dissociation-reduction of a hydrated eutectic electrolyte consisting of $Zn(ClO_4)_2{\cdot}6H_2O$, ethylene glycol (EG), and $InCl_3$ on the

surface of a zinc anode (Figure 4c). The top of the bilayer interphase is composed of the dissociation-reduction products of eutectic molecules ($Zn(ClO_4)_2{\cdot}6H_2O$ and EG), including organic components (C–Cl components) and inorganic components ($Zn_5(OH)_8Cl_2{\cdot}H_2O$ and $ZnCO_3$) (Figure 4d). On the one hand, this zincophobic layer inhibits side reactions by blocking direct contact between active water and the zinc anode. On the other hand, its organic-inorganic hybrid structure enhances the mechanical stability of the SEI interphase. The bottom of the bilayer interphase is a metal indium layer formed by the spontaneous displacement reaction of $InCl_3$ in the electrolyte and attached to the surface of the zinc anode (Figure 4e). This zincophilic layer exhibits a low zinc nucleation energy barrier, thereby facilitating the preferential deposition of (002) crystal planes and effectively suppressing dendrite formation. Combining the limiting effect of liquid eutectic network on H_2O molecules, the assembled Zn||Zn symmetric battery can cycle 3000 times at a current of 1 mA cm^{-2}, the cycle life can be extended to 2500 h at 50°C and 800 h at –50°C.

Adding organic compounds to eutectic electrolytes can spontaneously construct a dense and flexible organic-inorganic composite SEI film on the surface of zinc, effectively inhibiting dendrite growth. For example, Wang et al. [187]. developed a gradient-structured and robust solid gradient SEI, consisting of B, O-inner layers and F, O-exterior layers, for achieving uniform and reversible deposition of zinc (Figure 4f,g). This structure is in situ formed through a hydrated eutectic electrolyte system composed of zinc tetrafluoroborate ($Zn(BF_4)_2$) and acetamide. Specifically, BF_4^- is confined to the solvation sheath of Zn^{2+} in eutectic electrolytes, inhibiting its hydrolysis to HF and generating boron-containing oxides through electrochemical reduction reactions. The inner layer, rich in boron and oxygen, has high zinc ion permeability, enabling uniform lateral diffusion and preventing local accumulation (Figure 4h). The outer layer is coordinated by the C = O of acetamide and Zn^{2+}, and decomposes during electrodeposition to form an organic-inorganic hybrid interface enriched with F/O species. The high mechanical strength of ZnF_2 inhibits dendritic puncture, while organic components enhance interfacial flexibility. The assembled Zn||Zn symmetric battery was cycled for 4400 h at 0.5 mA cm^{-2}, and the Zn||PANI full battery maintained a capacity of 73.2% after 4000 cycles.

Similarly, Meng et al. [190] used a eutectic electrolyte (ZBFD) composed of BF_4^- and dimethyl ether (DME) to form a gradient organic/inorganic hybrid SEI layer on the surface of the zinc anode through in-situ chemical reconstruction. The ZnF_2 produced by BF_4^- hydrolysis accumulates near the zinc metal interface, while the decomposition products of DME, like hydrocarbons and carbon oxides, gradually decrease in the outer layer, forming an organic-to-inorganic compositional gradient (Figure 4i). The inner ZnF_2 layer prevents H_2O molecules from contacting the zinc anode, greatly reducing hydrogen evolution. It also improves Zn^{2+} diffusion at the interface, promoting epitaxial growth along the low-energy (002) crystal plane (Figure 4j). The flexible organic components in the outer layer alleviate the stress during the zinc deposition/stripping process, preventing the SEI layer from cracking. And the organic layer guides the uniform diffusion of Zn^{2+} through gradient component distribution, avoiding dendrites caused by excessive local concentration. The synergistic effect of the inner and outer layers achieves a "balance of rigidity and flexibility" interface stability, resulting in a lifespan of 2200 h at 5 mA cm^{-2} for Zn||Zn symmetric batteries, and no capacity degradation for Zn||V_2O_5 full battery after 22 000 cycles.

Overall, the key to constructing multiple interfacial layers using eutectic electrolytes is to achieve precise control of their "bottom-up" assembly process. It is necessary to ensure strong and stable chemical anchoring between the eutectic components and the zinc substrate, rather than physical adsorption, to ensure the structural integrity of the interfacial layer during cycling. In addition, the thickness and density of the interface layer need to reach an optimal balance. Excessive thickness will increase ion migration resistance, while excessive thickness may lead to insufficient protection.

3.5 | In-Situ Fabricating Multiple Molecular Layers With the Electrolyte Additive

Although in-situ or ex-situ fabrication of multiscale interface artificial SEI layers on the surface of zinc metal anodes offers notable advantages over single-interface artificial SEI layers, these artificial SEI layers still face certain limitations, including limited flexibility, low ionic conductivity, and potential environmental toxicity [44]. And the thickness of these coatings is usually over tens of micrometers, which reduces the energy density of the battery and hinders its further commercialization [24]. More importantly, the diffusion of zinc ions across the interface layer involves overcoming a certain energy barrier, thereby necessitating precise control of the layer thickness to minimize the diffusion path as much as possible [195]. In contrast, developing complex and robust biomolecular artificial interface layers through molecular-level chemical design holds significant research value. During the construction process, the functional molecules (such as amphiphilic molecules, biomolecules, or silane coupling agents) are usually firmly anchored to the zinc substrate through strong terminal chemical interactions (such as Zn–S, Zn–N covalent bonds or coordination bonds, electrostatic adsorption, etc.) to form the first layer of adsorption [211]. On this basis, through intermolecular hydrogen bonds, hydrophobic interactions, π–π stacking, or electrostatic interactions, the molecules are further guided to self-assemble in an ordered manner in the vertical or horizontal direction, thereby constructing multi-layer interfaces with clear chemical gradients and structural orientations [212]. These multi-molecular layers can effectively inhibit dendrite formation by regulating the migration pathway of zinc ions or guiding the preferred deposition of Zn (002) crystal planes [213]. From the perspective of construction principles, multi molecular layer artificial interfaces can be divided into the following three typical strategies, whose core lies in achieving ordered assembly and functional integration of interface structures through precise and controllable intermolecular interactions: (1) By utilizing a single amphiphilic molecule and relying on its different affinities with zinc metal/electrolyte, it spontaneously arranges vertically at the interface to form a functionally distinct bilayer structure. (2) By enhancing the interactions between the head or tail groups of molecules (such as hydrogen bonds), amphiphilic molecules can self-assemble in a "head-to-head" or "tail-to-tail" manner, forming a sandwich multilayer interface with a denser structure and higher mechanical strength. (3) Assemble two or more molecules with complementary functions through intermolecular forces

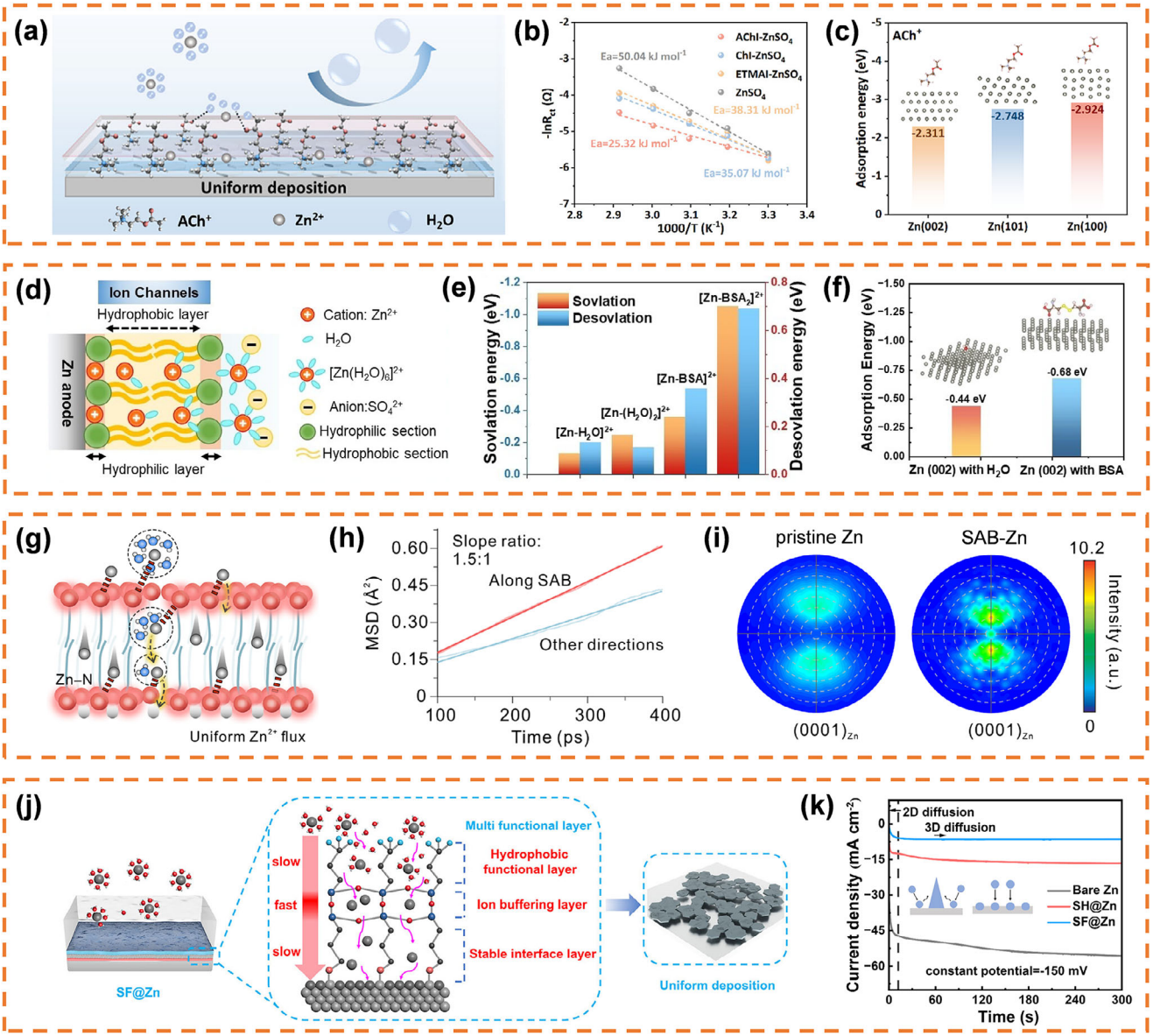

FIGURE 5 | (a) The schematic illustrations of the optimization mechanism of ACh^+ on the Zn surface. (b) Arrhenius curves of activation energies with different electrolytes. (c) Adsorption energy of ACh^+ on different crystal planes of Zn anode [191]. Copyright 2025, Wiley-VCH. (d) Cross-sectional schematic diagram of multifunctional BSA bilayer. (e) Solvation energy and desolvation energy of Zn^{2+} with H_2O and BSA molecules. (f) Comparison of adsorption energies of BSA and H_2O toward the Zn (002) plane [192]. Copyright 2024, Wiley-VCH. (g) Schematic representation of the proposed molecular mechanism of SAB enabling concurrent in-plane Zn/Zn^{2+} transport and electrochemical reaction. (h) MSD of Zn^{2+} ions along the SAB direction compared to other orientations derived from CMD simulations. (i) (0001) Zn pole figures for both bare Zn and SAB-Zn anodes following the initial charge-discharge cycle [193]. Copyright 2021, Wiley-VCH. (j) Schematic illustrations of Zn^{2+} diffusive deposition on SF@Zn anode. (k) *I–t* curves of different anodes [194]. Copyright 2024, American Association for the Advancement of Science.

like a "puzzle" to construct a composite interface layer that can simultaneously meet multiple requirements, such as strong anchoring and fast conduction.

For the first method, Li et al. [191] used the amphiphilic acetylcholine cation (Ach^+) as an interface modifier, and its asymmetric electrostatic potential distribution caused it to preferentially adsorb vertically on the surface of the zinc anode, forming a hydrophobic-hydrophilic gradient interface structure (Figure 5a). The hydrophobic groups ($-N^+(CH_3)_3$) in the inner layer are positioned near the zinc surface, minimizing H_2O molecule contact and forming a water-poor electric double layer (EDL) structure that reduces direct interaction between zinc and the electrolyte, thereby suppressing side reactions. The hydrophilic groups (—C═O or —OH) on the outer layer extend outward, disrupting the existing hydrogen bonding network between water molecules, reducing water activity, and the energy barrier for Zn^{2+} desolvation. This is evident in the $AChI\text{-}ZnSO_4$ electrolyte, which has the lowest activation energy (Figure 5b). In addition, Ach^+ selectively adsorbs onto the Zn (100)/(101) crystal plane, exposing the (002) crystal plane (Figure 5c). This guides Zn^{2+} deposition along the low-energy plane and suppresses dendrite formation. When coupled with an I_2 cathode, Ach^+ fixes I^{3-}/I^{5-} through electrostatic action, suppressing the iodine shuttle effect and

improving the cycling stability of zinc iodine batteries. Therefore, the zinc anode with optimized double-layer structure operates stably for over 3700 h at 1.0 mA cm^{-2}/1.0 mAh cm^{-2}, and for over 1500 h at a high-current density of 10 mA cm^{-2}/1.0 mAh cm^{-2}.

In contrast, a cross-linked network is formed through strong interactions between molecular heads or tails for lateral connections. This makes the interface layer more like a solid "thin film" rather than a simple stacking of single molecular layers, which can more effectively suppress the piercing of zinc dendrites and provide better interface shielding. And the tight arrangement between molecules can form ion channels with a more uniform size and clearer pathways. This highly ordered structure is conducive to more precise regulation of the migration kinetics of zinc ions, such as achieving a more uniform ion flow, thereby guiding the flat deposition of zinc. For example, Lu et al. [192] regulated zinc ion migration and facilitated their desolvation process by employing the self-assembly of bovine serum albumin (BSA) on a zinc metal anode to construct a bilayer architecture. The bilayer structure is formed by dynamic self-assembly of hydrophilic and hydrophobic fragments in BSA molecules, with hydrophilic chains facing outward and hydrophobic chains facing inward, forming a multifunctional interface layer with a "hydrophilic hydrophobic hydrophilic" sandwich structure (Figure 5d). The cysteine in the hydrophilic outer layer contains a large number of S–S bonds that can replace H_2O molecules in the solvation structure of Zn^{2+} ions, reducing the number and activity of H_2O molecules near the Zn anode surface. The hydrophobic inner layer prevents the invasion of solvated water molecules, thereby promoting the desolvation of $[Zn(H_2O)_6]^{2+}$ and reducing the direct contact between water molecules and the zinc anode. And the reduction of solvation energy provides more favorable conditions for the rapid and reversible insertion and extraction of Zn^{2+} ions through SEI (Figure 5e). Moreover, the high adsorption energy of BSA on the Zn (002) crystal plane further promotes the preferential deposition of Zn along the (002) orientation, effectively inhibiting the growth of Zn anode dendrites (Figure 5f). The assembled Zn||Zn symmetric cell exhibited stable cycling performance over 2400 h at a current density of 10 mA cm^{-2}. In contrast, the SH@Zn anode grafted with only a single layer of KH590 was cycled for merely 3000 h at the same cycling condition.

The core advantage of the third "multi-component functional assembly" method compared to the first two is the customizability of functional integration and performance. It overcomes the constraints of a single molecular structure, enabling specialized functional division and synergistic enhancement of efficiency. By carefully selecting and organizing different functional molecules, it is expected to construct a truly intelligent and robust artificial interface layer, thereby comprehensively improving the performance of zinc metal anodes. Inspired by the natural cell membranes conformation, Chen et al. [193] developed a lipopeptide molecule (C14-RWW-NH_2) with a supramolecular bilayer (SAB) structure formed by self-assembly of hydrophobic fatty chains (C_{14}) and arginine (R)–tryptophan dimer (WW) through noncovalent forces. This structure consists of two external peptide layers and a staggered alkyl chain in the middle, arranged in an upright array. On the zinc surface and electrolyte side, external peptide layers with high zincophilicity are arranged in a vertically ordered manner, achieving extensive and rapid Zn^{2+} transport, while the hydrophobic interior serves as a directional channel, allowing Zn^{2+} to dissolve and pass through the bilayer interface with a uniform ion flow (Figure 5g). From the molecular diffusion spectrum (MSD), it can be seen that the diffusion coefficient of Zn^{2+} ions in the SAB crystal array is larger than that in other directions, which proves the existence of directional transport properties (Figure 5h). In addition, the indole ring of tryptophan and the amino terminal (C–terminal–NH_2) of arginine form Zn–N bonds with the zinc surface through coordination. Under the electric field, the in-plane Zn–N bond further promotes the synchronous transport and redox reaction of Zn/Zn^{2+}, leading to the growth of the planar Zn (0001) crystal plane (Figure 5i).

Along the same lines, Yan et al. [194] developed a bilayer silane film (SF) with hydrophobicity, ion buffering, and strong interfacial adhesion by precisely assembling silane coupling agents. This process is developed through a two-step molecular assembly approach utilizing two distinct surfactant molecules: (3-mercaptopropyl)trimethoxysilane (KH590) and (3,3,3-trifluoropropyl)trimethoxysilane (TFPS). Simply put, the —SH group of KH590 covalently binds to the zinc surface through Zn–S, forming a monolayer modified SH@Zn. Subsequently, TFPS was hydrolyzed and condensed onto the KH590 layer to form a second layer, constructing a bilayer structure with a thickness of only 6 nm. The structure consists of a hydrophobic functional layer, an ion buffer layer, and a stable interface layer from top to bottom (Figure 5j). The —CF_3 group in the hydrophobic functional layer promotes dehydration of $[Zn(H_2O)_6]^{2+}$ and prevents H_2O from contacting the zinc anode. The ion buffer layer alleviates concentration polarization by adjusting the migration rate of Zn^{2+}. The stable interface layer ensures the firm adhesion of the solid fluorine layer through Zn–S bonds. The chronoamperometry (CA) results show that SF@Zn has a much shorter 2D diffusion time, indicating that the SF layer effectively guides uniform Zn^{2+} deposition and nucleation (Figure 5k). Thus, the SF@Zn anode demonstrates exceptional reversibility, achieving 4300 h of cycling at 1 mA cm^{-2} and 1230 h at 10 mA cm^{-2}. In contrast, the SH@Zn anode grafted with only a single layer of KH590 was cycled for merely 3000 h at the same cycling condition.

In conclusion, the core principle of constructing protective layers at the molecular scale is to move from physical mixing to chemical directional assembly and achieve customized optimization of interface performance through precise control of molecular arrangement. To successfully achieve and leverage its advantages, on the one hand, functional molecules must be stably anchored to the zinc substrate through strong chemical bonds to resist delamination during cycling. On the other hand, the molecular structure needs to be carefully designed to form a dense and uniform defect-free coverage to prevent dendrite initiation, while also incorporating efficient ion transport channels to ensure that zinc ions can quickly pass through instead of forming insulating barriers. To enhance the interface selectivity and functional compatibility of the molecular layer, another feasible strategy is to structurally integrate and functionally coordinate the constructed SEI layer with the self-assembled molecular layer. This "SEI-molecular layer" composite interface not only possesses chemical stability and structural orderliness, but also can optimize the ion transport and reaction microenvironment at the SEI-electrolyte interface through the dynamic adjustment of the molecular

layer. Thus, it enhances the uniformity of zinc deposition while improving the environmental adaptability and long-cycle stability of the interface. Lastly, the cost and environmental friendliness of the selected molecules are also practical considerations that cannot be ignored in the transition from laboratory to commercial applications.

4 | Multiscale Interface Construction Technologies in Zinc Powder Anode

As mentioned above, zinc foil electrodes remain the mainstream system in the research of aqueous zinc-ion battery anodes due to their advantages such as strong modifiability, high energy density, and low cost. However, the fatigue characteristics of metallic zinc itself limit its application in flexible devices, while its relatively low depth of discharge also constrains the improvement of actual energy efficiency. In comparison, zinc powder (ZnP) anodes possess unique advantages such as controllable active material usage, high discharge depth, excellent spatial adaptability, and structural designability, making them particularly suitable for large-scale production and flexible energy storage applications [214–216]. Specifically, the high specific surface area of ZnP can accelerate ion transport and electrochemical reactions, enabling the storage of more charges per unit volume, achieving higher energy density and longer cycle life [217]. Moreover, the particle characteristics of zinc powder allow easy integration into battery cells of various shapes and sizes, making it ideal for space-constrained applications [218]. However, there are also many problems with using zinc powder as an anode material for AZIBs: (1) Similar to zinc foil, uneven zinc deposition and dissolution during charge-discharge cycles cause dendrite formation. As the dissolution process proceeds, the original spherical morphology of ZnP is gradually compromised, and during subsequent electrodeposition, zinc ions preferentially accumulate at localized regions known as "hotspots", promoting dendritic growth [219]. These dendrites will grow into large dendritic clusters on their own, penetrate the separator, and ultimately lead to battery failure. (2) The extended ion migration pathway in ZnP may result in localized over-deposition of zinc, thereby accelerating performance degradation. (3) The high specific surface area and manufacturing defects of ZnP increase its susceptibility to HER, leading to catalytic corrosion, loss of active materials, and formation of non-uniform passivation layers that worsen the "tip effect" and dendrite growth [220]. Clearly, a single surface modification strategy can no longer comprehensively address these issues, necessitating systematic, multiscale interfacial regulation strategies.

The multiscale interfacial regulation strategies aim to start from guiding the migration and deposition behavior of zinc ions, simultaneously enhancing the microstructure stability of zinc powder electrodes, the uniformity of electrochemical reactions, and the overall integrity of macroscopic electrodes, thereby overcoming their inherent bottlenecks such as high contact resistance, large volume changes, and intense side reactions. The constructed interface layer not only needs to have basic functions such as anti-corrosion and dendrite inhibition, but also should possess characteristics like guiding the directional deposition of zinc ions, high ionic conductivity, and good mechanical strength, to ensure the controllability of zinc deposition positions and adapt to volume changes during the cycling process. For example, Zheng et al. developed a novel biomimetic quasi-skin-capillary ZnP anode, whose dual-interface protective layer consists of an outer interface of aramid nanofibers (ANF) and an inner interface interwoven with ANF and acetylene black (AB) (Figure 6a) [221]. The inner interface is formed by electrostatic self-assembly of negatively charged ANF and positively charged ZnP. During the interweaving process, AB is coated on the surface of ZnP to form a conductive network, ensuring the continuity of the ion-electron transport network. The ANF outer interface serves dual functions of ion redistribution and electron barrier formation, effectively homogenizing the Zn^{2+} ion flux and preventing direct contact between water and the ZnP anode. Moreover, the capillary-shaped ANF adhesive extends inward to firmly anchor the approximate unit of ZnP, offering high selectivity for Zn^{2+} and thereby enhancing the efficiency of Zn^{2+} plating and stripping (Figure 6b). From the COMSOL Multiphysics simulation results, it is evident that the designed biomimetic quasi-skin capillary full-chain ZnP-FC can further homogenize the surface electric field and Zn^{2+} ion flux, thereby promoting uniform zinc deposition (Figure 6c). Owing to the synergistic effect between the inner and outer layers, the ZnP-FC||ZnP-FC symmetric battery is capable of continuous operation for 1650 h under a current density of 5 mA cm^{-2}.

Analogously, a three-layer golf-type anode with high conductivity was developed by Hu et al. to enhance the Gibbs free energy and mitigate the volume change of the anode [222]. The process first carbonizes zinc citrate microspheres and removes zinc oxide to create carbon microspheres with an egg yolk-shell structure. Then, a powder carburizing method is used to embed zinc powder into the yolk-shell structure at high temperatures, forming composite zinc-carbon powder (ZCP). Then, a small amount of metallic Bi nanosheets was deposited on the surface of ZCP via liquid-phase reduction, forming a bismuth layer (Figure 6d). The inner carbon layer enhances the conductivity and specific surface area of the anode, and facilitates electron transfer while optimizing the surface electric field distribution through its continuous carbon network structure. The outer metallic Bi layer provides superconductivity, enhances the binding energy with zinc ions, suppresses HER, promotes uniform deposition of zinc ions, and reduces dendrite formation. Owing to the synergistic interaction between the carbon and bismuth layers, the gradient architecture significantly enhances Gibbs free energy while minimizing volumetric fluctuations in the anode, thereby enabling stable zinc-manganese electrochemical cycling. Therefore, the ZCBP//Ti battery manufactured has an average CE of 98.62% in 1400 cycles (Figure 6e), and the ZCBP symmetric battery has a cycle life of up to 5000 h (Figure 6f).

Dimethyl diallyl ammonium chloride (DMDAAC), a cationic surfactant characterized by high charge density, enables it to readily copolymerize with diverse unsaturated monomers and possesses inherent adhesive capabilities. In a research by Tang et al. [223], DMDAAC was employed as a multifunctional additive in the construction of a ZnP anode, where it was copolymerized with $Ti_3C_2T_x$ MXene to form a composite powder anode (DDA-MXene@Zn-p) with improved cycling performance. The incorporation of DMDAAC introduces a positive surface charge on ZnP particles, strengthening the electrostatic interaction between ZnP and $Ti_3C_2T_x$ MXene (Figure 6g). Moreover, by tuning the

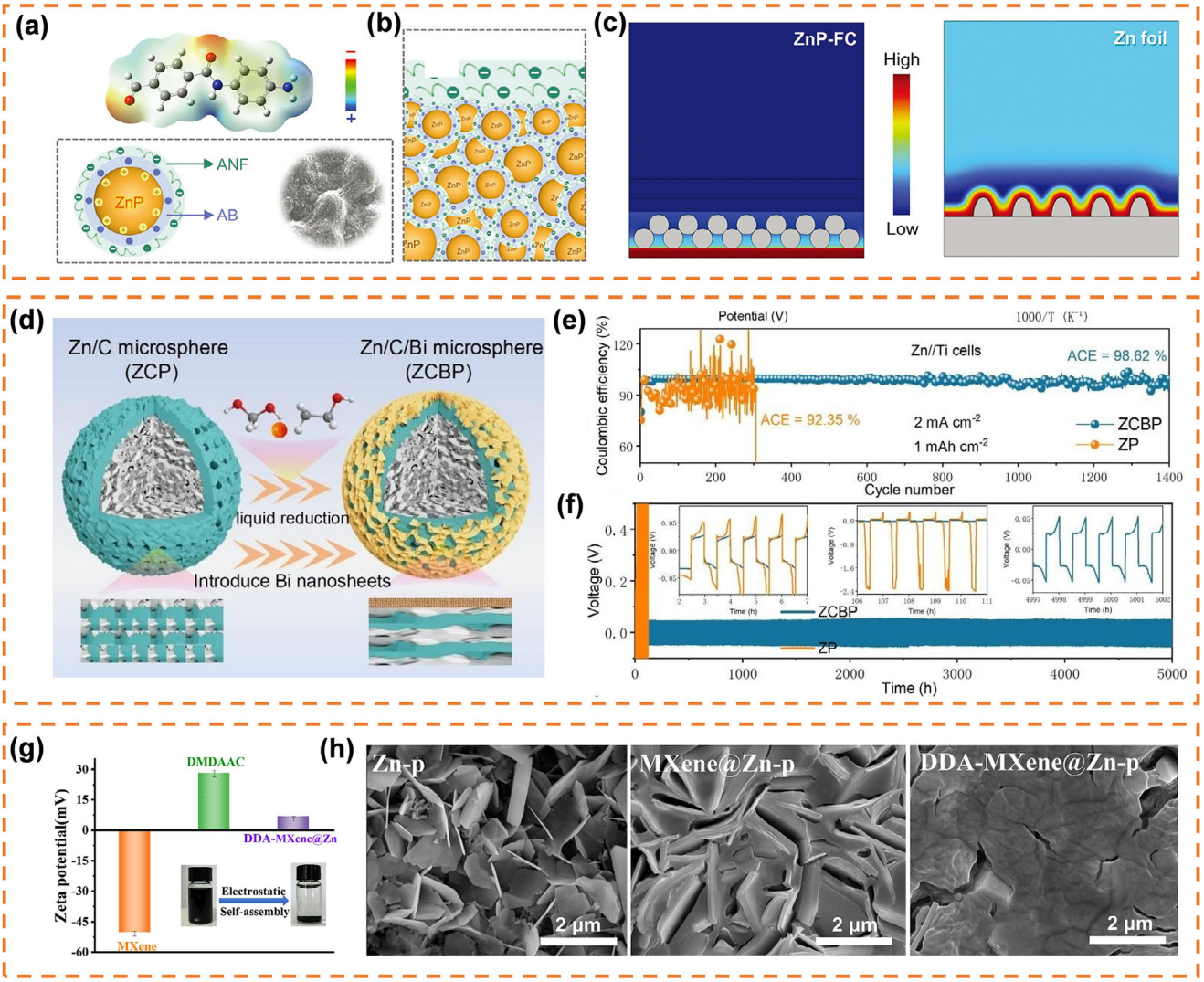

FIGURE 6 | (a) ESP of ANF unit. (b) Schematic assembly structure and corresponding SEM image of ZnP-ANF. (c) Schematic structure of ZnP-FC [221]. Copyright 2025, Wiley-VCH. (d) Schematic diagram of the construction of the outermost Bi layer in ZCBP. (e) CE plots of ZP//Ti and ZCBP//Ti cells at 2 mA cm^{-2} and 1 mAh cm^{-2}. (f) Galvanostatic charge/discharge cycling voltage profiles of ZP//ZP and ZCBP//ZCBP cells at 1 mA cm^{-2}/0.5 mAh cm^{-2} [222]. Copyright 2025, Wiley-VCH. (g) Zeta potential comparison of MXene, DDA, and DDA-MXene@Zn-p. (h) SEM images of the surface of Zn-p, MXene@Zn-p, and DDA-MXene@Zn-p after 50 cycles [223]. Copyright 2025, Elsevier.

interfacial surface tension, DMDAAC facilitates the formation of a hydrophobic layer within the composite anode, which effectively inhibits zinc dendrite formation and mitigates parasitic side reactions. The external $Ti_3C_2T_x$ MXene layer exhibits excellent electrical conductivity, which facilitates rapid electron transfer within the anode and reduces internal resistance. Moreover, the abundant surface functional groups (such as –OH, –O, and –F) on the $Ti_3C_2T_x$ MXene layer can selectively bind with ions in the electrolyte, thereby enhancing the transport behavior of both ions and electrons. Therefore, the synthesized ZnP composite anode effectively suppresses dendrite formation and mitigates corrosion, thereby achieving enhanced interfacial stability over extended periods. As shown in the SEM image of Figure 6h, the DDA-MXene@Zn-p electrode retains a relatively smooth surface without dendritic formation after cycling. The symmetric cell based on DDA-MXene@Zn-p demonstrates lower nucleation overpotentials and maintains stable cycling performance for over 300 h at a current density of 1 mA cm^{-2} and 1 mAh cm^{-2}, whereas the Zn-p and MXene@Zn-p cells fail due to polarization after 33 and 67 h, respectively. These observations and tests suggest that the zinc deposition/stripping process in the ZnP composite electrodes is highly reversible.

Overall, the core advantage of constructing a multi-layer protective coating on ZnP over a single layer is that it offers more comprehensive and stable three-dimensional protection for high surface area active materials. By ensuring uniform zinc ion deposition on each ZnP surface through the inner layer design, the dense middle layer effectively suppresses dendrite growth and side reactions, while the outer layer withstands electrolyte erosion and cyclic stress, collectively enhancing the composite anode's cycle life and coulombic efficiency. However, special attention should be paid to the uniformity and integrity of the multi-layer coating process on the micro/nano scale ZnP to avoid defects caused by uneven coating or particle aggregation. At the same time, it is essential to precisely control the thickness of

each layer to prevent excessive accumulation within the overall package, as this would significantly reduce the volumetric energy density of the anode. Additionally, a robust interlayer bond must be ensured to prevent delamination from the ZnP surface during volume changes associated with charge and discharge cycles.

5 | Multiscale Interface Construction Technologies in Zinc Host Anode

Although constructing multiple protective layers on the surface of ZnP significantly enhances its electrochemical performance and offers greater flexibility in electrode design, it remains undeniable that most ZnP anodes still face challenges in achieving high DOD. For example, first-principles calculations show that the adsorption energy of carbon for Zn^{2+} (E_{ads} = −4.83 eV) is slightly higher than that of metallic zinc (E_{ads} = −4.62 eV), indicating stronger zincophilicity [222]. The experimental results indicate that complete spatial confinement regeneration is difficult after zinc metal dissolves outside the carbon coating, and this irreversible effect worsens with more cycles (>500) and deeper discharge (DOD > 80%) [224]. More importantly, this results in the loss of internal physical support for the protective layer originally coating the surface, ultimately causing structural collapse, delamination, and functional failure [218].

In contrast, pre-constructing a mechanically robust deposition space can fundamentally address this issue by providing a stable, independent host framework [225]. The difference lies in that zinc host electrodes pre-construct a three-dimensional conductive skeleton as the deposition space for zinc, and then load zinc metal through methods such as electroplating or melt infiltration. This hollow host structure maintains structural integrity regardless of zinc deposition and dissolution cycles, offering continuous spatial confinement and mechanical support, ensuring electrode stability even under deep discharge and long-term cycling. However, a simple hollow structure cannot spontaneously guide zinc ions to deposit preferentially in its inner cavity, which may lead to the failure of the "confinement effect" over time. Therefore, multiscale interfacial regulation strategies should be employed to differentially and functionally modify the inner and outer surfaces of the hollow structure in a coordinated manner, achieving a synergistic enhancement effect through "internal and external repair". Specifically, its inner interface can be designed as a zincophilicity or interface with specific crystal plane orientation to guide zinc ions to preferentially nucleate uniformly, achieving precise localized deposition [226]. And its outer interface can be modified as a strongly hydrophobic or chemically inert interface, effectively isolating water molecules in the electrolyte from contacting the active substance, thereby synergistically inhibiting dendrite growth and side reactions, ultimately constructing an almost ideal zinc deposition microenvironment. The key to constructing this zinc host anode lies in ensuring the structural robustness of the skeleton and the rational functionalization of both inner and outer surfaces.

The application of electrospinning technology to fabricate carbon skeletons with hollow architectures has been extensively explored in the field of energy storage, demonstrating significant potential for use as zinc host anodes [227]. For example, Xue et al. [228]. developed a 3D porous hollow fiber scaffold incorporating well-dispersed TiO_2, SiO_2, and carbon, serving as a highly zincophilic host material for zinc anodes. This method involves electrospinning a mixed solution of polyvinylpyrrolidone (PVP) containing tetrabutyl titanate (TNB) and tetraethyl orthosilicate (TEOS), leading to phase separation, followed by hydrolysis and condensation reactions between TEOS and TNB, forming a 3D fiber-based framework consisting of cross-linked SiO_2 and TiO_2. During the carbonization process, hollow porous fibers with zincophilic substances are formed in the core layer, while a nitrogen-doped carbon layer develops due to the Kirkendall effect. The inner SiO_2 layer can effectively suppress the HER and markedly reduce the dissociation activity, thereby simplifying and stabilizing the zinc deposition kinetics. Furthermore, the TiO_2 present in the inner layer acts as a zincophilic site, facilitating a more uniform distribution of zinc ion flux and promoting homogeneous zinc deposition within the fibers during both plating and stripping processes (Figure 7a). This phenomenon can be substantiated by the DFT calculation results of SiO_2 and TiO_2 with varying structural configurations, as illustrated in Figure 7b. For amorphous SiO_2 and TiO_2 surfaces, the binding energy of zinc can reach −2.46 and −3.32 eV, respectively, which is much lower than that of the crystalline carbon, indicating strong zinc adsorption anchoring and excellent performance. The fiber outer surface coated with highly conductive nitrogen-doped carbon enhances wetting and conductivity, promoting zinc deposition inside the fiber rather than on its surface. Additionally, the 3D conductive network within the fibers provides extra pathways for zinc deposition and dissolution during electroplating and stripping, improving the rate performance of ZIBs. Due to the synergistic effect, HSTF exhibits significant mechanical strength during repeated electroplating/peeling processes, capable of withstanding a large amount of Zn loading, and the Zn@HSTF symmetric battery has a stable polarization voltage of ∼154 mV and significant cycling stability, with no dendrite growth after more than 2000 cycles.

Likewise, Li et al. [224] proposed a layered constraint strategy to regulate zinc affinity and construct spatial traps by employing a series of cobalt-embedded porous carbon cages. During the preparation process, cobalt-based metal organic frameworks (Co-MOF) were mixed with polyacrylonitrile (PAN) in N, N-dimethylformamide and electrospun to form a composite Co-MOF@PAN precursor fiber. After annealing treatment, it transforms into a cobalt carbon composite material (CoCC) with multi-level pores in structure. As shown in Figure 7c, during the zinc ion deposition process, the inner layer containing zincophilic cobalt sites acts as a preferential nucleation region with low nucleation barriers, effectively guiding the targeted nucleation of zinc. The outer carbon cage serves as a trap to spatially restrict and accommodate zinc deposition. This integrated framework with both internal and external interfaces not only reduces local current density and homogenizes zinc ion flux but also buffers significant volume changes during long-term zinc deposition/stripping processes. From Figure 7d, as deposition time increases, irregular protrusions develop on the surface of bare zinc and eventually form dendrites. In contrast, CoCC shows no obvious protrusions or dendrites throughout the entire electroplating process, maintaining uniform zinc deposition even after 90 min. These results further confirm the spatial confinement effect within the framework of cobalt carbon composite materials. Therefore, the assembled CoCC||CoCC symmetric battery has a significantly stable cycle life of over 800 cycles and an

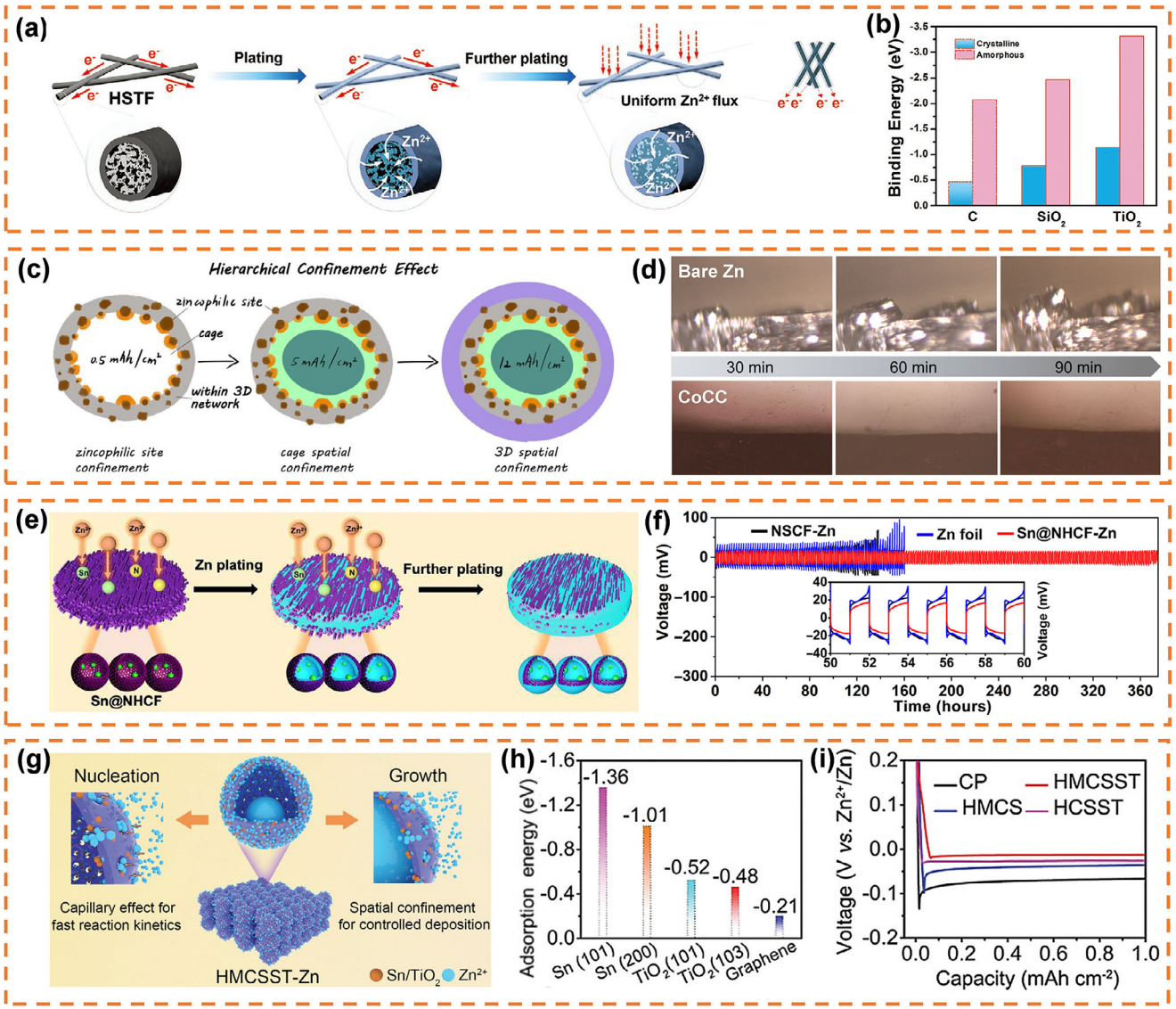

FIGURE 7 | (a) Schematic illustration of the deposition behavior of Zn^{2+} ion flux on 3D HSTF electrodes. (b) The calculated binding energies of Zn adsorbed on the surfaces of crystalline/amorphous TiO_2, SiO_2, and carbon [228]. Copyright 2021, Wiley-VCH. (c) Schematic illustration of Zn deposition on the CoCC electrode. (d) In-situ optical microscopy observations of zinc plating on both bare zinc foil and CoCC electrodes, conducted at a current density of 10 mA cm^{-2} [224]. Copyright 2022, American Chemical Society. (e) Schematic representation showing the process of Zn deposition on both bare Zn foil and Sn@NHCF. (f) GCD profiles of symmetric cells equipped with various composite Zn-based electrodes, along with the corresponding magnified voltage curves (inset) recorded at a current density of 1 mA cm^{-2} with a specific capacity of 1 mAh cm^{-2} [229]. Copyright 2022, American Association for the Advancement of Science. (g) Illustration depicting the deposition process of Zn on the HMCSST host. (h) Overview of the computed adsorption energies of Zn atoms interacting with Sn, TiO_2, and graphene. (i) Initial zinc plating voltage curves recorded on various hosts at a current density of 1 mA cm^{-2} [230]. Copyright 2024, Wiley-VCH.

overpotential as low as about 65 millivolts at 20 mA cm^{-2}. In contrast, when Co-MOF is not introduced, although the prepared carbon fibers (CFs) anode also has a long cycle life, it will eventually fail after hundreds of cycles due to a significant increase in voltage fluctuation. This phenomenon can be attributed to the increase in the accumulation of "failed zinc" substances at the interface caused by the lack of induced deposition.

Along the same lines, Yu et al. [229]. employed a hard template strategy to fabricate interconnected N-doped carbon spheres embedded with numerous Sn nanoparticles, forming a 3D hollow fiber skeleton (designated as Sn@NHCF), which serves as a high-performance anode for aqueous ZIBs. In this process, SiO_2 was employed as a hard template to fabricate hollow SnO_2 nanospheres through in situ coating combined with alkali etching. Subsequently, resorcinol-formaldehyde (RF) was coated onto its surface, and Sn@NHCF was synthesized via electrospinning technology. Within this structural design, Sn nanoparticles embedded in the inner layer exhibit strong zincophilicity, which facilitates the preferential binding of zinc ions to these sites during deposition. This characteristic facilitates both nucleation and growth on the surface of the inner layer, thereby inhibiting the formation of zinc dendrites and promoting uniform zinc deposition. In addition, metallic Sn with weak electrocatalytic

properties towards HER can prevent the generation of hydrogen bubbles inside the battery (Figure 7e). The outer N-doped carbon fiber enhances zinc ion interaction, promoting their adsorption and desorption on the electrode surface. It also protects the inner Sn nanoparticles and zinc deposits from electrolyte corrosion, maintaining electrode stability and reducing side reactions. In addition, the hollow structure of the outer layer provides sufficient space for zinc deposition, accommodating volume changes and suppressing zinc dendrite formation. Thanks to these advantages, the Sn@NHCF electrode achieved a very low nucleation overpotential, enabling dendrite-free zinc deposition, minimal voltage hysteresis, and stable performance over 370 h of cycling, which is much longer than that of the NHCF anode (Figure 7f).

In addition to using electrospinning technology, the prepared hollow material can also be directly coated onto the current collector. Sun et al. [230] synthesized SiO_2@SiO_2/resorcinol-formaldehyde (RF) spheres through the evaporation-induced self-assembly method to form tightly arranged opal arrays on carbon paper. Subsequently, a hollow mesoporous carbon sphere (HMCS) opal with a mesoporous hollow structure was synthesized through sequential calcination and etching strategies. Finally, metallic Sn and TiO_2 were encapsulated into the mesoporous channels and inner surface of HMCS through immersion and thermal reduction, forming a HMCS opal structure with enclosed Sn/TiO_2 nanoparticles (HMCSST), which serves as a high-performance zincophilic carrier for creating 3D zincophilic materials. As shown in Figure 7g, the high specific surface area and porosity of the outer hollow mesoporous carbon spheres allow rapid electrolyte penetration and diffusion during zinc ion deposition, improving Zn ion transport efficiency. The encapsulated Sn/TiO_2 nanoparticles act as zincophilic sites that enhance Zn atom adsorption (Figure 7h) and reduce Zn deposition nucleation overpotential (Figure 7i), leading to uniform Zn deposition. In addition, the platform potential of the HMCSST bulk is much lower than that of the carbon paper (CP), HMCS (which lacks a mesoporous wall), and HCSST hosts, which indicates that its mass transfer is faster, charge transfer is more rapid, and resistance is lower. The synergistic effect between the inner and outer layers of HMCSST enhances the Coulombic efficiency, accelerates Zn^{2+} diffusion, and prolongs the cycling stability of the Zn metal anode by facilitating electrolyte penetration, homogenizing current distribution, offering zincophilic sites, and suppressing side reactions.

In conclusion, pre-constructing hollow structures can significantly improve the discharge depth of zinc anodes and greatly reduce direct and disordered contact between the zinc surface and electrolyte, effectively suppressing side reactions such as HER and corrosion, which is more conducive to commercial use. However, when using this hollow structure to guide zinc deposition, it is important to note that the structure itself must have sufficient mechanical strength to resist significant volume changes during zinc deposition/dissolution, avoiding rupture or collapse. On the other hand, excellent ionic conductivity must be ensured to enable zinc ions to quickly migrate into the cavity and prevent deposition from occurring outside the structure due to slow kinetics. In addition, precise control of cavity size and distribution is necessary, and differentiated functional interfaces must be designed for the inner and outer surfaces of the structure to achieve efficient and stable dendrite-free zinc deposition in synergy.

6 | Multiscale Interfacial Construction Technologies in Separators

In AZIBs, the core of separator regulation lies in actively regulating ion transport behavior and interface environment through its own properties, such as pore size, hydrophilicity, hydrophobicity, surface chemistry, and ionic conductivity, thereby achieving precise optimization of battery performance [231]. The regulation mechanism mainly includes three types: [232–233] (1) optimizing the nanopores and surface functional groups of the separator to regulate the uniform distribution of ion flow, avoiding the formation of ion concentration gradients on the surface of the zinc anode, thereby suppressing the local preferential growth of dendrites from the source. (2) By endowing the separator with hydrophobic properties or functional coatings, direct contact between dissolved oxygen and water molecules and the zinc anode can be physically blocked and chemically isolated, effectively suppressing corrosion and HER. (3) By guiding the preferential deposition of Zn (002) crystal surface through surface functional groups, a smoother and more stable electrode/electrolyte interface is formed. However, to effectively suppress dendrite formation, the modified layer typically requires increased density or a high concentration of functional groups, which often leads to elevated ion transport impedance and reduced separator porosity. Furthermore, the modified layer may exhibit poor compatibility with the chemical environment of the cathode material or bulk electrolyte, potentially triggering undesirable side reactions.

Therefore, separators with Janus structures (such as different material types, dispersion concentrations, or functional group contents) have attracted much attention from researchers. This Janus-type separator ensures the storage of electrolyte on the cathode side and the rapid transport of ions, while physically blocking the shuttle of substances dissolved in the anode. On the other hand, it can guide the uniform deposition of Zn^{2+} at the zinc anode and suppress side reactions. Currently, the traditional method for creating Janus-type separators involves functionalizing one side of the GF separator while leaving the other side reserved for the high chemical stability, high porosity, and excellent wettability of GF [234]. For example, Li et al. [235] fabricated a double-sided functional separator by integrating chemical vapor deposition (CVD) with air plasma treatment, enabling the in-situ formation of a vertically oriented graphene (VG) mesh structure co-doped with oxygen and nitrogen atoms on one side of a GF separator. The 3D VG conductive network adjacent to the zinc anode effectively promotes uniform electric field distribution, reduces localized current density, and postpones the initial formation of dendrites. The co-doping of oxygen and nitrogen further enhances the zincophilicity of the VG network structure and significantly improves the wettability of the $ZnSO_4$ electrolyte, thereby facilitating zinc ion transport. In addition, the 3D VG adjacent to the zinc anode can be regarded as a continuation of the zinc anode perpendicular to its plane direction, providing spatial extension for guiding zinc deposition. Other materials also with similar functions include sulfonic acid-functionalized cellulose-modified graphene [236],

SnS_2 [237], MXene [238], halloysite nanotubes [239], etc., which promote the parallel deposition of Zn^{2+} along the (002) crystal plane and effectively suppress dendrite formation.

However, an ideal separator requires simultaneous optimization of the deposition kinetics of zinc ions on the anode side and the whole diffusion behavior on the cathode side, and this traditional type of Janus separator ignores the regulation of zinc ions on the cathode side, which limits the regulation process and range, ultimately limiting the cycling performance and lifespan of zinc metal batteries. Therefore, the new Janus-type separator needs to be modified on both sides to transform into a key component that can actively regulate the internal chemical environment of the battery through its unique asymmetric structure and multiscale interfacial regulation. Its dual-face design can precisely target and adapt the interface microenvironment between the anode and cathode. The prepared Janus-type separator primarily follows two design strategies: one involves imparting distinct functional properties to each side to synergistically regulate zinc ion deposition and suppress the dissolution and shuttle effect of the cathode active material. The second approach involves creating a separator with a gradient distribution by applying different functional materials to the cathode and anode sides, effectively suppressing side reactions at each interface. The specific preparation principles and regulatory mechanisms will be discussed in this section. Table 2 summarizes the reporting strategies and performance of different Janus-type separators.

6.1 | Double-Sided Decoration Type Separator

As mentioned above, the GF separator relies solely on fiber stacking to form pores of different sizes, and its inherent low conductivity is not conducive to the rapid and uniform transmission of ions. Therefore, a new generation of Janus-type separators with double-sided decoration has been developed, which can overcome the limitations of single-sided modified GF separators. Specifically, one method involves modifying both surfaces of the original GF separator, enabling its upper and lower surfaces to selectively isolate harmful anions and regulate zinc ion deposition, respectively. Another method is using functionalized materials such as cellulose, polymer, Nafion, etc., as the separator base and modifying one of its surfaces. These functionalized separators themselves have high porosity and rich active functional groups, which can directly serve as high-quality surfaces for regulating zinc ion transfer. By combining the modified surface on the opposing side, a synergistic effect can be achieved, which effectively regulates the flux distribution of zinc ions and the interfacial electric field strength, thereby enhancing the deposition kinetics of zinc metal anodes and suppressing dendrite formation.

For the double-sided modified GF separators, Bi et al. [255] prepared Co-HNMXS and Cu-HMXS with hollow conductive structures using a hard template method, and loaded them onto the cathode and anode sides of a GF separator through vacuum filtration. The prepared Janus separator with a heterogeneous double-sided interface mediated by highly conductive MXene simultaneously controls zinc deposition and accelerates the kinetics of iodine adsorption conversion reaction (Figure 8a). Among them, the Cu-HMXS on the anode side of the Janus separator contains a large number of zincophilic Cu sites, which reduces the nucleation energy barrier of zinc (Figure 8b). Its conductive hollow sphere structure alleviates the tip effect and induces horizontally oriented dendrite-free growth of zinc. In addition, the relatively high fluorine content in Cu-HMXS ensures the hydrophobicity of its interface and eliminates competitive side reactions caused by water on the anode side. For the Co-HNMXS located on the cathode side of the Janus separator, its high porosity and abundant Co-N-C active sites strongly chemically adsorb I_3^- intermediate and inhibit the iodine shuttle effect (Figure 8c). Moreover, the Co-N-C active site optimizes the electronic structure, promotes the charge transfer of I_2/I^- redox, and accelerates the redox kinetics. In addition, the hydrophilic interface and hierarchical pore structure of Co-HNMXS accelerate the transport kinetics of charge carriers on the cathode side. Owing to the synergistic effects of this dual-interface engineering approach, this Janus separator enabled Zn||Zn symmetric batteries to achieve over 2900 h of stable cycling, while also delivering an ultra-high capacity of 274 mAh g^{-1} and a cycle life exceeding 20 000 cycles for Zn–I_2 batteries.

Compared with the GF separator, using separator materials rich in hydrophilic functional groups (such as –OH, –COOH) can significantly improve electrolyte wettability and zincophilicity, promote uniform ion transport; using separator materials rich in sulfonic acid groups (SO_3^-) can selectively guide the uniform migration of Zn^{2+}, while partially repelling anions, which helps to suppress concentration polarization [264]. For example, Zheng et al. [251] employed bacterial cellulose (BC) and silver nanowires (AgNWs) as raw materials to fabricate an ultrathin Janus separator featuring abundant zincophilic sites, a uniform electric field distribution, and enhanced ion transport kinetics, through a two-step vacuum-assisted filtration process. The Janus separator features two distinct sides: one composed of a BC layer and the other consisting of an AgNWs/BC composite layer (Figure 8d). Among them, BC nanofibers form a dense network structure through intermolecular hydrogen bonding and van der Waals forces, endowing the separator with excellent mechanical strength and puncture resistance. Moreover, BC nanofibers are rich in –OH and highly compatible with aqueous electrolytes, helping to balance current density and suppress dendrite formation. The uniformly distributed zincophilic silver nanowires in the anode side of AgNWs/BC separator exhibit excellent electrical and thermal conductivity, acting as ion pumps that efficiently transport Zn^{2+} through the electrolyte and guide uniform nucleation for subsequent zinc deposition. This results in dense and dendrite-free zinc plating, which can be confirmed from the laser confocal scanning microscopy (LCSM) images (Figure 8e). In addition, the tightly interwoven AgNWs/BC network structure reduces hydrogen bonds between BC nanofibers, thereby adjusting the pore structure and improving the diffusion kinetics of Zn^{2+} carriers. Therefore, the Zn||Zn symmetrical battery employing this Janus separator has a stable cycle life of over 2400 h at 2 mA cm^{-2} with 1 mA h cm^{-2} (Figure 8f).

Similarly, Zheng et al. [254] fabricated a double-sided cellulose fiber (CF)/polyvinyl alcohol (PVA)/ZrO_2 composite separator through the vacuum filtration method. During the vacuum filtration process, ZrO_2 nanoparticles tend to precipitate and aggregate at the bottom of the separator, resulting in the formation of composite films with asymmetric surfaces (Figure 8g). In this

TABLE 2 | Summary of the construction methods and cell performances of the reported Janus- or gradient-type separators.

Modified method	Modified material	Symmetric cells (cycling time, cycling condition)	Asymmetric cells (Coulombic efficiency, cycling condition, cycling number)	Reference
Single-sided decoration	Vertical graphene/GF	250 h, 1 mA cm^{-2}/1 mAh cm^{-2}	95%, 2 mA cm^{-2}/1 mAh cm^{-2}, 20 cycles	[235]
Single-sided decoration	Butter paper/GF	>5000 h, 0.5 mA cm^{-2}/0.5 mAh cm^{-2}	99.0%, 1 mA cm^{-2}/0.5 mAh cm^{-2}, 200 cycles	[240]
Single-sided decoration	$Ti_3C_2T_x$ MXene/GF	1180 h, 1 mA cm^{-2}/1 mAh cm^{-2}	96.2%, 2 mA cm^{-2}/0.5 mAh cm^{-2}, 200 cycles	[238]
Single-sided decoration	Graphene sheets modified with sulfonic cellulose/GF	1400 h, 10 mA cm^{-2}/10 mAh cm^{-2}	99.6%, 1 mA cm^{-2}/1 mAh cm^{-2}, 890 cycles	[236]
Single-sided decoration	$Ti_3C_2T_x$ MXene/GF	2500 h, 1 mA cm^{-2}/1 mAh cm^{-2}	95.3%, 1 mA cm^{-2}/0.5 mAh cm^{-2}, 200 cycles	[241]
Single-sided decoration	Sulfonated poly(arylene ether sulfone)/GF	2000 h, 1 mA cm^{-2}/1 mAh cm^{-2}	99.3%, 2 mA cm^{-2}/1 mAh cm^{-2}, >250 cycles	[242]
Single-sided decoration	Cu/GF	3500 h, 1 mA cm^{-2}/1 mAh cm^{-2}	99.88%, 2 mA cm^{-2}/-, >2400 cycles	[243]
Single-sided decoration	GO-TiO_2/GF	>2000 h, 1 mA cm^{-2}/1 mAh cm^{-2}	~100%, 2 mA cm^{-2}/0.5 mAh cm^{-2}, 200 cycles	[244]
Single-sided decoration	Halloysite nanotubes/GF	3000 h, 1 mA cm^{-2}/1 mAh cm^{-2}	99.87%, 1 mA cm^{-2}/1 mAh cm^{-2}, 950 cycles	[239]
Single-sided decoration	Acid-treated carbon/GF	2400 h, 1 mA cm^{-2}/1 mAh cm^{-2}	99.6%, 1 mA cm^{-2}/1 mAh cm^{-2}, 900 cycles	[245]
Single-sided decoration	CNT-PAN-Ag/GF	>1000 h, 1 mA cm^{-2}/0.5 mAh cm^{-2}	96.58%, 2 mA cm^{-2}/1 mAh cm^{-2}, 450 cycles	[246]
Single-sided decoration	CAU-17/GF	4450 h, 1 mA cm^{-2}/1 mAh cm^{-2}	99.9%, 2 mA cm^{-2}/1 mAh cm^{-2}, 500 cycles	[247]
Single-sided decoration	SnS_2(001)/GF	2100 h, 1 mA cm^{-2}/1 mAh cm^{-2}	99.32%, 1 mA cm^{-2}/1 mAh cm^{-2}, 200 cycles	[237]
Single-sided decoration	D-ZrP/GF	3000 h, 1 mA cm^{-2}/1 mAh cm^{-2}	99.2%, 1 mA cm^{-2}/1 mAh cm^{-2}, 420 cycles	[248]
Single-sided decoration	BC/$Ti_{0.87}O_2$/GF	1400 h, 1 mA cm^{-2}/1 mAh cm^{-2}	99.5%, 1 mA cm^{-2}/1 mAh cm^{-2}, >600 cycles	[249]
Double-sided decoration	rGO-MOF/PP-PE	>500 h, 2 mA cm^{-2}/1 mAh cm^{-2}	97.8%, 0.5 mA cm^{-2}/0.5 mAh cm^{-2}, 320 cycles	[250]

(Continues)

TABLE 2 | (Continued)

Modified method	Modified material	Symmetric cells (cycling time, cycling condition)	Asymmetric cells (Coulombic efficiency, cycling condition, cycling number)	Reference
Double-sided decoration	Ag nanowires/bacterial cellulose	>2400 h, 2 mA cm^{-2}/1 mAh cm^{-2}	98.1%, 1 mA cm^{-2}/1 mAh cm^{-2}, 430 cycles	[251]
Double-sided decoration	$Ti_3C_2T_x$ MXene/nanofibrillated cellulose	1000 h, 5 mA cm^{-2}/5 mAh cm^{-2}	98.95%, 1 mA cm^{-2}/0.5 mAh cm^{-2}, 1000 cycles	[252]
Double-sided decoration	Chitosan/commercial cotton pad	1500 h, 1 mA cm^{-2}/1 mAh cm^{-2}	98.5%, 1 mA cm^{-2}/1 mAh cm^{-2}, 350 cycles	[253]
Double-sided decoration	Cellulose fiber/PVA/ZrO_2	>1500 h, 1 mA cm^{-2}/0.5 mAh cm^{-2}	99.18%, -/0.6 mAh cm^{-2}, 150 cycles	[254]
Double-sided decoration	Cu-HMXS/GF/Co-HNMXS	2900 h, 1 mA cm^{-2}/1 mAh cm^{-2}	99.4%, 2 mA cm^{-2}/1 mAh cm^{-2}, 2000 cycles	[255]
Double-sided decoration	In_2O_3-SiO_2/GF/Co@CNF	>3400 h, 1 mA cm^{-2}/1 mAh cm^{-2}	99.8%, 5 mA cm^{-2}/1 mAh cm^{-2}, >3500 cycles	[256]
Double-sided decoration	RHNTs/bacterial cellulose	800 h, 4.4 mA cm^{-2}/1.1 mAh cm^{-2}	97.2%, 2 mA cm^{-2}/1 mAh cm^{-2}, 168 cycles	[257]
Double-sided decoration	PAN-PVDF-UIO-66/PAA	>500 h, 5 mA cm^{-2}/5 mAh cm^{-2}	99.3%, 1 mA cm^{-2}/1 mAh cm^{-2}, >250 cycles	[258]
Gradient distribution	SiO_2/bacterial cellulose	2900 h, 1 mA cm^{-2}/1 mAh cm^{-2}	99.81%, 1 mA cm^{-2}/1 mAh cm^{-2}, >800 cycles	[259]
Gradient distribution	CeF_3/GF	2500 h, 1 mA cm^{-2}/1 mAh cm^{-2}	99.7%, 1 mA cm^{-2}/1 mAh cm^{-2}, >320 cycles	[260]
Gradient distribution	$BaTiO_3$/GF	1600 h, 10 mA cm^{-2}/2.5 mAh cm^{-2}	~100%, 1 mA cm^{-2}/-, 500 cycles	[261]
Gradient distribution	MCM-41/GF	>2400 h, 1 mA cm^{-2}/1 mAh cm^{-2}	98.61%, -, 350 cycles	[262]
Gradient distribution	NMP-$ZnCl_2$/GF	>4800 h, 3 mA cm^{-2}/1 mAh cm^{-2}	99.7%, 5 mA cm^{-2}/1 mAh cm^{-2}, 2500 cycles	[263]

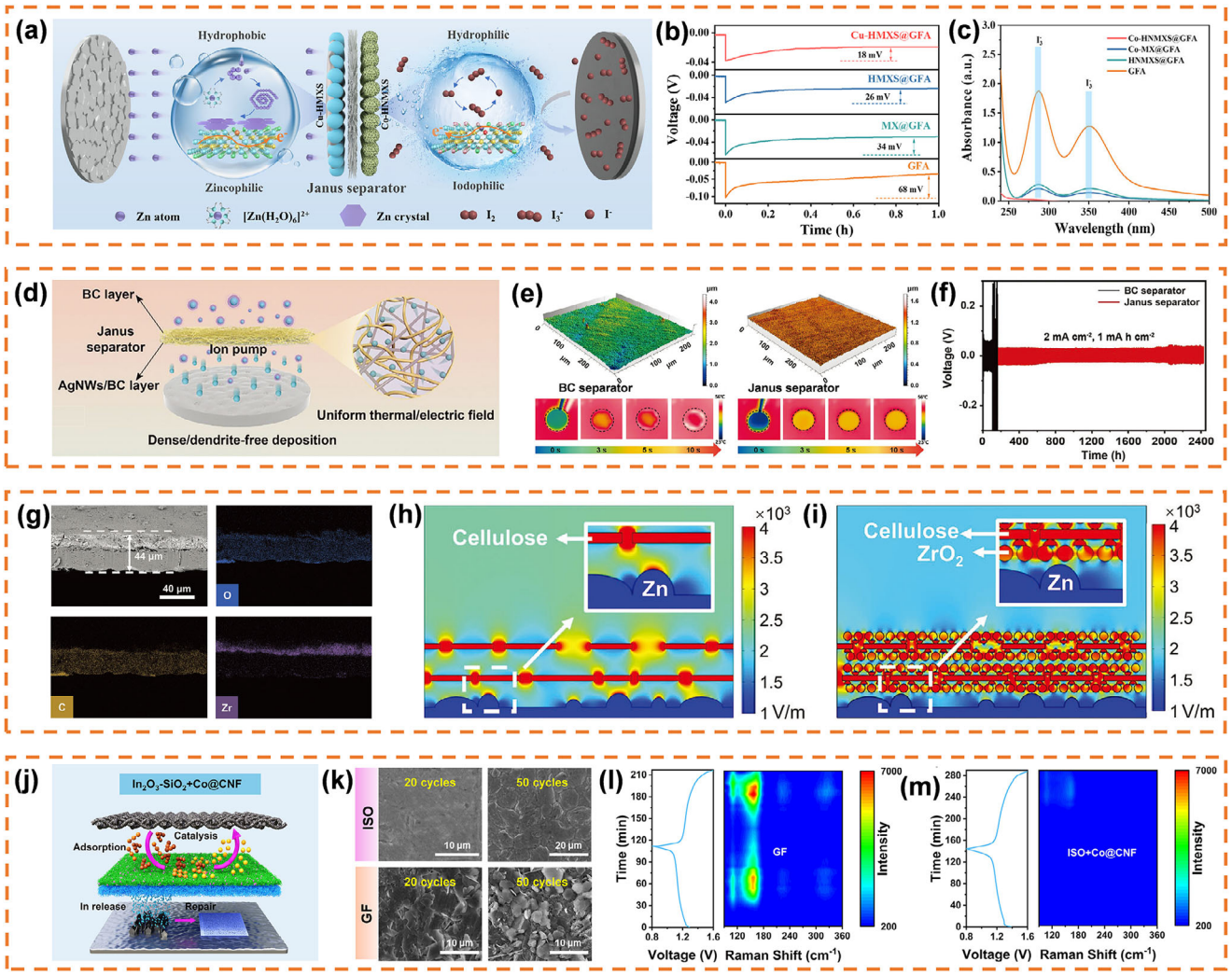

FIGURE 8 | (a) Mechanism illustration of Cu-HMXS/Co-HNMXS@GFA separator. (b) Nucleation overpotential at 1 mA cm^{-2} of various materials. (c) The UV–vis spectra with different separators after standing for 60 min [255]. Copyright 2025, Wiley-VCH. (d) Schematic illustration of the function mechanism of the AgNWs/BC Janus separators. (e) LCSM 3D topographic images of zinc deposition with BC and AgNWs/BC Janus separators. (f) Cycling performances of Zn||Zn symmetrical battery of 2 mA cm^{-2} and 1 mA h cm^{-2} [251]. Copyright 2023, Wiley-VCH. (g) Cross-sectional SEM image and the corresponding elemental maps of O, C, and Zr taken from the CF/PVA/ZrO_2 separator. Simulated electric field distribution near the Zn anode in contact with (h) a CF separator and (i) a CF/PVA/ZrO_2 separator [254]. Copyright 2025, Wiley-VCH. (j) Schematic representation of interfacial processes in Zn–I_2 batteries employing the ISO + Co@CNF Janus separator. (k) SEM images of Zn electrodes after 20 and 50 cycles using GF and ISO separators, respectively. In-situ Raman spectra combined with time-dependent voltage profiles of Zn||I_2 full cells equipped with (l) GF and (m) ISO + Co@CNF separators during the initial charge-discharge cycle at a rate of 0.5 C [256]. Copyright 2025, Wiley-VCH.

asymmetric configuration, the fibrous surface on the cathode side retains a porous architecture, which facilitates efficient ion transport. Moreover, the hydroxyl groups present in cellulose exhibit favorable wetting characteristics for aqueous electrolytes, which facilitates the desolvation of hydrated zinc ions, $[Zn(H_2O)_6]^{2+}$, thereby reducing the activation energy required for the process. The anode side surface of the asymmetric separator is embedded with numerous ZrO_2 nanoparticles possessing a high dielectric constant. These nanoparticles generate a polarizing electric field under an applied voltage, thereby facilitating uniform zinc ion deposition and transport pathways (Figure 8h,i). In addition, DFT shows a strong chemical affinity between the ZrO_2 (220) crystal surface and Zn (101) crystal surface, which facilitates rapid Zn (101) growth and results in a compact, flat, and dendrite-free zinc anode. Therefore, the Zn||Zn symmetric battery demonstrates excellent electrochemical performance, operating for over 1500 h at 1 mA cm^{-2} and 400 h at 6 mA cm^{-2}.

In addition to the above two methods, another method is to prepare different types of separators in advance and stack them for use. This method has higher flexibility and can design corresponding separator surfaces based on the selected anode and cathode materials. For example, Li et al. [256] prepared a separator with an integrated series structure consisting of an In_2O_3-SiO_2 (ISO) layer and a carbon nanofiber layer encapsulated with cobalt nanoparticles (Co@CNF) using a two-step electrospinning combined with a calcination process (Figure 8j). In this separator, the zwitterionic In_2O_3 present in the ISO layer on the anode side can effectively neutralize the OH^- generated by local HER, while releasing soluble indium species (In_2O_3 +

$2OH^- \rightarrow 2[In(OH)_4]^-$). The indium species generated during electrodeposition are reduced to indium metal and deposited onto the damaged areas of the zinc anode. The loaded indium metal offers zincophilic sites and inhibits the HER, helping to restore the interfacial environment and reduce anode degradation. As shown in Figure 8k, the zinc anode with the ISO separator shows denser and flatter deposition than that with the GF separator, clearly indicating the ISO layer's regulation of zinc deposition. In addition, dual protection of the zinc anode interface is achieved through physical isolation of SiO_2 and chemical dynamic repair of In_2O_3. The 3D porous carbon fiber network of Co@CNF on the cathode side provides abundant adsorption sites to anchor multi-iodides (I_3^-, I_5^-), suppress shuttle effects, and prevent anode corrosion caused by multi-iodides. In detail, due to the strong hybridization between the d-orbitals of Co and the p-orbitals of I, the I–I bond strength is significantly weakened. This facilitates the preferential chemical adsorption of I_3^- by cobalt nanoparticles, leading to their dissociation into I_2^- intermediates and the formation of Co–I bonds. The conductive network formed by nitrogen-doped carbon enhances electron transfer, thereby promoting the rapid reduction of I_2^- to I^-. The in-situ Raman spectra show that with an ISO separator, the intensity of I_3^- (110 cm^{-1}) and I_5^- (150 cm^{-1}) in the electrolyte is significantly lower than with a GF separator (Figure 8l,m). This confirms the synergistic effect of cobalt nanoparticles and nitrogen-doped carbon materials in reducing the energy barrier from I_3^- to I_5^- and accelerating the redox reaction rate. Owing to the complementary stabilization effect provided by both electrode interfaces, the fabricated full cell exhibited a remarkable areal capacity of 2.97 mAh cm^{-2} and showed outstanding cycling performance with stability maintained over 20 000 cycles.

In conclusion, constructing a dual-functional surface-regulated separator can achieve multi-step fine regulation of zinc deposition behavior through bilateral synergistic effects. Compared to single-sided modified separators, this strategy provides richer regulatory dimensions and simultaneously inhibits dendrite growth and side reactions on the zinc anode side. At the same time, the functional layer facing the cathode effectively blocks the dissolution and shuttle effect of the active material. This dual-pronged design, initiated at the key interfaces on both sides of the battery, significantly enhances the overall electrochemical stability of the system. However, this strategy still needs to pay attention to the following two points in practical applications: (1) the introduction of a multi-layer structure may increase the overall impedance of the separator, and the thickness and properties of each functional layer need to be precisely controlled to ensure high ion conductivity and fast reaction kinetics. (2) The long-term bonding strength between different functional layers is crucial, and it is necessary to avoid interlayer separation caused by uneven swelling or shrinkage during the cycling process, which poses a challenge to the preparation process.

6.2 | Gradient Distribution Type Separator

The gradient distributed separator refers to a continuous or layered gradient in its physical or chemical properties (such as pore size, hydrophilicity, hydrophobicity, functional group density, etc.) along the thickness direction of the separator. It does not have a sudden interface switch like a double-sided decorative separator. This gradient structure can guide zinc ions more smoothly from one side to the other, avoiding sudden changes in ion flow at the interface, thereby more effectively achieving uniform ion flux and suppressing dendrites from the root. In addition, the gradient mechanical modulus can better match the volume change of the electrode. The side closer to the zinc cathode can be designed to be more durable to physically block dendrites, while the middle layer provides flexibility to adapt to deformation during cycling and reduce internal stress. Although its preparation process is more complex than that of double-sided modified separators, the gradient structure effectively avoids long-term stability issues that may arise from interlayer interfaces, providing a more promising overall solution for achieving highly stable AZIBs.

The first method is to introduce high dielectric materials into the separator and form a gradient distribution. Under the action of an electric field, they will polarize and generate an induced electric field in the opposite direction to the external electric field internally. This polarization effect effectively weakens the local electric field strength near the surface of the zinc anode, especially in the "hot spot" areas that are prone to dendrite formation. The final homogenization of zinc ion flow induces uniform deposition of zinc. For example, Liang et al. [261] developed a dual-functional gradient-type separator by optimizing the concentration of $BaTiO_3$ (BTO)/polyvinylidene fluoride (PVDF) dispersion and by immobilizing BTO nanoparticles on the surface and within the pores of a GF separator through a filtration-based approach. This process enhances the efficiency of zinc ion deposition through a two-stage regulatory mechanism. First, when zinc ions pass through the GF separator in the electrolyte, the asymmetric crystal structure of BTO causes misalignment between positive and negative charge centers, resulting in a spontaneous polarization and an electric dipole moment. This polarization creates an internal electric field that selectively attracts positively charged Zn^{2+} ions and accelerates their migration (Figure 9a). Furthermore, the electric field directs Zn^{2+} ions to move orderly along the (110) plane, preventing random diffusion (Figure 9b). Subsequently, the BTO enrichment layer creates a uniform electric field at the separator–anode interface, preventing localized charge accumulation. This uniform ion flow reduces the exposed active area of the Zn anode, suppressing zinc dendrite and by-product formation. Simply put, the fiber-electrolyte interface acts as an "ion accelerator" that enhances transport rates through polarized electric fields and zincophilicity. The separator–anode interface serves as an "ion redistribution device", achieving ion flow homogenization through uniform filling. Thanks to the synergistic effect of the dual interface, efficient zinc ion regulation is achieved. The Zn||Zn symmetrical battery with this dual-interface engineering separator operates stably for 1600 h with minimal voltage fluctuations, outperforming the unmodified version.

The gradient-type separator can also be designed from the perspective of adjusting the desolvation and diffusion of hydrated zinc ions. Specifically, the cathode side ensures excellent electrolyte wettability and ion conductivity, ensuring good rate performance, while the anode side strongly suppresses side reactions. The intermediate gradient transition layer ensures the continuity of ion transport and avoids sudden changes in performance. For example, Dong et al. [259] used hydrophilic BC as the substrate material to prepare BC separators with

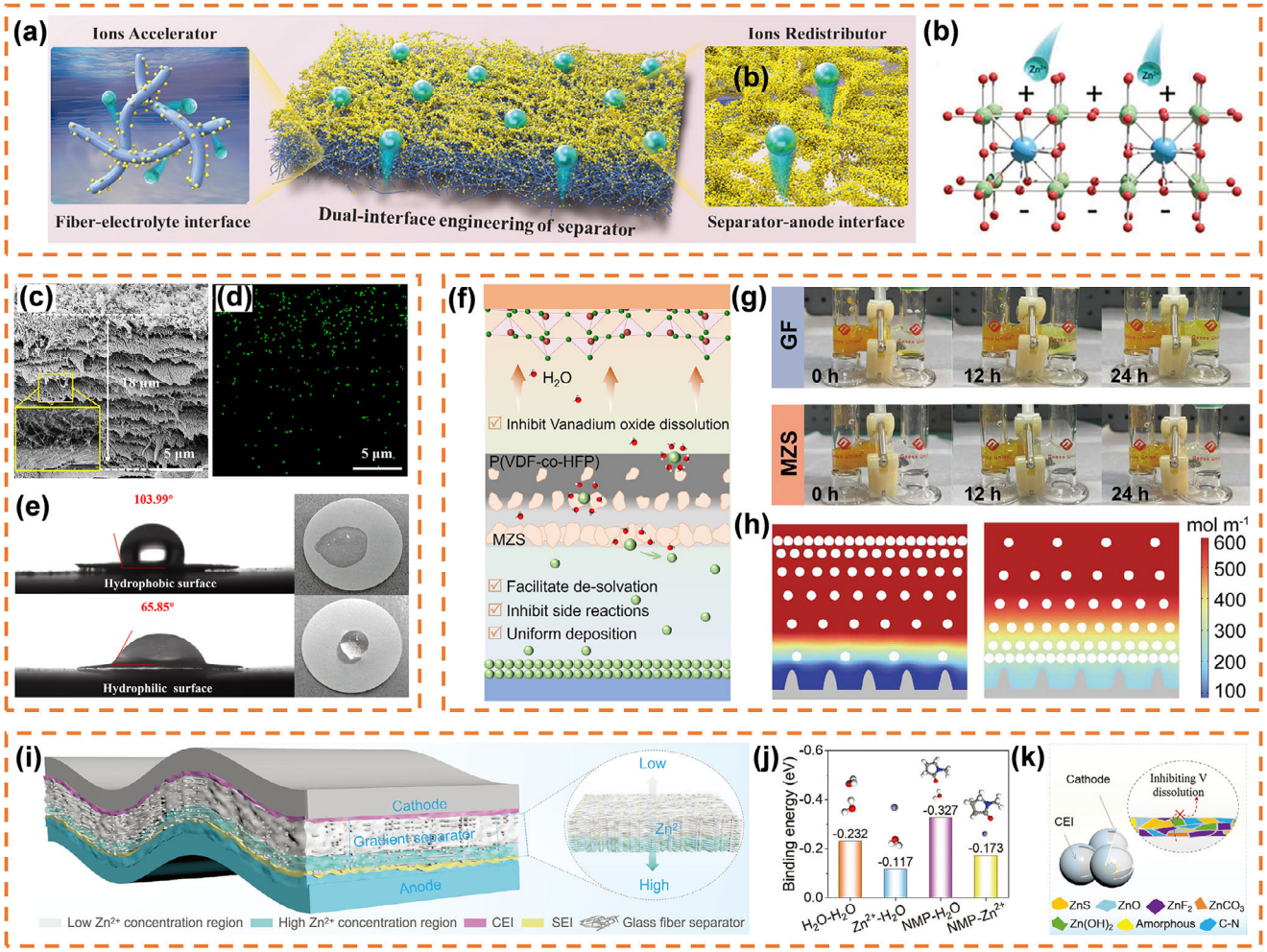

FIGURE 9 | (a) The schematic diagram of dual-interface engineering of the separator. (b) Schematic diagram of enhanced mechanism for Zn^{2+} transport [261]. Copyright 2022, Wiley-VCH. (c) Cross-sectional SEM image and (d) the corresponding EDS mapping of the Si element of the gradient-type BC separator. (e) Contact angle measurement of the gradient-type BC separator and the corresponding optical images [259]. Copyright 2025, Wiley-VCH. (f) Schematic diagram illustrating the bifunctional MZS separator to stabilize both the cathode and Zn anode. (g) Permeation experiments with an H-type equipped with a GF and MZS separator. (h) Ion distribution field simulations of MZS using finite element analysis [262]. Copyright 2025, Wiley-VCH. (i) Schematic illustration of a Zn metal battery with a gradient separator. (j) Binding energies of H_2O–H_2O, Zn^{2+}–H_2O, NMP–H_2O, and Zn^{2+}–NMP and corresponding structures. (k) Mechanism illustration of the gradient separator on the cathode [263]. Copyright 2024, Wiley-VCH.

a thickness of only 18 μm through vacuum filtration. They then impregnated the BC skeleton with a hydrophobic gas-SiO_2 solution to form a continuous gradient distribution from hydrophilic to hydrophobic (Figure 9c–e). On the hydrophilic side, the oxygen-containing functional groups on the BC surface anchor free water through hydrogen bonds, converting it into low activity bound water. And the negatively charged groups of the BC skeleton selectively block the penetration of Cl^- through electrostatic repulsion, while accelerating the diffusion of Zn^{2+} ions. The introduction of SiO_2 nanoparticles in the hydrophobic side disrupts the dense hydrogen bonds of cellulose, reconstructs the pore structure, and forms a continuous ion transport channel. This further weakens the interaction between Zn^{2+} ions and water molecules, forming a highly aggregated electrolyte. Ultimately, the two achieved synergy through gradient design, jointly suppressing Cl^- corrosion and moisture-induced side reactions. Therefore, Zn||Zn symmetric batteries can operate stably for 2900 h at a current density of 1 mA cm^{-2}/1 mAh cm^{-2} in natural seawater electrolytes, and can operate for 1300 h at a discharge depth of 50%. Materials with similar functionalities also include CeF_3, which, when dispersed in a gradient concentration within GF, can regulate Zn^{2+} ion flux and suppress SO_4^{2-} migration, thus facilitating dense and uniform zinc deposition. The strong interaction between CeF_3 nanoparticles and water molecules effectively desolvates Zn^{2+} ions at the electrolyte/zinc anode interface, thereby inhibiting parasitic side reactions [260].

On this basis, gradient-type separators can be extended to two-component systems, which can not only improve the dendrite and hydrogen evolution problems at the anode but also suppress the dissolution and shuttle of cathode active materials. For example, Chang et al. [262] prepared MCM-41 zeolite separators (named MZS) with a gradient distribution using a template-assisted method. During the preparation process, MCM-41 zeolite is uniformly dispersed under the action of a magnetic stirrer and forms a concentration gradient distribution in the subsequent film drying stage due to natural gravity. Ultimately, the distribution of upper layer (MZS-U) zeolite is relatively sparse, while the

distribution of lower layer (MZS-D) zeolite is dense (Figure 9f). The MCM-41 zeolite distribution in the MZS-U layer is relatively light while the polymer concentration is high, forming a relatively dense structural layer. This effectively inhibits the dissolution and shuttle of VO^{2+}, reducing the loss of cathode material (Figure 9g). In contrast, gravity-induced MCM-41 zeolite accumulates in the MZS-D layer, forming a porous structure. On the one hand, the hydrophilicity of MCM-41 zeolite and the attractive effect of P(VDF-co-HFP) on Zn^{2+} synergistically reduce the desolvation energy barrier, inhibit HER and related corrosion reactions. On the other hand, the loose and porous structure of heavy zeolite distribution effectively regulates the flux of Zn^{2+} ions (Figure 9h), promotes 3D Zn^{2+} diffusion behavior, and inhibits the formation of zinc dendrites caused by 2D diffusion. This dual-function design enables the Zn||Zn symmetric battery to have a cycle life of over 2400 h, and the entire battery maintains a high capacity of 212.5 mAh g^{-1} after 1000 cycles at a current density of 1 A g^{-1}, demonstrating excellent electrochemical stability. Similarly, Tian et al. [263] utilized capillary action to load a semi-solid NMP slurry containing polyethylene oxide (PEO) binder and $ZnCl_2$ onto a glass fiber separator, forming a densely packed high Zn^{2+} concentration region. Subsequently, 1.0 M $Zn(OTf)_2$ + H_2O electrolyte is injected into the upper layer of the separator to form a low Zn^{2+} concentration region, ultimately forming a stable concentration layered structure (Figure 9i). The low Zn^{2+} concentration region maintains the wettability of the cathode interface, while NMP diffused from the high concentration region coordinates with Zn^{2+} through strong electrostatic interactions, disrupting the hydrogen bonding network of water molecules and reducing water-induced side reactions (Figure 9j). In addition, NMP will form a cathode electrolyte interface rich in $N/ZnS/ZnF_2$, thereby inhibiting the leaching of vanadium ions (Figure 9k). The high Zn^{2+} concentration region homogenizes the ion flow, and its synergistic in-situ generated flexible SEI inhibits dendrite growth and hydrogen evolution reaction.

In conclusion, the core advantage of gradient separators in AZIBs lies in their "partition design" concept, which can synergistically solve the two major problems of dendrites and side reactions. The side near the zinc anode is usually designed with a smaller pore size or hydrophobicity to guide the uniform deposition of zinc and isolate water molecules, effectively suppressing dendrite growth and corrosion, hydrogen evolution side reactions. On the side closer to the cathode, it maintains a larger pore size and good hydrophilicity, ensuring efficient ion transport. This synergistic effect significantly improves the cycle life and safety of the battery, but specific parameters need to be finely optimized according to the specific battery system, and an unreasonable gradient design may have the opposite effect. For example, if the hydrophobic layer is too thick or the hydrophilicity is too poor, it may lead to a decrease in overall ionic conductivity. If the aperture gradient design is improper, it may cause uneven ion flow at the interface.

7 | Multiscale Interface Construction Technologies in Hydrogel Electrolyte

The water in the hydrogel electrolyte is immobilized within the polymer scaffold (typically through interactions with polar functional groups on the polymer chains), preventing electrolyte depletion caused by the high reactivity of water in batteries that use traditional aqueous electrolytes [72]. Rich functional groups and hydrophilic polymer chains can form cross-linked networks with water molecules, not only establishing ordered ion migration pathways, but also promoting uniform distribution of ion flux [265]. Although the traditional hydrogel electrolyte provides a good application prospect for aqueous system AZIBs due to its inherent flexibility and ionic conductivity, its inherent structural symmetry and chemical uniformity constitute the theoretical and practical bottleneck for further performance breakthroughs. This homogeneous system exposes its fundamental shortcomings when facing the heterogeneous and dynamic electrochemical interface inside the battery: it cannot provide "tailored" microenvironment regulation for the positive and anodes with vastly different physical and chemical environmental requirements. Specifically, strategies aimed at stabilizing the zinc anode and suppressing dendrites and side reactions (such as reducing water activity) often contradict the conditions required to maintain the structural stability of the cathode material and achieve high-capacity storage (such as sufficient solvation environment) [120]. This "one size fits all" design philosophy results in the electrolyte being in a suboptimal state at both electrode interfaces, leading to limited cycle life of the battery, difficulty in further improving Coulombic efficiency, and actual energy density lower than theoretical expectations at a macro level.

The multiscale interface construction methods in hydrogel electrolytes can perfectly solve the above problems. Specifically, the hydrogel electrolyte is designed as two different components inside and outside. One of the main obstacles to the application of AZIBs is the conflicting demand between the zinc metal anode and cathode. On the anode side, water can cause severe corrosion and dendrite growth, significantly inhibiting the reversibility of zinc deposition/stripping. On the cathode side, water is essential because many cathode materials require simultaneous insertion/extraction of H^+ and Zn^{2+} to achieve high capacity and long lifespan.

7.1 | Janus-Type Hydrogel Electrolyte

The Janus-type hydrogel electrolytes are primarily composed of asymmetric structures derived from distinct chemical components, with common configurations including polymer-polymer composites, polymer-inorganic hybrids, and functionally modified systems. Compared with traditional homogeneous hydrogel electrolytes, the core advantage of the Janus-type hydrogel electrolytes lies in overcoming the limitation of single-component systems, which struggle to simultaneously optimize multiple performance metrics [266]. It achieves synergistic functionality through spatially defined functional zones, enabling each region to perform its designated role effectively. The anode-facing side can be designed as a high mechanical modulus layer to suppress dendrite growth and regulate zinc ion solvation, reducing side reactions. The cathode-facing side can feature high ion conductivity and interface compatibility to ensure efficient reaction kinetics, significantly improving cycling stability, coulombic efficiency, and interface performance without compromising ion transport.

One of the common methods is to combine the hydrogel with the SEI interface of the zinc anode, such as porphyrin paddlewheel

framework (PPFs) [267], PEDOT:PSS [268], CALF-20 [266], etc. Its core advantage is to build a "rigid and flexible" cooperative protection mechanism: the flexible hydrogel layer can perfectly fit the surface of the zinc anode, effectively alleviate the volume change during the charging and discharging process, and maintain close interface contact. At the same time, its internal free water molecules provide a rapid migration channel for zinc ions. The SEI interface acts as a mechanically robust barrier that effectively prevents zinc dendrite penetration and blocks water molecules from contacting zinc metal due to its chemical stability, significantly suppressing HER and corrosion. This structure balances interface stability with ion transport kinetics, enabling efficient ion conduction and enhancing the reversibility of zinc deposition/dissolution and battery cycle life. For example, Chen et al. [267]. proposed an asymmetric design using an inorganic solid-state electrolyte (SSE) and a hydrogel electrolyte to simultaneously meet the differing requirements of the anode and cathode (Figure 10a). The surface of the asymmetric electrolyte adjacent to the zinc metal anode is a solid electrolyte layer featuring 2D PPF metal-organic framework sheets (PPF-SSEs), fabricated via an ion diffusion impregnation coating method. Conversely, the surface facing the cathode side consists of a polyacrylamide (PAM) hydrogel, prepared using a pre-polymerization combined coating technique. Finally, these two pre-prepared electrolyte layers were subjected to hot pressing and in-situ polymerization to form a PPF-SSEs/PAM bilayer asymmetric structure. In this asymmetric configuration, the PPF-SSE solid electrolyte layer effectively separates the zinc electrode from direct contact with water, thereby preventing water-induced corrosion of zinc and the accompanying hydrogen evolution. And through the physical desolvation effect of MOF channels, $[Zn(H_2O)_6]^{2+}$ coordination ions are forced to remove water molecules, reducing uneven deposition of zinc and further achieving dendrite-free and HER-free zinc deposition/dissolution. The Raman spectrum shows that the peak intensities of ZnO and $Zn(OH)_2$ in the zinc foil with asymmetric electrolyte are significantly weaker than those with the ordinary hydrogel electrolyte, further indicating that the PPF-SSEs layer suppresses side reactions (Figure 10b,c). On the cathode side, the PAM hydrogel layer serves a dual function. Firstly, it provides water molecules as both the source and lubricant for H^+ ions, facilitating H^+/Zn^{2+} synergistic intercalation and deintercalation in cathode materials like MnO_2 and V_2O_5, thus enabling high capacity. Secondly, the PAM hydrogel exhibits a conductivity of 84.79 mS cm^{-1}, effectively enhancing the cathodic reaction kinetics. Owing to the synergistic effect of the asymmetric structure, the fabricated $Zn//MnO_2$ battery maintains excellent stability after 1000 charge-discharge cycles, demonstrating an initial capacity retention of up to 94% (Figure 10d).

In contrast, a Janus-type hydrogel electrolyte formed by combining two kinds of hydrogels achieves a higher degree of interface fusion and performance homogenization. Both sides of this Janus-type gel electrolyte structure are composed of flexible hydrogels, ensuring excellent interface compatibility and ionic conductivity continuity within the entire electrolyte, and avoiding the risk of poor contact or peeling due to modulus mutation between the water gel and the rigid solid layer. At the same time, through the precise design of the chemical composition of the hydrogels on both sides, the dendrite suppression function facing the anode side and the high ion transmission capability facing the cathode side can be given respectively on the premise of maintaining the overall flexibility, to synergistically improve the magnification performance and cycle stability of the battery without introducing significant interface impedance, which is especially suitable for the application scenarios of flexible devices that need to withstand repeated deformation. For example, Zhao et al. [269] developed an anhydrous Janus quasi-solid-state electrolyte to achieve excellent cycling performance of AZIBs, aiming at the two problems of the hydrogel electrolyte's significant kinetic barrier and the lack of free water, which will lead to a significant decline in cathode capacity. This Janus-type electrolyte is composed of two different polymer components, namely polymethyl methacrylate (PMMA) and poly (vinylidene fluoride hexafluoropropylene copolymer) (P(VDF-co-HFP)), which allows the characteristics of the cathode and anode interface to be independently adjusted (Figure 10e). Specifically, the abundant carbonyl groups (C═O) in the PMMA polymer backbone temporarily capture and evenly distribute Zn^{2+}, forming a Zn^{2+} enrichment layer at the anode interface, which ensures rapid replenishment of Zn^{2+}, significantly reducing concentration polarization on the electrode surface and avoiding dendrite growth caused by ion depletion at the root. In addition, the lower LUMO energy levels of the PMMA and $CF_3SO_3^-$ make them more prone to reduction and decomposition on the anode surface, forming a unique in-situ "organic-outer/inorganic-inner" gradient SEI (Figure 10f). The PHEC layer near the cathode incorporates 1-ethyl-3-methylimidazolium chloride (EMIMCl) ionic liquid, reducing internal resistance and enabling high-rate performance. The $EMIM^+$ cation in the ionic liquid has the highest HOMO energy level among all components, making it highly resistant to oxidation. This provides the PHEC layer with excellent high-voltage stability and helps stabilize the cathode/electrolyte interface. More importantly, at the interface between PHEC and PAZT, a spontaneous ion bilayer forms due to differences in built-in electric field and ion solubility, with Cl^- and Zn^{2+} confined to their respective layers (Figure 10g). During charging and discharging, Zn^{2+} works on the anode side, while Cl^- works on the cathode side. They rely on the ionic double layer to complete charge transfer together, while avoiding side reactions and concentration polarization caused by ion crossing. The Zn||Zn symmetric battery prepared with the PHEC/PAZT solid electrolyte operated for over 13 300 h at 0.1 mA cm^{-2} at 25°C and for 3000 h at 60°C. In contrast, the Zn||Zn symmetric battery using a single PAZT solid electrolyte can only cycle for 1200 h, and obvious voltage fluctuations occur during the cycling process, indicating that its ability to suppress side reactions is relatively weak. Furthermore, the Zn||PANI full battery based on the PHEC/PAZT solid electrolyte was cycled 10000 times at 3 A g^{-1}, with a capacity retention rate of 75%.

In the same way, Liu et al. [270] adopted the superimposition pouring method to develop a hierarchical structure hydrogel electrolyte based on high water content polyacrylamide (PAM) hydrogel and low water content poly (sulfonated ethanol methacrylate) (PSBMA) hydrogel, aiming to reduce the corrosion of the zinc anode and enhance the proton storage capacity of the cathode (Figure 10h). In this structure, the low water content hydrogel electrolyte at the zinc anode side reduces the H^+ concentration at the interface, thus effectively inhibiting the corrosion of the zinc anode and the HER. In addition, the low water content zwitterionic hydrogel contributes to the dehydration of zinc ions

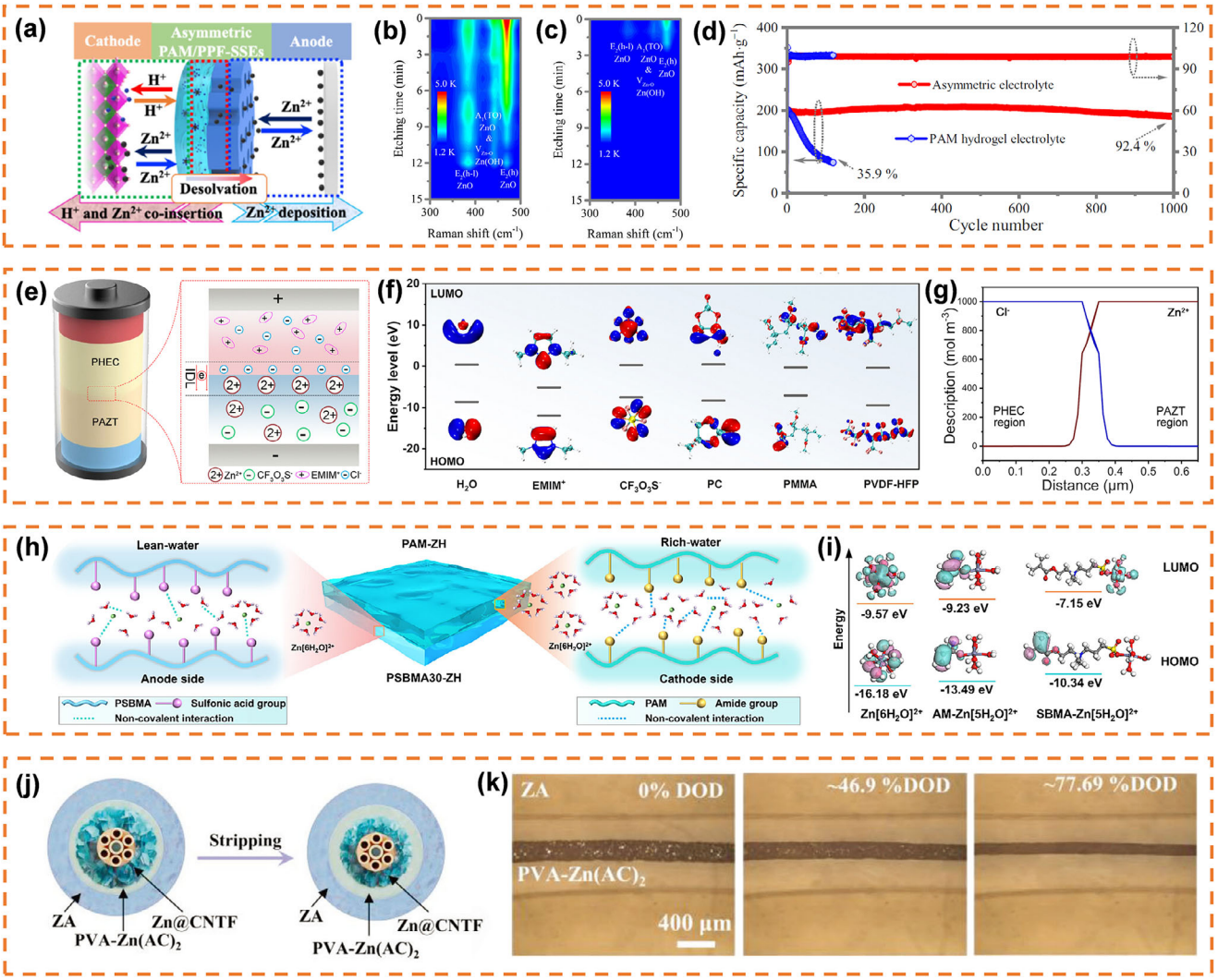

FIGURE 10 | (a) Schematic illustration of the PAM/PPF-SSEs asymmetric electrolyte. Raman spectra of Zn electrode with (b) hydrogel electrolyte and (c) PAM/PPF-SSEs asymmetric electrolyte. (d) The cyclic stability of Zn//MnO_2 full cells using PAM/PPF-SSEs asymmetric electrolyte and hydrogel electrolyte [267]. Copyright 2023, Springer Nature. (e) Schematic illustration of a battery model with the Janus quasi-solid-state electrolyte. (f) HOMO and LUMO energy of H_2O, $EMIM^+$, $CF_3O_3S^-$, PC, PMMA, and P(VDF-co-HFP). (g) Simulations reveal the quantitative concentration profiles of Zn^{2+} and Cl^- [269]. Copyright 2025, Royal Society of Chemistry. (h) Schematic diagram of the hierarchical structure hydrogel. (i) Lowest unoccupied molecular orbital and highest occupied molecular orbital of $Zn[6H_2O]^{2+}$, AM-$Zn[5H_2O]^{2+}$, and SBMA-$Zn[5H_2O]^{2+}$ [270]. Copyright 2025, Wiley-VCH. (j) The schematic illustration of as-made Zn@CNTF with a dual-layer gel electrolyte with lysine during the Zn stripping process. (k) Optical photographs of Zn@CNTF in a dual-layer gel electrolyte with lysine at different DOD of Zn metal [271]. Copyright 2024, Wiley-VCH.

and further inhibits the HER, which can be proved by the calculation of the molecular orbital energy level. The energy level difference of SBMA-$Zn[5H_2O]^{2+}$ is relatively small, and the unoccupied molecular orbital (LUMO) is also lower than that of $Zn[6H_2O]^{2+}$ and AM-$Zn[5H_2O]^{2+}$, indicating that water reduction at the PAMS30-ZH junction is not very favorable, thereby inhibiting HER behavior (Figure 10i). Moreover, the sulfonic acid group in PSBMA coordinates with Zn^{2+}, altering its solvation structure and reducing the desolvation energy barrier. And PSBMA preferentially adsorbs on the surface of the zinc anode, guiding Zn^{2+} to deposit at low surface energy sites and avoiding dendrite formation. The high water content hydrogel on the cathode side provides more H^+ for the electrochemical reaction, thus improving the energy storage capacity of the cathode. And high moisture content helps to buffer the volume change of the cathode during charging and discharging, improving structural stability. Based on the synergistic effect of the two hydrogel electrolytes, the prepared Zn||Zn symmetric battery was cycled for 1200 h at 80% DOD, and the Zn||VN full battery was cycled 4000 times at 2 A g^{-1}, with a capacity retention rate of 91.2%. In contrast, the Zn||Zn symmetrical battery cycle life of a single PAM hydrogel is only over 800 h, and the performance of the assembled Zn||VN full battery also deteriorates sharply.

On these basics, Li et al. [271] extended the Janus-type hydrogel electrolyte to the field of fiber-shaped batteries. They used ion crosslinking and confinement encapsulation strategies to prepare a double-layer gel electrolyte with a high-fluidity inner layer and a high-strength outer layer. Using this double-layer gel electrolyte with a fibrous zinc anode can solve the problems of interface separation and zinc dendrite growth in flexible batteries. In the preparation process, the polyvinyl alcohol-Zn acetate

[PVA-Zn$(AC)_2$] solution is first coated onto the fibrous Zn@carbon nanotube fiber [Zn@CNTF] electrode. Then the composite fiber is immersed in a sodium alginate (SA) solution, forming an outer layer of zinc alginate (ZA) through Zn^{2+} cross-linking, resulting in a double-layer gel electrolyte composed of an inner PVA-Zn$(AC)_2$ layer and an outer ZA layer (Figure 10j). The high-fluidity gel formed by PVA-Zn$(Ac)_2$ with a low degree of crosslinking enables dynamic filling of the interfacial gaps caused by zinc anode stripping or deformation, thereby maintaining intimate contact between the electrode and the electrolyte during the charge-discharge process (Figure 10k). Moreover, the outer layer of ZA forms a dense structure through electrostatic interactions, thereby exhibiting high mechanical strength, which can constrain the flow of the inner layer, prevent electrolyte leakage, and avoid short circuits caused by direct electrode contact. Meanwhile, lysine is incorporated into this dual-layer gel electrolyte as an additive. The amino (–NH_2) and carboxyl (–COOH) functional groups within its molecular structure can selectively adsorb onto the surface of the zinc anode, thereby forming a stable SEI film. In addition, the lowest unoccupied molecular orbital (LUMO) energy level of lysine is lower than that of water molecules, making it easier to bind with Zn^{2+}, thereby regulating the solvation structure of Zn^{2+} and inhibiting HER. Benefiting from the synergistic effect of inner and outer gel electrolytes combined with lysine additives, the fabricated fibrous Zn||Zn symmetric battery exhibited an extended cycle life exceeding 800 h under a current density of 1 mA cm^{-2} and a dynamic bending frequency of 0.1 Hz.

In conclusion, Janus-type hydrogel electrolyte achieves the advantages of functional synergy and spatial separation by building an asymmetric structure with different physical/chemical properties on both sides: one side is committed to promoting the uniform deposition of zinc ions to inhibit dendrites, and the other side focuses on regulating the solvation structure of $[Zn(H_2O)_6]^{2+}$ and inhibiting the dissolution of cathode materials to reduce side reactions, thereby simultaneously improving the cycle stability and reversibility of the battery. However, special attention should be paid to the chemical compatibility and stable bonding of the two interfaces during the construction process to avoid delamination failure caused by volume changes or increased interface impedance during charging and discharging. At the same time, it is necessary to accurately balance the ion conductivity and mechanical strength of the components on both sides to ensure the long-term stability of ion transport kinetics and interface contact.

7.2 | Gradient-Type Hydrogel Electrolyte

The gradient hydrogel electrolyte is different from the Janus electrolyte hydrogel mentioned above, and its internal composition presents a continuous gradient distribution without obvious mutation, which eliminates the clear interface in the Janus structure caused by sudden changes in the physical and chemical properties of the two components. This transition structure without mutation can achieve seamless connection of material physical and chemical properties such as ionic conductivity and mechanical modulus in space, bringing two key benefits: first, it can effectively avoid uneven zinc ion flow distribution, increased interface impedance, and interlayer delamination problems that may occur at the Janus interface due to modulus or conductivity mismatch, providing a more uniform dynamic environment for zinc ion deposition and fundamentally reducing the risk of local dendrite growth; Second, the gradient structure enables a precisely controlled functional transition from the zinc anode side, characterized by high modulus and strong suppression capability, to the cathode side, which exhibits high conductivity and efficient ion transport. This integrated gradient design ensures excellent dendrite suppression capability while providing better ion transport paths and interface stability, which is particularly beneficial for improving the cycle life and overall reliability of the battery at high rates. The constructed gradient-type hydrogels are of three types: electrolyte concentration gradient type, dispersoid concentration gradient type, and polymer backbone gradient distribution.

In high-concentration electrolytes, abundant zinc ions promote dense zinc deposition and enhance electrochemical stability by binding most solvent molecules into a solvation shell, minimizing free water. However, the poor wettability between high-concentration electrolytes and GF separators, along with a tendency for the electrolytes to become water-poor during circulation, hinders zinc ion transport and limits battery performance. In response to this issue, Lu et al. [272] proposed an electrolyte gradient strategy, which achieved dense and dendrite-free deposition of zinc by constructing a zinc ion concentration gradient from the zinc anode to the separator direction, significantly improving the cycle life of AZIBs (Figure 11a). This method involves coating a mixture of high-concentration $ZnSO_4$ electrolyte and carboxymethyl cellulose sodium (CMC) on the surface of a zinc anode (HCE@CMC). The high-concentration electrolytes provide sufficient Zn^{2+}, promote uniform nucleation and dense deposition, and inhibit dendrite formation (Figure 11b,c). CMC anchors high-concentration electrolytes on the zinc anode surface via water absorption and molecular chain structure, creating a stable concentration gradient. And the terminal oxygen atoms in CMC molecules can coordinate with water, reducing free water content and regulating Zn^{2+} solvation to promote dense deposition. On the contrary, filling the GF separator with low-concentration $ZnSO_4$ electrolyte ensures good wetting and ion migration, preventing polarization and dendrite growth due to ion depletion. The exchange current density of this electrolyte gradient system is higher than that of conventional electrolytes, indicating its faster zinc deposition kinetics. In Zn||Zn symmetrical batteries, batteries using 4 M@CMC|1 M|4 M@CMC gradient electrolytes cycled over 14 000 times (>8 months) at 5 mA cm^{-2}, far superior to conventional electrolytes.

As mentioned in section 2, using high dielectric performance materials as “electric field pumps” significantly enhances the vertical electric field strength on the electrode surface under the action of an external electric field, suppresses the horizontal electric field component, and eliminates the local growth of zinc dendrites caused by the tip effect. When incorporated into the gel electrolyte, it establishes a 3D, dynamic ion-regulating network that actively guides zinc ions toward uniform distribution along their migration pathway before reaching the electrode surface, thereby suppressing dendritic nucleation at its origin. For example, Wang et al. [273] constructed an asymmetric piezoelectric gradient polymer electrolyte based on PVDF-based polymer matrix (PVHF), and introduced piezoelectric ceramic

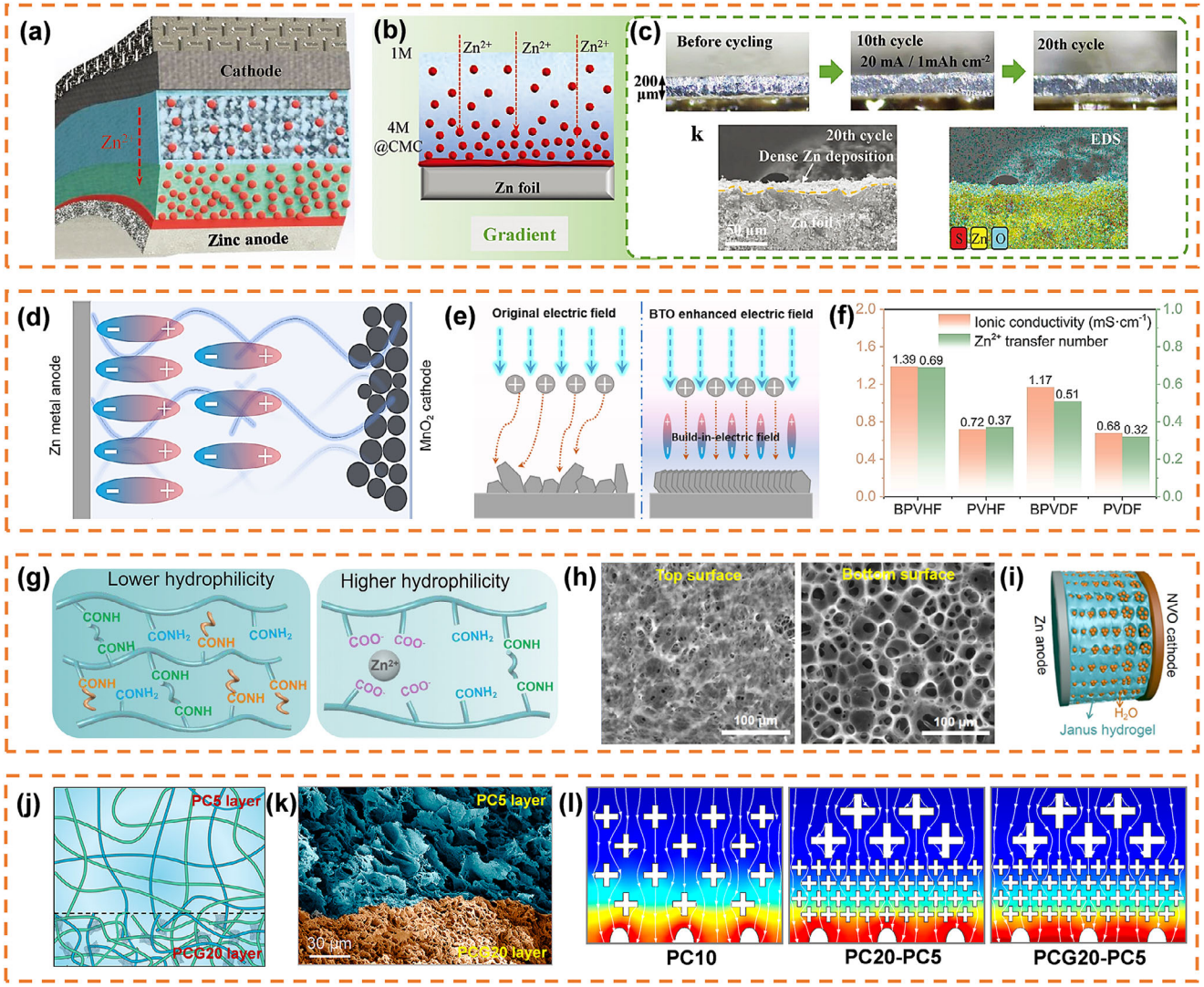

FIGURE 11 | (a) Schematic of gradient electrolyte strategy in the zinc-ion battery. (b) Schematic of zinc deposition with a gradient electrolyte. (c) In situ optical images, SEM image, and EDS image of dense zinc growth in 4 M@CMC|1 M ($ZnSO_4$) gradient electrolyte [272]. Copyright 2023, Wiley-VCH. (d) Illustration showing the design of Zn||MnO_2 batteries utilizing the BPVHF electrolyte with an asymmetric configuration. (e) Conceptual diagram illustrating the process of Zn^{2+} deposition. (f) Comparative analysis of ionic conductivity and Zn^{2+} transference numbers across various electrolyte systems [273]. Copyright 2025, Elsevier. (g) The distribution of functional groups on the hydrophilic and hydrophobic sides of the Janus PAZPM hydrogel electrolyte. (h) Top and bottom surface perspectives of the Janus PAZPM hydrogel electrolyte. (i) Illustration of the Zn||NVO full cell incorporating the Janus PAZPM hydrogel electrolyte featuring graded pore architecture [274]. Copyright 2024, Royal Society of Chemistry. (j) Schematic illustration of the PCG20-PC5 gradient-networked hydrogel electrolyte. (k) SEM image of the PCG20-PC5 hydrogel. (l) Simulated ionic field distributions for PC10, PC20-PC5, and PCG20-PC5 [275]. Copyright 2025, American Chemical Society.

barium titanate (BTO) nanofillers. This design introduces a built-in gradient electric field in the direction of electrolyte thickness, utilizing the electromagnetic properties of BTO to regulate zinc ion transport and interface dynamics (Figure 11d). On the zinc anode side, the spontaneous polarization of high-concentration BTO forms an internal electric field, guiding Zn^{2+} to migrate uniformly along the electric field lines (Figure 11e). The mechanical stress induced by dendritic growth activates the piezoelectric effect of BTO, thereby generating localized electric fields that enable real-time regulation of ion distribution and effectively suppress dendrite deterioration. On the contrary, the MnO_2 cathode surface contains a softer and higher polymer content phase with lower BTO content, which ensures better interface compatibility and lower contact resistance, achieving efficient ion transport without causing excessive polarization. Therefore, based on this asymmetric gradient polymer electrolyte, an ion conductivity of 1.39 mS cm^{-1} and a high zinc ion transfer number of 0.69 were achieved, which is superior to traditional solid electrolytes (Figure 11f). Thanks to this gradient electrolyte, the assembled Zn||Zn symmetric batteries exhibit excellent cycling stability and can sustain operation for over 1500 h, while Zn||MnO_2 full batteries demonstrate stable cycling performance after 1200 cycles.

The third method is to use two or more polymers to form an asymmetric gradient hydrogel electrolyte. The similarities with Janus-type hydrogel electrolyte mentioned above are that it adapts to the cathode and anode, respectively, according

to the water locking capacity, hydrophilicity, and porosity of different polymers, and cooperatively regulates the transfer and deposition of zinc ions. The difference is that all the polymers in the gradient hydrogel electrolyte run through the entire electrolyte in the thickness direction, presenting a continuous and gradual transition state, which is often more advantageous in alleviating interlayer stress concentration and ensuring continuous transition of ion flow. For example, Zhu et al. [274] innovatively designed an integrated Janus gradient hydrogel with two different hydrophilic surfaces and a gradient pore structure inside to meet the needs of the cathode and anode for different water content. The Janus gradient hydrogel is driven by the polarity difference of the mold. In detail, in an aqueous solution containing four organic monomers, the hydrophilic acrylamide (AM) and zinc acrylate (Zn-AC) monomers tend to diffuse towards glass surfaces with higher polarity, while hydrophobic monomers, such as N-isopropylacrylamide (NIPAM), tend to aggregate towards the hydrophobic PTFE surface (Figure 11g). During this process, the hydrophobic isopropyl group of NIPAM induces the polymer chains to coil tightly, thereby repelling water molecules and facilitating the formation of a compact pore structure. The hydrophilic groups ($-CONH_2$, $-COO^-$) of AM and Zn-AC extend the polymer chains to accommodate more aqueous solutions, forming a large pore structure (Figure 11h). In this gradient hydrogel, the hydrophobic surface is positioned next to the zinc metal anode. Its dense polymer chains and highly entangled hydrophobic segments effectively guide uniform and concentrated zinc deposition on the anode, while also reducing water activity and inhibiting water-induced corrosion through the formation of a dense polymer network and small pore structure. Furthermore, the high polymer density on the hydrophobic side endows the hydrogel with excellent mechanical strength, supporting the stability of the battery under extreme conditions such as bending or cutting. The hydrophilic surface next to the cathode facilitates hydrogen ion insertion. It also stabilizes water molecules through strong hydrogen and ionic bonds ($-COO^-$, $-NH_2$), buffers pH changes, and reduces cathodic dissolution by-products (Figure 11i). Moreover, the large pore structure on the hydrophilic side provides a fast ion transport channel with an ion conductivity of 17.0 mS cm^{-2}, nearly matching the symmetric hydrophilic gel (20.6 mS cm^{-2}), ensuring high rate performance of the battery. The AZIBs exhibit a high capacity of 475 mA h g^{-1} and excellent cycle stability of 88% capacity retention after 1000 cycles when employing this Janus gradient hydrogel electrolyte, significantly outperforming both symmetric hydrogel and liquid electrolytes.

To achieve higher performance goals, three different gradient designs can be coupled to comprehensively improve the overall performance of the AZIBs. For example, Wang et al. [275] drew inspiration from articular cartilage and integrated the network-forming capabilities of PVA and cellulose nanofibers (CNF), along with the dielectric properties of graphene oxide (GO), to develop a Janus-type hydrogel electrolyte featuring a gradient network structure and optimized interfacial chemistry (Figure 11j). In brief, the Janus-type hydrogel with the density difference between the upper and lower layers was prepared by adjusting the solid content of the pouring solution, combining the two-step pouring molding process and the freezing-thawing molding method (Figure 11k). Among these, the low-network-density polyvinyl alcohol/cellulose nanofiber (PC) hydrogel layer on the cathode side features a broad network of channels and a high water content, which facilitates the rapid transport of zinc ions. The high-network-density polyvinyl alcohol/cellulose/graphene oxide (PCG) hydrogel layer on the anode side features a dense network with abundant carboxyl and hydroxyl groups that desolvate zinc ions, reduce water molecule activity, homogenize ion flow, and improve mechanical strength (Figure 11l). In addition, the presence of polar oxygen-containing groups, such as carboxyl (–COOH) and hydroxyl (–OH) groups in GO within PCG, endows it with dielectric and negatively charged characteristics. These features reduce the binding energy between Zn^{2+} and water molecules, thereby enhancing the Zn^{2+} transference number and ionic conductivity in the hydrogel electrolyte. Thanks to its Janus-type gradient network structure and optimized interface chemistry, this hydrogel electrolyte exhibits excellent electrochemical stability and high-performance magnification. It allows Zn||Zn symmetric batteries to maintain stability for over 2200 h at 1 mA cm^{-2} and enhances the rate capability and safety of Zn-MnO_2 full batteries.

Along the same lines, Zhou et al. [276] constructed a double-layer hydrogel electrolyte with a spatial concentration gradient based on the regulation of different anions in the Hofmeister sequence on polymer solubility and crosslinking degree. Specifically, the process uses a cyclic freeze-thaw method to construct a dual crosslinked network consisting of PVA and hydroxyethyl cellulose (HEC) physically crosslinked. Zinc acetate ($Zn(OAc)_2$) is used as the salt solution, and the middle position characteristic of acetate ions (OAc^-) in the Hofmeister sequence is utilized to construct a high concentration layer on the zinc anode side and a low concentration layer on the cathode side, forming a continuous concentration gradient and hydrogen bond network gradient. The non-uniform structure restricts free water in local hydrogen bond traps at the molecular scale, while promoting rapid dehydration and transport of zinc ions, effectively suppressing HER and corrosion. A uniform ion flow guides zinc to deposit along the (002) crystal plane at the electrode interface, thereby suppressing dendrite growth and forming a flat crystal structure.

In conclusion, the gradient hydrogel electrolyte has constructed a smooth gradient distribution of physical and chemical properties, such as ionic conductivity and mechanical modulus, from anode to cathode through its continuously changing internal dispersion concentration. Its core advantage is that it can achieve spatially accurate matching of functions: the side close to the anode can be designed with a high modulus to mechanically inhibit dendritic growth, while the high concentration network helps guide the uniform flow of zinc ions. On the cathode side, it can be optimized for high ion conductivity to ensure fast reaction kinetics. This seamless transition structure can more effectively synergistically improve the cycle life and rate performance of the battery. However, the key to the construction of such electrolytes is to precisely control the formation and stability of the concentration gradient. It is necessary to ensure that the gradient structure can be accurately formed during the gel process and does not relax or migrate under long-term use. At the same time, it is necessary to optimize the ion transport path at the gradient interface to avoid new interface impedance or uneven ion flow caused by sudden property changes, which may lead to local deposition or corrosion.

8 | Summary and Prospects

In summary, AZIBs are a promising alternative to LIBs due to their high safety, low cost, and high energy density. However, practical applications of high-performance AZIBs are limited by issues such as dendrite growth, HER, corrosion, and passivation during electrochemical cycling. Among numerous solutions, interface regulation has become the most effective strategy to address these issues [49]. This review first systematically explores the formation mechanisms of zinc anode dendrites, hydrogen evolution reactions, and side reactions, and then lists various interface regulation methods to address these issues. In addition, to overcome the limitations of single interface regulation, this review emphasizes and provides examples of multiscale interfacial regulation strategies to synergistically address multiple challenges in zinc anodes, aiming to provide valuable insights into the synergistic effects of multiscale interfaces in electrode and electrolyte design. Firstly, four approaches for constructing multiple SEI layers on the surface of zinc anodes are summarized: the pre-construction method, the multiphase conversion method, the electrolyte additive-based in-situ construction method, and the eutectic electrolyte-based in-situ construction method. The respective advantages and limitations of each method are systematically analyzed. Furthermore, the protective interface on the surface of the zinc anode has been extended and systematically summarized at the molecular level. Subsequently, this review examines the design principles and regulatory mechanisms of multiscale interface layers for zinc powder anodes and zinc host anodes, to enable the development of zinc-based anodes capable of achieving high depths of discharge. Finally, this review summarizes the application of multiscale interfacial regulation strategies in AZIBs separators and hydrogel electrolytes, categorizing them primarily into Janus-type and gradient-type structures. We further discuss the respective advantages and limitations of these two configurations, along with key considerations for their design and implementation. Although significant progress has been achieved in enhancing the performance of zinc anodes through multiscale interfacial regulation strategies, further optimization remains necessary to fully realize their potential in AZIBs. This section discusses key challenges and outlines prospective research directions for advancing multiscale interfacial regulation approaches in zinc anode development (Scheme 4).

1. Prefabricated multi-layer coatings typically rely on physical or weak chemical interactions to adhere to the surface of zinc foil. During the zinc deposition/stripping process, cracking or interlayer delamination is prone to occur due to volume changes and mechanical stress, leading to the failure of protective functions. In addition, the total thickness of multi-layer coatings often reaches tens of micrometers, significantly reducing the energy density of batteries and limiting their application in high-energy demand scenarios. In the future, dynamic self-healing coating systems with strong interfacial bonding capabilities should be developed, such as introducing reversible covalent bonds or supramolecular interactions to enhance the structural integrity of coatings during cycling. At the same time, the design of nanoscale ultra-thin multifunctional composite coatings should be explored to achieve a balance between high ion conductivity and high mechanical strength.
2. The induction of multiphase transformation in single-layer coatings relies on controllable chemical reactions (such as displacement and decomposition) between the coating and zinc or electrolyte. The degree, uniformity, and kinetics of these reactions are influenced by various factors such as electrolyte composition, current density, and temperature, making it difficult to accurately control and leading to uneven interfacial layers or the formation of non-ideal products. In addition, the applicable precursor materials are limited, and the research and development barriers are high. Suggest combining DFT theoretical calculations with high-throughput experimental screening to develop precursor materials with clear reaction pathways and high selectivity. By optimizing the composition of the electrolyte and assisting with external fields such as thermal and electric fields, precise control of interface reaction kinetics and spatial distribution can be achieved, promoting the controllable preparation and practical application of such intelligent responsive interface layers.
3. When using electrolyte additives to construct a multi-layer SEI, it irreversibly consumes active Zn^{2+} ions and electrolyte during the first charge and discharge process, resulting in a decrease in initial coulombic efficiency and capacity loss of the battery, which is particularly unfavorable for high-energy density batteries. In addition, the continuous consumption of additives may weaken their long-term protective effects, and some additive molecules may cause environmental toxicity issues. In the future, efforts should be made to develop "zero consumption" or "low consumption" intelligent additives that can dynamically repair SEI during the cycling process without being continuously consumed. The research focus can be on the design of polymer additives with self-healing function or inorganic organic hybrid molecules that can form ultra-stable SEI on zinc surfaces, while paying close attention to the environmental friendliness and cost of additives.
4. The core challenge of using eutectic electrolytes to construct multi-layer interfacial layers in situ on the surface of zinc anodes lies in the precise control of the "bottom-up" assembly process. A stable chemical bond between the eutectic components and the zinc substrate is essential, not mere physical adsorption, to ensure interfacial structural integrity during cycling. In addition, the thickness and density of the interface layer need to reach an optimal balance point. An excessively thick interface layer can significantly increase ion migration resistance, while an excessively thin layer may lead to insufficient protection and fail to effectively suppress dendrite penetration and side reactions. Future research should focus on molecular design to regulate the functional groups of each molecule in eutectic components and their reactivity with zinc surfaces, in order to achieve controllable interfacial layer growth kinetics and thermodynamics. Develop eutectic systems with self-limiting growth characteristics, enabling them to automatically form multi-layer structures with optimal thickness, density, and uniformity. At the same time, advanced in-situ characterization techniques should be combined to monitor the formation and evolution process of the

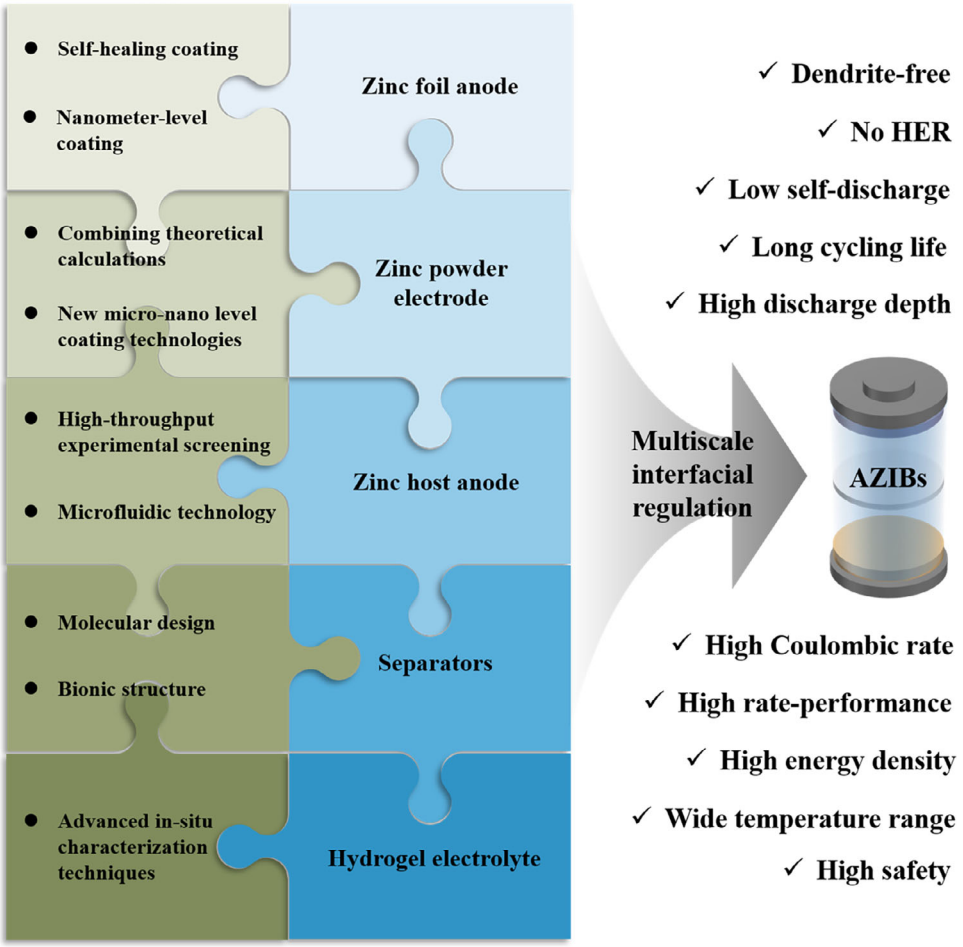

SCHEME 4 | Summary and prospects of the application of multiscale interfacial regulation in stabilizing the Zn anode.

interface layer in real time, providing theoretical guidance for the rational design of eutectic electrolyte formulations.

5. The main challenge in constructing protective layers at the molecular scale is how to achieve stable, oriented, and defect-free assembly of functional molecules on zinc surfaces. Functional molecules must be stably anchored on a zinc substrate through strong chemical bonds (such as Zn–S, Zn–N) to resist peeling forces during cycling. At the same time, the molecular structure needs to be carefully designed to form a dense and uniform coverage, prevent dendrite initiation from defects, and integrate efficient ion transport channels to avoid the formation of ion insulation barriers. In addition, the cost and environmental friendliness of the selected molecules are also practical considerations that cannot be ignored in the transition from laboratory to commercialization. Future research directions should focus on the "multi-component functional assembly" strategy, integrating molecules with complementary functions such as strong anchoring, rapid conduction, and hydrophobic isolation through intermolecular forces like a "puzzle" to construct a truly intelligent and robust artificial interface layer. We need to vigorously develop precise synthesis methods for interface molecular engineering to achieve precise control over molecular arrangement, stacking methods, and channel sizes. At the same time, inspiration should be drawn from the structure of natural biological membranes (such as cell membranes) to design biomimetic multi-molecular layer structures with ordered ion channels, opening up new avenues for achieving ultra-high rate and ultra-long lifespan zinc metal anodes.

It is particularly important to emphasize that in the repetitive cycle with high discharge depth, the stress on the interface protective layer continuously accumulates, posing a severe challenge to its structural stability, and the risk of instability and even collapse significantly increases. Therefore, future multi-scale interface layers must simultaneously meet two strict conditions: first, they must possess excellent mechanical adaptability and toughness, capable of withstanding the significant volume changes caused by the intense deposition/dissolution of zinc without cracking or peeling off. Second, it ensures uniform ion redistribution and deposition guidance. Even at high absolute deposition rates, it can still strongly regulate the zinc ion current, inhibit dendrite growth and side reactions, thereby achieving coordinated stability at both the physical barrier and electrochemical regulation levels.

6. It is extremely challenging to achieve a uniform, complete, and strong multi-layer coating on the surface of zinc powder particles with high specific surface area. Coating defects or particle agglomeration can lead to uneven zinc deposition, exacerbating dendrites and side reactions. During deep

discharge, the drastic changes in the volume of zinc powder can easily cause the collapse of the coating structure and functional failure. Develop new micro-nano level coating technologies, such as atomic layer deposition combined with molecular self-assembly, to achieve uniform coating of zinc powder surface with sub-nanometer precision. Meanwhile, a "soft hard" alternating structure coating with gradient modulus can be designed to better adapt to volume changes, and the three-dimensional conductive network can be utilized to enhance the structural stability and reaction reversibility of the zinc powder electrode.

7. When pre-constructing hollow structures as deposition carriers, if the mechanical strength of the hollow structure itself is insufficient, it is prone to rupture or collapse under the stress of repeated zinc deposition/dissolution. In addition, if the ion conductivity of the structure is poor, zinc ions will find it difficult to quickly enter the cavity, resulting in zinc preferentially depositing outside the structure and losing the meaning of spatial confinement. The precise control of cavity size and distribution is also a major preparation challenge. In the future, the focus should be on developing new hollow frame materials with high strength and ionic conductivity, such as COFs or composite ceramic materials. Through advanced imaging technology and simulation calculations, the relationship between cavity structure (size, shape, distribution) and zinc deposition behavior is accurately correlated to guide optimal structural design. At the same time, differential functional modifications should be applied to the inner and outer surfaces of the structure to achieve zincophilicity and hydrophobicity/inertness, respectively, in order to synergistically enhance performance.

8. There may be compatibility and adhesion issues between the functional layers of double-sided modified separators, which can lead to interlayer separation due to changes in electrode volume over long-term cycling, resulting in increased impedance and loss of function. In addition, the introduction of functional layers usually increases the total thickness of the separator and ion migration resistance, which may sacrifice the rate performance of the battery. The research direction should lean towards developing integrated Janus separators rather than simple physical stacking to enhance interlayer bonding. Functional layers can be directly constructed on substrates using grafting polymerization or in situ growth techniques. At the same time, it is necessary to carefully design the pore structure and chemical properties of each functional layer to ensure that it can selectively regulate ions without significantly increasing the overall impedance.

9. The preparation process of gradient structure separators is usually complex (such as requiring control of component settling, phase separation, etc.), making it difficult to achieve large-scale, low-cost continuous production. Unreasonable gradient design, such as excessive hydrophilic-hydrophobic transition or improper pore size gradient, may lead to uneven distribution of ion flow at the interface, and even trigger new local corrosion or dendrite growth points. Simple and controllable gradient-forming techniques should be developed, such as using electric and magnetic fields to drive the directional arrangement of nanoparticles or achieving continuous gradient changes in components through microfluidic technology. Combining finite element analysis to simulate the transport behavior of ions in different gradient structures, to reverse engineer the optimal gradient parameters. Developing gradient materials with dynamic adaptability to fine-tune their properties based on battery states is the forefront direction of the future.

10. The components on both sides of the Janus hydrogel usually have different swelling degrees, moduli, or chemical properties. Due to moisture migration or electrode volume changes during charging and discharging, it is easy to generate internal stress at the interface between the two layers, leading to delamination or increased interface impedance. The strong coupling relationship between the performance on both sides also makes independent optimization difficult. In the future, efforts should be made to design Janus hydrogels with chemical bonding interfaces, such as interpenetrating polymer networks or chemical reactions at the interface, to fundamentally solve the layering problem. Develop a dual network structure with a "soft hard" gradient or complementary performance to achieve synergistic suppression of anode side dendrites and high ion conductivity on the cathode side. For flexible devices, it is necessary to ensure that the overall electrolyte can maintain interface integrity under bending and stretching.

11. The core challenge of gradient hydrogels is the stability of their concentration gradient or network density gradient during long-term use and storage. The components may be gradually homogenized due to diffusion, leading to functional degradation. The precise control of gradient formation during the preparation process is also a major technical challenge. The research focus can be on using cross-linking density gradient or fixed charge density gradient to construct stable non-equilibrium structures, which are not easily relaxed due to simple diffusion. A novel bionic gradient hydrogel was developed to mimic the structural characteristics of biological tissues, such as cartilage, to achieve the optimal spatial distribution of mechanical and ion transport properties. Real-time monitoring of the evolution of gradient structures during battery operation using in-situ characterization techniques provides a direct basis for optimizing design.

In summary, while multiscale interfacial regulation of zinc anodes significantly enhances battery performance, significant challenges persist. These include limited long-term interfacial stability, compromised energy density, scalability of fabrication processes, and environmental compatibility. To address these issues, future research should prioritize in-situ and dynamic interfacial engineering, multi-scale theoretical modeling integrated with artificial intelligence, the development of sustainable materials, and system-level optimization. Such an integrated approach is indispensable for translating high-performance, long-life, and low-cost AZIBs from the laboratory to commercial viability.

Acknowledgements

The authors appreciate the financial support by National Natural Science Foundation of China (No. 22272150).

Conflicts of Interest

The authors declare no conflicts of interest.

Data Availability Statement

Research data are not shared.

References

1. Z. Feng, Y. Feng, F. Fan, et al., "Functionalization Design of Zinc Anode for Advanced Aqueous Zinc-Ion Batteries," *SusMat* 4 (2024): 184.

2. Y. Wang, Y. Kong, T. Zhang, C. Chen, H. Wang, and Y. Hu, "Fluorine-Functionalized Chemistry toward Stable Zn Anode in Aqueous Zn-Ion Batteries," *Advanced Energy Materials* 15 (2025): 2502353, https://doi.org/10.1002/aenm.202502353.

3. Y. Liu, J. Huang, X. Li, J. Li, J. Yang, and K. Cai, "MIL-100(V) Derived Porous Vanadium Oxide/Carbon Microspheres with Oxygen Defects and Intercalated Water Molecules as High-Performance Cathode for Aqueous Zinc Ion Battery," *Journal of Energy Chemistry* 90 (2024): 578–589, https://doi.org/10.1016/j.jechem.2023.11.029.

4. J. Du, Y. Han, H. Zhang, X. Gao, J. Guan, and A. Chen, "CoP_2O_6-Assisted Copper/Carbon Catalyst for Electrocatalytic Reduction of CO_2 to Formate," *ACS Nano* 17 (2023): 10055–10064, https://doi.org/10.1021/acsnano.2c12426.

5. J. Du, M. Sun, K. Zheng, and A. Chen, "Engineering Short-Range Ordered Mesoporous Carbon toward Balanced Activity-Stability in Oxygen Reduction," *Advanced Functional Materials* 36 (2025): 08058.

6. L.-F. Zhou, T. Du, J.-Y. Li, et al., "A Strategy for Anode Modification for Future Zinc-Based Battery Application," *Materials Horizons* 9 (2022): 2722–2751, https://doi.org/10.1039/D2MH00973K.

7. Y. Zhang, X. Zheng, N. Wang, et al., "Anode Optimization Strategies for Aqueous Zinc-Ion Batteries," *Chemical Science* 13 (2022): 14246–14263, https://doi.org/10.1039/D2SC04945G.

8. S. Liu, R. Zhang, C. Wang, et al., "Zinc Ion Batteries: Bridging the Gap from Academia to Industry for Grid-Scale Energy Storage," *Angewandte Chemie, International Edition* 63 (2024): 202400045.

9. Y. Zong, H. He, Y. Wang, et al., "Functionalized Separator Strategies toward Advanced Aqueous Zinc-Ion Batteries," *Advanced Energy Materials* 13 (2023): 2300403, https://doi.org/10.1002/aenm.202300403.

10. Z. Hu, F. Zhang, Y. Zhao, et al., *Advanced Materials* (2022): 34.

11. R. Qin, Y. Wang, L. Yao, et al., "Progress in Interface Structure and Modification of Zinc Anode for Aqueous Batteries," *Nano Energy* 98 (2022): 107333, https://doi.org/10.1016/j.nanoen.2022.107333.

12. X. Guo, Z. Zhang, J. Li, et al., "Alleviation of Dendrite Formation on Zinc Anodes via Electrolyte Additives," *ACS Energy Letters* 6 (2021): 395–403, https://doi.org/10.1021/acsenergylett.0c02371.

13. Z. Li, J. Tan, Y. Wang, et al., "Building Better Aqueous Zn-Organic Batteries," *Energy & Environmental Science* 16 (2023): 2398–2431, https://doi.org/10.1039/D3EE00211J.

14. Y. Liu, T. Wang, Y. Sun, et al., "Fast and Efficient in-Situ Construction of Low Crystalline PEDOT-Intercalated V_2O_5 Nanosheets for High-Performance Zinc-Ion Battery," *Chemical Engineering Journal* 484 (2024): 149501, https://doi.org/10.1016/j.cej.2024.149501.

15. L. Jia, H. Hu, X. Cheng, et al., "Toward Low-Temperature Zinc-Ion Batteries: Strategy, Progress, and Prospect in Vanadium-Based Cathodes," *Advanced Energy Materials* 14 (2023): 2304010, https://doi.org/10.1002/aenm.202304010.

16. Y. Liu, Y. Sun, J. Zhang, et al., "Electrochemically Inducing V2O5·nH2O Nanoarrays Vertically Growth on VSx Microrods for Highly Stable Zinc Ion Battery Cathode," *Nano Energy* 120 (2024): 109152, https://doi.org/10.1016/j.nanoen.2023.109152.

17. G. Li, L. Sun, S. Zhang, et al., "Developing Cathode Materials for Aqueous Zinc Ion Batteries: Challenges and Practical Prospects," *Advanced Functional Materials* 34 (2023): 2301291, https://doi.org/10.1002/adfm.202301291.

18. Y. Xu, J. Zhu, J. Feng, et al., "A Rechargeable Aqueous Zinc/Sodium Manganese Oxides Battery with Robust Performance Enabled by Na2SO4 Electrolyte Additive," *Energy Storage Materials* 38 (2021): 299–308, https://doi.org/10.1016/j.ensm.2021.03.019.

19. T. Zhou, B. Wu, C. Li, X. Zhang, W. Li, and H. Pang, "Advancements in Manganese-Based Cathode for Sustainable Energy Utilization," *Chemsuschem* 17 (2024): 202400890.

20. T. Zhou, L. Xie, Q. Han, et al., "Progress and Prospect of Vanadates as Aqueous zn-ion Batteries Cathodes," *Coordination Chemistry Reviews* 498 (2024): 215461, https://doi.org/10.1016/j.ccr.2023.215461.

21. Y. Bai, H. Zhang, W. Liang, C. Zhu, L. Yan, and C. Li, *Small* 20 (2023): 202306111.

22. J. Du, Y. Liu, M. Sun, J. Guan, A. Chen, and B. Han, "Highly Selective Oxygen Electroreduction to Hydrogen Peroxide on Sulfur-Doped Mesoporous Carbon," *Angewandte Chemie, International Edition* 64 (2025): 202503385.

23. J. Du, X. Peng, X. Gao, et al., "Engineering Three-Dimensional Interconnected Pores with Plentiful Edge Sites via a Confined Space for Enhanced Oxygen Reduction," *Nano Letters* 24 (2024): 12140–12147, https://doi.org/10.1021/acs.nanolett.4c02780.

24. C. Nie, G. Wang, D. Wang, et al., "Recent Progress on Zn Anodes for Advanced Aqueous Zinc-Ion Batteries," *Advanced Energy Materials* 13 (2023): 2300606, https://doi.org/10.1002/aenm.202300606.

25. J. Du, Q. Han, Y. Chen, M. Peng, L. Xie, and A. Chen, "Micro/Meso-Porous Double-Shell Hollow Carbon Spheres through Spatially Confined Pyrolysis for Supercapacitors and Zinc-Ion Capacitor," *Angewandte Chemie, International Edition* 63 (2024): 202411066.

26. Q. Zhang, Y. Su, Z. Shi, X. Yang, and J. Sun, "Artificial Interphase Layer for Stabilized Zn Anodes: Progress and Prospects," *Small* 18 (2022): 202203583.

27. X. Xu, X. Feng, M. Li, et al., "Overcoming Challenges: Extending Cycle Life of Aqueous Zinc-Ion Batteries at High Zinc Utilization through a Synergistic Strategy," *Small* 20 (2024): 2308273, https://doi.org/10.1002/smll.202308273.

28. W. Zhang, Y. Dai, R. Chen, et al., "Highly Reversible Zinc Metal Anode in a Dilute Aqueous Electrolyte Enabled by a pH Buffer Additive," *Angewandte Chemie, International Edition* 62 (2023): 202212695.

29. B. Niu, X. Jian, Z. Hu, P. Wang, and X. Wang, "Thermal Phase Transition Electrolyte for High-Temperature Aqueous Zinc-Metal Batteries," *Advanced Materials* 38 (2025): 14164.

30. Z. Zhao, J. Zhao, Z. Hu, et al., "Long-life and Deeply Rechargeable Aqueous Zn Anodes Enabled by a Multifunctional Brightener-inspired Interphase," *Energy & Environmental Science* 12 (2019): 1938–1949, https://doi.org/10.1039/C9EE00596J.

31. Z. Zhang, Y. Zhang, M. Ye, et al., *Angewandte Chemie, International Edition* (2023): 62.

32. M. Chen, W. Fu, C. Hou, Y. Zhu, and F. Meng, "Recent Functionalized Strategies of Metal-Organic Frameworks for Anode Protection of Aqueous Zinc-Ion Battery," *Small* 20 (2024): 2403724, https://doi.org/10.1002/smll.202403724.

33. L. Wang, S. Zhou, K. Yang, et al., "Screening Selection of Hydrogen Evolution-Inhibiting and Zincphilic Alloy Anode for Aqueous Zn Battery," *Advancement of Science* 11 (2024): 202307667.

34. Y. Gong, B. Wang, H. Ren, et al., "Recent Advances in Structural Optimization and Surface Modification on Current Collectors for High-Performance Zinc Anode: Principles, Strategies, and Challenges," *Nano-Micro Letters* 15 (2023): 208, https://doi.org/10.1007/s40820-023-01177-4.

35. G. Weng, Z. Dong, P. Xiang, et al., "Critical Criteria Depicting the Rational Design of Zn Anode Current Collector," *Advanced Functional Materials* 34 (2024): 2400839, https://doi.org/10.1002/adfm.202400839.

36. T. Liu, X. Dong, B. Tang, et al., "Engineering Electrolyte Additives for Stable Zinc-based Aqueous Batteries: Insights and Prospects," *Journal of Energy Chemistry* 98 (2024): 311–326, https://doi.org/10.1016/j.jechem.2024.06.036.

37. P. Wang, X. Xie, Z. Xing, et al., "Mechanistic Insights of Mg2+-Electrolyte Additive for High-Energy and Long-Life Zinc-Ion Hybrid Capacitors," *Advanced Energy Materials* 11 (2021): 2101158.

38. L. Li, S. Jia, S. Yue, et al., "Hydrogel-stabilized Zinc Ion Batteries: Progress and Outlook," *Green Chemistry* 26 (2024): 6404–6422, https://doi.org/10.1039/D4GC01465K.

39. Z. Hao, Y. Dai, X. Xu, et al., "Strategies for Addressing the Challenges of Aqueous Zinc Batteries Enabled by Functional Separators," *Journal of Materials Chemistry A* 11 (2023): 11031–11047, https://doi.org/10.1039/D3TA01706K.

40. S. Bai, Z. Huang, G. Liang, et al., "Electrolyte Additives for Stable Zn Anodes," *Advancement of Science* 11 (2023): 202304549.

41. S. Zheng, W. Zhao, J. Chen, X. Zhao, Z. Pan, and X. Yang, "2D Materials Boost Advanced Zn Anodes: Principles, Advances, and Challenges," *Nano-Micro Letters* 15: 46, https://doi.org/10.1007/s40820-023-01021-9.

42. Y. Dai, C. Zhang, X. Zhang, et al., "Interfacial Energy Storage in Aqueous Zinc-ion Batteries," *Energy & Environmental Science* 18 (2025): 9018–9030, https://doi.org/10.1039/D5EE03741G.

43. B. Li, X. Zhang, T. Wang, et al., "Interfacial Engineering Strategy for High-Performance Zn Metal Anodes," *Nano-Micro Letters* 14 (2021): 6, https://doi.org/10.1007/s40820-021-00764-7.

44. J. Yang, R. Zhao, Y. Wang, et al., "Insights on Artificial Interphases of Zn and Electrolyte: Protection Mechanisms, Constructing Techniques, Applicability, and Prospective," *Advanced Functional Materials* 33 (2023): 2213510, https://doi.org/10.1002/adfm.202213510.

45. J. Jiang, Z. Li, Z. Pan, et al., "Recent Progress and Prospects on Dendrite-free Engineerings for Aqueous Zinc Metal Anodes," *Energy Environ Mater* 6 (2022): 12410.

46. B. Ge, L. Hu, X. Yu, et al., "Engineering Triple-Phase Interfaces around the Anode toward Practical Alkali Metal–Air Batteries," *Advanced Materials* 36 (2024): 2400937, https://doi.org/10.1002/adma.202400937.

47. S.-J. Yang, L.-L. Zhao, Z.-X. Li, et al., "Achieving Stable Zn Anode via Artificial Interfacial Layers Protection Strategies toward Aqueous Zn-ion Batteries," *Coordination Chemistry Reviews* 517 (2024): 216044.

48. L. Li, Y. Zheng, J. Xu, et al., "Structural and Interfacial Engineering Strategies for Constructing Dendrite-Free Zinc Metal Anodes," *ACS Energy Letters* 9 (2024): 3269–3289, https://doi.org/10.1021/acsenergylett.4c01123.

49. P. A. Shinde, N. R. Chodankar, L. K. Shrestha, A. Al Ghaferi, E. Alhajri, and K. Ariga, "Stable and Dendrite-Free Zinc Metal Anodes via Interface Nanoarchitectonics for Aqueous Zinc-Ion Batteries," *Advanced Functional Materials* 35 (2025): 2424242, https://doi.org/10.1002/adfm.202424242.

50. H. Liu, Q. Zhou, Q. Xia, et al., "Interface Challenges and Optimization Strategies for Aqueous Zinc-ion Batteries," *Journal of Energy Chemistry* 77 (2023): 642–659, https://doi.org/10.1016/j.jechem.2022.11.028.

51. H. Jia, Z. Wang, B. Tawiah, et al., "Recent Advances in Zinc Anodes for High-performance Aqueous Zn-ion Batteries," *Nano Energy* 70 (2020): 104523, https://doi.org/10.1016/j.nanoen.2020.104523.

52. T. Wang, C. Li, X. Xie, et al., "Anode Materials for Aqueous Zinc Ion Batteries: Mechanisms, Properties, and Perspectives," *ACS Nano* 14 (2020): 16321–16347, https://doi.org/10.1021/acsnano.0c07041.

53. X. Liu, G. Wang, Z. Lv, A. Du, S. Dong, and G. Cui, "A Perspective on Uniform Plating Behavior of Mg Metal Anode: Diffusion Limited Theory versus Nucleation Theory," *Advanced Materials* 36 (2023): 202306395.

54. B. Sambandam, V. Mathew, F. Ahmad Nurul, S. Kim, M. Song, and J. Kim, "Aqueous Rechargeable Zinc–Metal Batteries: a Critical Analysis," *ACS Energy Letters* 9 (2024): 3058–3065, https://doi.org/10.1021/acsenergylett.4c00792.

55. C. Xie, S. Liu, Z. Yang, et al., "Discovering the Intrinsic Causes of Dendrite Formation in Zinc Metal Anodes: Lattice Defects and Residual Stress," *Angewandte Chemie, International Edition* 62 (2023): 202218612.

56. J. Zhang, J. Sun, D. Yang, et al., "Trade-Off between Rough and Smooth Electrode Surfaces toward Stable Zn Stripping/Plating in Aqueous Electrolytes," *Nano Letters* 24 (2024): 688–695, https://doi.org/10.1021/acs.nanolett.3c03983.

57. F. Tao, Y. Liu, X. Ren, et al., "Different Surface Modification Methods and Coating Materials of Zinc Metal Anode," *Journal of Energy Chemistry* 66 (2022): 397–412, https://doi.org/10.1016/j.jechem.2021.08.022.

58. L. Kang, M. Cui, F. Jiang, et al., "Nanoporous CaCO 3 Coatings Enabled Uniform Zn Stripping/Plating for Long-Life Zinc Rechargeable Aqueous Batteries," *Advanced Energy Materials* 8 (2018): 1801090, https://doi.org/10.1002/aenm.201801090.

59. K. Zhao, C. Wang, Y. Yu, et al., "Ultrathin Surface Coating Enables Stabilized Zinc Metal Anode," *Adv Mater Interfaces* 5 (2018): 201800848.

60. X. Luo, Q. Nian, Q. Dong, et al., "Anti-Swelling Supramolecule-Crosslinked Hydrogel Interphase for Stable Zn Metal Anodes," *Advanced Energy Materials* 15 (2024): 2403187, https://doi.org/10.1002/aenm.202403187.

61. Q. Cheng, T. Jin, Y. Miao, et al., "Stabilizing Lithium Plating in Polymer Electrolytes by Concentration-polarization-induced Phase Transformation," *Joule* 6 (2022): 2372–2389, https://doi.org/10.1016/j.joule.2022.08.001.

62. Y. Li, C. B. Musgrave, M. Y. Yang, et al., "The Zn Deposition Mechanism and Pressure Effects for Aqueous Zn Batteries: a Combined Theoretical and Experimental Study," *Advanced Energy Materials* 14 (2023): 2303047, https://doi.org/10.1002/aenm.202303047.

63. C. Lin, L. Zeng, M. Liu, et al., "Dynamic Regulation for the Well-Distribution of Electrons and Zn2+ Ions Achieving Uniform Zn Redox in Ah-Scale Pouch Cells," *Advanced Materials* 37 (2025): 11484.

64. M. Zhu, J. Hu, Q. Lu, et al., "A Patternable and in Situ Formed Polymeric Zinc Blanket for a Reversible Zinc Anode in a Skin-Mountable Microbattery," *Advanced Materials* 33 (2021): 202007497.

65. Y. Jiao, F. Li, X. Jin, et al., "Engineering Polymer Glue towards 90% Zinc Utilization for 1000 H to Make High-Performance Zn-Ion Batteries," *Advanced Functional Materials* 31 (2021): 2107652, https://doi.org/10.1002/adfm.202107652.

66. X. Zhang, J. Li, D. Liu, et al., "Ultra-long-life and Highly Reversible Zn Metal Anodes Enabled by a Desolvation and Deanionization Interface Layer," *Energy & Environmental Science* 14 (2021): 3120–3129, https://doi.org/10.1039/D0EE03898A.

67. Y. Cui, Q. Zhao, X. Wu, et al., "An Interface-Bridged Organic–Inorganic Layer That Suppresses Dendrite Formation and Side Reactions for Ultra-Long-Life Aqueous Zinc Metal Anodes," *Angewandte Chemie International Edition* 59 (2020): 16594–16601, https://doi.org/10.1002/anie.202005472.

68. Y. Wang, Z. Deng, B. Luo, et al., "Highly Reversible Zn Metal Anodes Realized by Synergistically Enhancing Ion Migration Kinetics and

Regulating Surface Energy," *Advanced Functional Materials* 32 (2022): 2209028, https://doi.org/10.1002/adfm.202209028.

69. Z. Cao, X. Zhu, D. Xu, et al., "Eliminating Zn Dendrites by Commercial Cyanoacrylate Adhesive for Zinc Ion Battery," *Energy Storage Materials* 36 (2021): 132–138, https://doi.org/10.1016/j.ensm.2020.12.022.

70. R. Zhang, T. Shui, A. Li, et al., "Novel in Situ SEI Fabrication on Zn Anodes for Ultra-high Current Density Tolerance Enabled by Electrical Excitation–conjugation of Iminoacetonitriles," *Energy & Environmental Science* 18 (2025): 1011–1026, https://doi.org/10.1039/D4EE03624G.

71. X. Lu, L. Chen, W. Li, et al., "Accelerating Desolvation and Constructing Dual-Storage Channels for Zn2+ by Ligand Field Engineering of Polar Organic Molecules for High-Performance Zinc-Ion Batteries," *Advanced Functional Materials* 36 (2025): 13457.

72. J. Li, A. Azizi, S. Zhou, et al., "Hydrogel Polymer Electrolytes toward Better Zinc-ion Batteries: a Comprehensive Review," *eScience* 5 (2025): 100294.

73. H. Gan, J. Wu, F. Zhang, R. Li, and H. Liu, "Uniform Zn2+ Distribution and Deposition Regulated by Ultrathin Hydroxyl-rich Silica Ion Sieve in Zinc Metal Anodes," *Energy Storage Materials* 55 (2023): 264–271, https://doi.org/10.1016/j.ensm.2022.11.044.

74. P. Liu, W. Liu, Y. Huang, P. Li, J. Yan, and K. Liu, "Mesoporous Hollow Carbon Spheres Boosted, Integrated High Performance Aqueous Zn-Ion Energy Storage," *Energy Storage Materials* 25 (2020): 858–865, https://doi.org/10.1016/j.ensm.2019.09.004.

75. Y. Mu, Z. Li, B.-K. Wu, et al., "3D hierarchical Graphene Matrices Enable Stable Zn Anodes for Aqueous Zn Batteries," *Nature Communications* 14 (2023): 4205, https://doi.org/10.1038/s41467-023-39947-8.

76. X. Pu, B. Jiang, X. Wang, et al., "High-Performance Aqueous Zinc-Ion Batteries Realized by MOF Materials," *Nano-Micro Letters* 12 (2020): 152, https://doi.org/10.1007/s40820-020-00487-1.

77. Y. Wang, X. Jiang, W. Liang, et al., "Directionally Modulated Zinc Deposition by a Robust Zincophilic Cu-Phthalocyanine Protective Layer in Dendrite-Free Aqueous Zinc Ion Batteries," *Advanced Materials* 37 (2025): 202503086.

78. Y. Wang, T. Pan, S. Zhang, Q. Li, and H. Pang, "MOF-based Electrode Materials for Aqueous Zinc-ion Batteries: Design Strategy and Future Challenges," *Inorganic Chemistry Frontiers* 12 (2025): 2988–3017, https://doi.org/10.1039/D5QI00159E.

79. J. Zheng, Z. Huang, F. Ming, et al., "Surface and Interface Engineering of Zn Anodes in Aqueous Rechargeable Zn-Ion Batteries," *Small* 18 (2022): 202200006.

80. H. Yu, S. Sun, M. Wu, C. Yuan, X. Yang, and L. Yu, *Advanced Materials* (2025): 17197.

81. D. Wang, Y. Li, G. Zhang, et al., "Invoking Hybrid-Ion Correlation Electrochemistry to Enable Optimal Aqueous Zn-Ion Batteries," *Advanced Materials* 37 (2025): 202511339.

82. D. Du, L. Zeng, N. Lan, et al., "Understanding and Mastering Multiphysical Fields toward Dendrite-Free Aqueous Zinc Batteries," *Advanced Energy Materials* 14 (2024): 2403153, https://doi.org/10.1002/aenm.202403153.

83. F. Liu, Y. Zhang, H. Liu, et al., "Advances of Nanomaterials for High-Efficiency Zn Metal Anodes in Aqueous Zinc-Ion Batteries," *ACS Nano* 18 (2024): 16063–16090, https://doi.org/10.1021/acsnano.4c06008.

84. N. Zhang, S. Huang, Z. Yuan, J. Zhu, Z. Zhao, and Z. Niu, "Direct Self-Assembly of MXene on Zn Anodes for Dendrite-Free Aqueous Zinc-Ion Batteries," *Angewandte Chemie International Edition* 60 (2020): 2861–2865, https://doi.org/10.1002/anie.202012322.

85. Q. Lu, C. Liu, Y. Du, et al., "Uniform Zn Deposition Achieved by Ag Coating for Improved Aqueous Zinc-Ion Batteries," *ACS Applied Materials & Interfaces* 13 (2021): 16869–16875, https://doi.org/10.1021/acsami.0c22911.

86. M. Qiu, D. Wang, B. Tawiah, H. Jia, B. Fei, and S. Fu, "Constructing PEDOT:PSS/Graphene Sheet Nanofluidic Channels to Achieve Dendrite-free Zn Anode," *Composites Part B: Engineering* 215 (2021): 108798, https://doi.org/10.1016/j.compositesb.2021.108798.

87. S. Zhou, Y. Wang, H. Lu, et al., "Anti-Corrosive and Zn-Ion-Regulating Composite Interlayer Enabling Long-Life Zn Metal Anodes," *Advanced Functional Materials* 31 (2021): 2104361, https://doi.org/10.1002/adfm.202104361.

88. Z. Wen, Z. Hu, X. Wang, et al., "Weakening the Space Charge Layer Effect through Tethered Anion Electrolyte and Piezoelectric Effect toward Ultra-Stable Zinc Anode," *Advanced Materials* 36 (2024): 202407390.

89. Y. Li, B. Ping, J. Qu, et al., "Constructing Autoregulative Electric Double Layer through Dielectric Effect toward Fast Charging Zinc Metal Anode," *Advanced Energy Materials* 15 (2025): 2405804, https://doi.org/10.1002/aenm.202405804.

90. K. Zhang, C. Li, J. Liu, S. Zhang, M. Wang, and L. Wang, *Small* 20 (2023): 202306406.

91. Q. Zhang, J. Luan, Y. Tang, X. Ji, and H. Wang, "Interfacial Design of Dendrite-Free Zinc Anodes for Aqueous Zinc-Ion Batteries," *Angewandte Chemie International Edition* 59 (2020): 13180–13191, https://doi.org/10.1002/anie.202000162.

92. M. Wang, Y. Meng, K. Li, et al., "Toward Dendrite-free and Anti-corrosion Zn Anodes by Regulating a Bismuth-based Energizer," *eScience* 2 (2022): 509–517.

93. M. Liu, K. Yang, Q. Xie, et al., "Operando Evolution of a Hybrid Metallic Alloy Interphase for Reversible Aqueous Zinc Batteries," *Angewandte Chemie, International Edition* 64 (2025): 202416047.

94. Q. Wen, H. Fu, C. Sun, et al., "Buried Interface Engineering towards Stable Zinc Anodes for High-performance Aqueous Zinc-ion Batteries," *Science Bulletin* 70 (2025): 518–528, https://doi.org/10.1016/j.scib.2024.12.017.

95. R. Zhao, X. Dong, P. Liang, et al., "Prioritizing Hetero-Metallic Interfaces via Thermodynamics Inertia and Kinetics Zincophilia Metrics for Tough Zn-Based Aqueous Batteries," *Advanced Materials* 35 (2023): 202209288.

96. H. Li, R. Zhao, W. Zhou, et al., "Trade-off between Zincophilicity and Zincophobicity: toward Stable Zn-Based Aqueous Batteries," 3 (2023): 2107–2116.

97. J. Hao, X. Li, S. Zhang, et al., "Designing Dendrite-Free Zinc Anodes for Advanced Aqueous Zinc Batteries," *Advanced Functional Materials* 30 (2020): 2001263, https://doi.org/10.1002/adfm.202001263.

98. L. Ren, Z. Hu, C. Peng, et al., "Suppressing Metal Corrosion through Identification of Optimal Crystallographic Plane for Zn Batteries," *PNAS* 121 (2024): 2309981121.

99. X. Yang, Z. Dong, G. Weng, et al., "Crystallographic Manipulation Strategies toward Reversible Zn Anode with Orientational Deposition," *Advanced Energy Materials* 14 (2024): 2401293, https://doi.org/10.1002/aenm.202401293.

100. Z. Peng, X. Shen, B. Li, et al., "Comprehensive Crystallographic Engineering for High-efficiency and Durable Zinc Metal Anodes," *Progress in Materials Science* 152 (2025): 101453, https://doi.org/10.1016/j.pmatsci.2025.101453.

101. T. Wei, H. Zhang, Y. Ren, et al., "Building near-Unity Stacked (002) Texture for High-Stable Zinc Anode," *Advanced Functional Materials* 34 (2023): 2312506, https://doi.org/10.1002/adfm.202312506.

102. Y. Zou, X. Yang, L. Shen, et al., "Emerging Strategies for Steering Orientational Deposition toward High-performance Zn Metal Anodes," *Energy & Environmental Science* 15 (2022): 5017–5038, https://doi.org/10.1039/D2EE02416K.

103. J. Zheng, Q. Zhao, T. Tang, et al., "Reversible Epitaxial Electrodeposition of Metals in Battery Anodes," *Science* 366 (2019): 645–648, https://doi.org/10.1126/science.aax6873.

104. H. Liu, Z. Xu, B. Cao, et al., "Marangoni-Driven Self-Assembly MXene as Functional Membrane Enables Dendrite-Free and Flexible Zinc–Iodine Pouch Cells," *Advanced Energy Materials* 14 (2024): 2400318, https://doi.org/10.1002/aenm.202400318.

105. Y. Wang, T. Ren, Z. Wang, et al., "Enabling and Boosting Preferential Epitaxial Zinc Growth via Multi-Interface Regulation for Stable and Dendrite-Free Zinc Metal Batteries," *Advanced Energy Materials* 14 (2024): 2400613, https://doi.org/10.1002/aenm.202400613.

106. Z. Yi, J. Liu, S. Tan, et al., *Advanced Materials* 34 (2022): 202203835.

107. Z. Hao, Y. Zhang, Z. Hao, et al., "Metal Anodes with Ultrahigh Reversibility Enabled by the Closest Packing Crystallography for Sustainable Batteries," *Advanced Materials* 35 (2023): 2209985, https://doi.org/10.1002/adma.202209985.

108. W. Yuan, X. Nie, G. Ma, et al., "Realizing Textured Zinc Metal Anodes through Regulating Electrodeposition Current for Aqueous Zinc Batteries," *Angewandte Chemie, International Edition* 62 (2023): 202218386.

109. X. Yang, C. Li, Z. Sun, et al., "Interfacial Manipulation via in Situ Grown ZnSe Cultivator toward Highly Reversible Zn Metal Anodes," *Advanced Materials* 33 (2021): 202105951.

110. K. K. Sonigara, J. V. Vaghasiya, and M. Pumera, "Corrosion-Resistant Shape-Programmable Zn–I2 Battery," *Advanced Energy Materials* (2024): 2401321.

111. L. Chang, J. Li, Q. Sun, X. Liu, X. Lu, and H. Cheng, *Small* (2024): 202408124.

112. Z. Chen, Q. Wu, X. Han, et al., "Converting Commercial Zn Foils into Single (002)-Textured Zn with Millimeter-Sized Grains for Highly Reversible Aqueous Zinc Batteries," *Angewandte Chemie, International Edition* 63 (2024): 202401507.

113. J. Zheng, Y. Deng, J. Yin, et al., *Advanced Materials* 34 (2021): 202106867.

114. Z. Chen, Y. Wang, Q. Wu, et al., "Grain Boundary Filling Empowers (002)-Textured Zn Metal Anodes with Superior Stability," *Advanced Materials* 36 (2024): 2411004, https://doi.org/10.1002/adma.202411004.

115. J. Cao, X. Wang, S. Qian, et al., "De-Passivation and Surface Crystal Plane Reconstruction via Chemical Polishing for Highly Reversible Zinc Anodes," *Advanced Materials* 36 (2024): 2410947, https://doi.org/10.1002/adma.202410947.

116. M. Zhou, Z. Tong, H. Li, et al., "Regulating Preferred Crystal Plane with Modification of Exposed Grain Boundary toward Stable Zn Anode," *Advanced Functional Materials* 35 (2024): 2412092, https://doi.org/10.1002/adfm.202412092.

117. D. Xu, B. Chen, X. Ren, et al., "Selectively Etching-off the Highly Reactive (002) Zn Facet Enables Highly Efficient Aqueous Zinc-metal Batteries," *Energy & Environmental Science* 17 (2024): 642–654, https://doi.org/10.1039/D3EE02522E.

118. S. La, Y. Gao, Q. Cao, et al., "A Thermal Transfer-enhanced Zinc Anode for Stable and High-energy-density Zinc-ion Batteries," *Matter* 8 (2025): 102013, https://doi.org/10.1016/j.matt.2025.102013.

119. J. Chen, W. Zhao, J. Jiang, et al., "Challenges and Perspectives of Hydrogen Evolution-free Aqueous Zn-Ion Batteries," *Energy Storage Materials* 59 (2023): 102767, https://doi.org/10.1016/j.ensm.2023.04.006.

120. H. Peng, D. Wang, F. Zhang, et al., "Improvements and Challenges of Hydrogel Polymer Electrolytes for Advanced Zinc Anodes in Aqueous Zinc-Ion Batteries," *ACS Nano* 18 (2024): 21779–21803, https://doi.org/10.1021/acsnano.4c06502.

121. C. Zhu, P. Li, G. Xu, H. Cheng, and G. Gao, "Recent Progress and Challenges of Zn Anode Modification Materials in Aqueous Zn-ion Batteries," *Coordination Chemistry Reviews* 485 (2023): 215142, https://doi.org/10.1016/j.ccr.2023.215142.

122. A. Rana, K. Roy, J. N. Heil, et al., "Realizing the Kinetic Origin of Hydrogen Evolution for Aqueous Zinc Metal Batteries," *Advanced Energy Materials* 14 (2024): 2402521, https://doi.org/10.1002/aenm.202402521.

123. X. Chen, X. Xie, P. Ruan, S. Liang, W.-Y. Wong, and G. Fang, "Thermodynamics and Kinetics of Conversion Reaction in Zinc Batteries," *ACS Energy Letters* 9 (2024): 2037–2056, https://doi.org/10.1021/acsenergylett.4c00450.

124. Y. Aniskevich and S.-T. Myung, "Gains and Losses in Zinc-ion Batteries by Proton- and Water-assisted Reactions," *Chemical Society Reviews* 54 (2025): 4531–4566, https://doi.org/10.1039/D4CS00810C.

125. Z. Wang, L. Bai, H. Fan, Y. Wang, and W. Liu, "Solvation Strategies in Various Electrolytes for Advanced Zinc Metal Anode," *Journal of Energy Chemistry* 94 (2024): 740–757, https://doi.org/10.1016/j.jechem.2024.03.021.

126. C. Li, X. Xie, S. Liang, and J. Zhou, "Issues and Future Perspective on Zinc Metal Anode for Rechargeable Aqueous Zinc-Ion Batteries," *ENERGY & ENVIRONMENTAL MATERIALS* 3 (2020): 146–159, https://doi.org/10.1002/eem2.12067.

127. J. Zhang, L. Mao, Z. Xia, M. Fan, Y. Deng, and Z. Chen, "Zincophilic Design for Highly Stable and Dendrite-Free Zinc Metal Anodes in Aqueous Zinc-Ion Batteries," *Advanced Functional Materials* 35 (2024): 2412547, https://doi.org/10.1002/adfm.202412547.

128. L. F. Shen, B. A. Lu, Y. Y. Li, et al., "Interfacial Structure of Water as a New Descriptor of the Hydrogen Evolution Reaction," *Angewandte Chemie International Edition* 59 (2020): 22397–22402, https://doi.org/10.1002/anie.202007567.

129. Y.-Q. Liu, Y.-H. Song, G.-D. Yang, et al., "Construction of Hydrophilic and Hydrophobic Hybrid Interface to Achieve Controlled Zinc Deposition for Aqueous Zn-ion Batteries," *Energy Storage Materials* 72 (2024): 103761, https://doi.org/10.1016/j.ensm.2024.103761.

130. W. Zhou, Z. Chen, S. Zhao, and S. Chen, "Superhydrophobic and Highly Flexible Artificial Solid Electrolyte Interphase Inspired by Lotus Effect toward Highly Stable Zn Anode," *Advanced Functional Materials* 34 (2024): 2409520, https://doi.org/10.1002/adfm.202409520.

131. G. Liu, Y. Tang, Y. Wei, et al., "Hydrophobic Ion Barrier-Enabled Ultradurable Zn (002) Plane Orientation towards Long-Life Anode-Less Zn Batteries," *Angewandte Chemie, International Edition* 63 (2024): 202407639.

132. L. Li, Y. Duan, Y. Cheng, P. Meng, W.-J. Jiang, and Q. Liang, "Bottom-up Dense Zinc Electrodeposition Mediated by Hydrophobic Redox-active Coating for Ultralong-life Aqueous Zn-metal Batteries," *eScience* (2025): 100458.

133. B. Zhang, Y. Huang, S. Gao, et al., "Uncovering Diverse Roles of Zincophilic and Hydrophobic Interactions at Composite Interfaces to Enhance the Longevity of Zinc-ion Batteries," *Journal of Energy Chemistry* 107 (2025): 908–918, https://doi.org/10.1016/j.jechem.2025.05.017.

134. W. J. Kim, J. W. Choi, H. J. Lee, et al., "Ionically Cross-Linked Composite Hydrogel Modulating an Electrical Double Layer on Zn Metal Anodes for Enhanced Kinetics and Stability," *Advanced Energy Materials* 15 (2025): 2501610, https://doi.org/10.1002/aenm.202501610.

135. J. Yan, J. Qian, Y. Wang, et al., "Biomass-Derived Polyanionic Interface Modulates the Electrical Double Layer to Achieve Ultrareversible Zinc Metal Anodes," *Advanced Energy Materials* 15 (2025): 04350, https://doi.org/10.1002/aenm.202504350.

136. D. Lin, Y. Lin, R. Pan, et al., "Water-Restrained Hydrogel Electrolytes with Repulsion-Driven Cationic Express Pathways for Durable Zinc-Ion Batteries," *Nano-Micro Letters* 17 (2025): 193, https://doi.org/10.1007/s40820-025-01704-5.

137. J. Xu, P. Han, Y. Jin, et al., "Hybrid Molecular Sieve-Based Interfacial Layer with Physical Confinement and Desolvation Effect for Dendrite-free Zinc Metal Anodes," *ACS Nano* 18 (2024): 18592–18603, https://doi.org/10.1021/acsnano.4c04632.

138. C. Zhao, Y. Lin, Q. Lin, et al., "C-P/C=O Bonds Assisted Desolvation Effect in Ultra-micropores Carbon for Boosting Zn-ion Storage Capability," *Energy Storage Materials* 58 (2023): 332–343, https://doi.org/10.1016/j.ensm.2023.03.039.

139. X. Liu, Y. Guo, F. Ning, et al., "Fundamental Understanding of Hydrogen Evolution Reaction on Zinc Anode Surface: a First-Principles Study," *Nano-Micro Letters* 16 (2024): 111, https://doi.org/10.1007/s40820-024-01337-0.

140. X. Bu, M. Li, Z. Liu, S. Liang, and G. Fang, "In-situ Alloying Interface Inducing Zn(002) Texture towards Stable High-utilization Zinc Anodes," *Advanced Powder Materials* 4 (2025): 100332, https://doi.org/10.1016/j.apmate.2025.100332.

141. J. Sun, X. Zheng, K. Li, et al., "Scalable Production of Hydrogen Evolution Corrosion Resistant Zn-Al Alloy Anode for Electrolytic MnO2/Zn Batteries," *Energy Storage Materials* 54 (2023): 570–578, https://doi.org/10.1016/j.ensm.2022.10.059.

142. Y. Gao, M. Wang, H. Wang, et al., "Kinetic and Thermodynamic Synergy of Organic Small Molecular Additives Enables Constructed Stable Zinc Anode," *Journal of Energy Chemistry* 84 (2023): 62–72, https://doi.org/10.1016/j.jechem.2023.05.021.

143. W. Nie, H. Cheng, Q. Sun, et al., *Small Meth* 8 (2023): 202201572.

144. Y. Shi, L. Li, C. Tan, et al., ""Framework Channel Catalysis": a Multiphase Synergistic Zn-based Coating Strategy for High-performance Zinc-ion Batteries," *Chemical Engineering Journal* 519 (2025): 165581, https://doi.org/10.1016/j.cej.2025.165581.

145. B. Sun, P. Wang, L. Yang, X. Wei, Y. Jin, and H. Wu, "Rational Design of an Interfacial Bilayer for Aqueous Dendrite-Free Zinc Anodes," *ACS Applied Materials & Interfaces* 14 (2021): 954–960, https://doi.org/10.1021/acsami.1c19438.

146. L. Han, Y. Guo, F. Ning, et al., "Lotus Effect Inspired Hydrophobic Strategy for Stable Zn Metal Anodes," *Advanced Materials* 36 (2023): 2308086, https://doi.org/10.1002/adma.202308086.

147. Y. Zhang, Z. Hu, Y. Bi, et al., "Epitaxial Zn (002) Growth Directed by Cu (111): a Dual-layer Strategy toward Stable and Reversible Zn Metal Anodes," *Energy Storage Materials* 79 (2025): 104366, https://doi.org/10.1016/j.ensm.2025.104366.

148. S. Wang, Z. Yang, B. Chen, et al., "A Highly Reversible, Dendrite-free Zinc Metal Anodes Enabled by a Dual-layered Interface," *Energy Storage Materials* 47 (2022): 491–499, https://doi.org/10.1016/j.ensm.2022.02.024.

149. L. Wang, B. Zhang, W. Zhou, et al., "Tandem Chemistry with Janus Mesopores Accelerator for Efficient Aqueous Batteries," *Journal of the American Chemical Society* 146 (2024): 6199–6208, https://doi.org/10.1021/jacs.3c14019.

150. W. Chen, J. Tang, F. Ji, J. Sun, Q. Zhu, and B.-T. Liu, "A Multifunctional Gradient Coating Enables Dendrite-free and Side Reaction-free Zinc Anodes for Stable Zinc-ion Batteries," *Cell Reports Physical Science* 4 (2023): 101344, https://doi.org/10.1016/j.xcrp.2023.101344.

151. Z. Liu, X. Li, Z. Li, et al., "Stable Dendrite-free Zn Anode with Janus MXene-Ag Interfacial Bifunctional Protective Layer for Aqueous Zinc-ion Batteries," *Chemical Engineering Journal* 479 (2024): 147412, https://doi.org/10.1016/j.cej.2023.147412.

152. J. Ba, X. Yin, F. Duan, et al., "Synergistic Cation-π Interactions and PEDOT-Based Protective Double-Layer for High Performance Zinc Anode," 8 (2024): 202301731.

153. W. Li, L. Li, X. Fu, Y. Hu, and Y. Deng, *Small* 21 (2025): 202411915.

154. W. Zhang, M. Chen, C. Sun, C. Lai, Y. Zhu, and M. Tong, "Design of a Multifunctional Gradient Double Coating Layer for a Stable Thin Zinc Anode with High Depth of Discharge," *Journal of Materials Chemistry A* 13 (2025): 9651–9659, https://doi.org/10.1039/D4TA09246E.

155. Z. Jiang, S. Fan, Z. Du, et al., "Gradient Interlayer Promotes Highly Stable Zn Metal Anodes for High-Performance Zn-Ion Batteries," *Advanced Functional Materials* (2025): 24105.

156. Q. Cao, Y. Gao, J. Pu, et al., "Gradient Design of Imprinted Anode for Stable Zn-ion Batteries," *Nature Communications* 14 (2023): 641, https://doi.org/10.1038/s41467-023-36386-3.

157. Z. Na, H. Qi, S. Li, Y. Wu, Q. Wang, and G. Huang, "Stable Zinc Metal Anode by Nanosecond Pulsed Laser Enabled Gradient Design," *ACS Energy Letters* 8 (2023): 3297–3306, https://doi.org/10.1021/acsenergylett.3c01206.

158. X. Cai, X. Wang, Z. Bie, et al., "A Layer-by-Layer Self-Assembled Bio-Macromolecule Film for Stable Zinc Anode," *Advanced Materials* 36 (2023): 2306734, https://doi.org/10.1002/adma.202306734.

159. K. Fu, H. Wang, M. Xie, et al., "Self-assembly of Super-hydrophobic and Zincophilic Surface Monolayer for Durable Zn Anodes," *Energy Storage Materials* 78 (2025): 104281, https://doi.org/10.1016/j.ensm.2025.104281.

160. C. Cao, H. Lu, Z. Yang, et al., "Feather-Effect-Inspired Superhydrophobic and Zincophilic Strategy for Ultrastable Zn Metal Anodes," *Nano Letters* 25 (2025): 14384–14394, https://doi.org/10.1021/acs.nanolett.5c03724.

161. Q. Luo, S. Xia, J. Liu, et al., "In Situ Constructing a Porous Organic Component-zincophilic Cu Clusters Layer on Zinc Anode for High Performance Aqueous Zinc Ion Batteries," *Chemical Engineering Journal* 494 (2024): 152789, https://doi.org/10.1016/j.cej.2024.152789.

162. S. Zhang, J. Ye, H. Ao, et al., "In-situ Formation of Hierarchical Solid-electrolyte Interphase for Ultra-long Cycling of Aqueous Zinc-ion Batteries," *Nano Research* 16 (2022): 449–457, https://doi.org/10.1007/s12274-022-4688-5.

163. H. Zhang, Y. You, D. Sha, et al., "Planar Deposition via in Situ Conversion Engineering for Dendrite-Free Zinc Batteries," *Advanced Materials* 36 (2024): 202409763.

164. Z. Shi, M. Yang, Y. Ren, et al., "Highly Reversible Zn Anodes Achieved by Enhancing Ion-Transport Kinetics and Modulating Zn (002) Deposition," *ACS Nano* 17 (2023): 21893–21904, https://doi.org/10.1021/acsnano.3c08197.

165. R. Xue, Y. Zou, Z. Wang, et al., "Enhancing Temperature Adaptability of Aqueous Zinc Batteries via Antifreezing Electrolyte and Site-Selective ZnSe-Ag Interface Layer Design," *ACS Nano* 17 (2023): 17359–17371, https://doi.org/10.1021/acsnano.3c05369.

166. X. Wu, Z. Yang, Q. Song, et al., "Dual Plating Zinc Foam of Three-dimensional Reconstruction as a High-flux and Stable Zinc Metal Anode for Aqueous Zinc-ion Batteries," *Chemical Engineering Journal* 497 (2024): 154395, https://doi.org/10.1016/j.cej.2024.154395.

167. X. Liu, Y. Zhang, L. Wang, et al., "Highly Reversible Dendrite-Free Zinc Anode Enabled by a Bilayered Inorganic-Metal Interface Layer," *ACS Nano* 18 (2024): 35325–35335, https://doi.org/10.1021/acsnano.4c11486.

168. C. Zhou, Z. Ding, S. Ying, et al., "Electrode/Electrolyte Optimization-Induced Double-Layered Architecture for High-Performance Aqueous Zinc-(Dual) Halogen Batteries," *Nano-Micro Letters* 17 (2024): 58, https://doi.org/10.1007/s40820-024-01551-w.

169. Y. Meng, M. Wang, J. Wang, et al., "Robust Bilayer Solid Electrolyte Interphase for Zn Electrode with High Utilization and Efficiency," *Nature Communications* 15 (2024): 8431, https://doi.org/10.1038/s41467-024-52611-z.

170. K. Zhu, W. Zhuang, N. Wang, et al., "Rational Design of a Bilayer Interface for Long-Term Stability of Zn Anodes and MnO2 Cathodes," *Advanced Materials* 37 (2025): 202502366.

171. D. Li, L. Cao, T. Deng, S. Liu, and C. Wang, "Design of a Solid Electrolyte Interphase for Aqueous Zn Batteries," *Angewandte Chemie International Edition* 60 (2021): 13035–13041, https://doi.org/10.1002/anie.202103390.

172. A. Li, J. Hao, K. Wu, et al., "Turning Zn(PO 3) 2 -Enriched Inorganic/Organic Hybrid Interfacial Chemistry with Chelating Ligands toward Robust Aqueous Zn Anodes," *ACS Nano* 19 (2025): 13016–13028, https://doi.org/10.1021/acsnano.4c17583.

173. R. Sun, J. Ma, Y. Gao, et al., "A Dynamic Organic-inorganic Bilayer Solid/Electrolyte Interphase Employed L-carnosine Additive for Highly Stable Zinc Metal Anode," *Energy Storage Materials* 79 (2025): 104293, https://doi.org/10.1016/j.ensm.2025.104293.

174. Z. Shao, L. Lin, W. Zhuang, et al., "In Situ Self-Reconfiguration Induced Multifunctional Triple-Gradient Artificial Interfacial Layer toward Long-Life Zn-Metal Anodes," *Advanced Materials* 36 (2024): 202406093.

175. H. Jiang, L. Tang, Y. Fu, et al., "Chloride Electrolyte Enabled Practical Zinc Metal Battery with a near-unity Coulombic Efficiency," *Nature Sustainability* 6 (2023): 806–815, https://doi.org/10.1038/s41893-023-01092-x.

176. Y. Zhao, M. Ouyang, Y. Wang, et al., "Biomimetic Lipid-Bilayer Anode Protection for Long Lifetime Aqueous Zinc-Metal Batteries," *Advanced Functional Materials* 32 (2022): 2203019, https://doi.org/10.1002/adfm.202203019.

177. J. Yang, Y. Zhang, Z. Li, et al., "Three Birds with One Stone: Tetramethylurea as Electrolyte Additive for Highly Reversible Zn-Metal Anode," *Advanced Functional Materials* 32 (2022): 2209642, https://doi.org/10.1002/adfm.202209642.

178. D. Wang, R. Li, J. Dong, et al., "Bidentate Coordination Enables Anions-Regulated Solvation Structure for Advanced Aqueous Zinc Metal Batteries," *Angewandte Chemie, International Edition* 64 (2024): 202414117.

179. W. Shao, C. Li, C. Wang, et al., "Stabilization of Zinc Anode by Trace Organic Corrosion Inhibitors for Long Lifespan," *Chinese Chemical Letters* 36 (2025): 109531, https://doi.org/10.1016/j.cclet.2024.109531.

180. M. Cui, L. Yu, J. Hu, S. He, C. Zhi, and Y. Huang, "Tailored Polymer-Inorganic Bilayer SEI with Proton Holder Feature for Aqueous Zn Metal Batteries," *Angewandte Chemie, International Edition* 64 (2025): 202423531.

181. Q. Zong, X. Liu, Q. Zhang, et al., "Interfacial Gradient Engineering Synergized with Self-adaptive Cathodic Defense for Durable Zn-ion Batteries," *Energy & Environmental Science* 18 (2025): 8256–8267, https://doi.org/10.1039/D5EE02236C.

182. Y. Mu, Y. Zhou, Y. Chu, et al., "Robust Piezoelectric-Derived Bilayer Solid Electrolyte Interphase for Zn Anodes Operating from −60 to 60°C," *ACS Nano* 19 (2025): 14161–14176, https://doi.org/10.1021/acsnano.5c00178.

183. G. Qu, Y. Zhao, C. Li, et al., "Hierarchical Interface Enabled by a Guest-Anionic Chemistry for High-Rate Aqueous Zinc-Ion Batteries," *Angewandte Chemie, International Edition* 64 (2025): 202422036.

184. H. Zhang, H. Yang, Y. Ai, et al., "All-Round Stannic Iodide as Electrolyte Additive Enables High-capacity and Long-Life Aqueous Zinc Ion Batteries," *Chemical Engineering Journal* 505 (2025): 159323, https://doi.org/10.1016/j.cej.2025.159323.

185. L. Cao, D. Li, F. A. Soto, et al., "Highly Reversible Aqueous Zinc Batteries Enabled by Zincophilic–Zincophobic Interfacial Layers and Interrupted Hydrogen-Bond Electrolytes," *Angewandte Chemie International Edition* 60 (2021): 18845–18851, https://doi.org/10.1002/anie.202107378.

186. J. Wan, R. Wang, Z. Liu, et al., "Hydrated Eutectic Electrolyte Induced Bilayer Interphase for High-Performance Aqueous Zn-Ion Batteries with 100° C Wide-Temperature Range," *Advanced Materials* 36 (2023): 202310623.

187. G. Wang, H. Fu, J. Lu, et al., "Gradient-Structured and Robust Solid Electrolyte Interphase in Situ Formed by Hydrated Eutectic Electrolytes for High-Performance Zinc Metal Batteries," *Advanced Energy Materials* 14 (2024): 2303549, https://doi.org/10.1002/aenm.202303549.

188. M. Zhao, Y. Lv, J. Qi, et al., "Crystallographic Reorientation Induced by Gradient Solid-Electrolyte Interphase for Highly Stable Zinc Anode," *Advanced Materials* 36 (2024): 202412667.

189. M. Li, X. Zhu, C. Jiang, et al., *Small* 20 (2024): 202402925.

190. C. Meng, W.-D. He, H. Tan, X.-L. Wu, H. Liu, and J.-J. Wang, "A Eutectic Electrolyte for an Ultralong-lived Zn//V 2 O 5 Cell: an in Situ Generated Gradient Solid-electrolyte Interphase," *Energy & Environmental Science* 16 (2023): 3587–3599, https://doi.org/10.1039/D3EE01447A.

191. J. Li, X. Zhang, X. Xu, et al., "Cation-Engineered Gradient Interfacial Structure toward Dendrite-Free and Shuttle-Free Aqueous Zn-Iodine Batteries," *Advancement of Science* (2025): 202509239.

192. J. Lu, T. Wang, J. Yang, et al., "Multifunctional Self-Assembled Bio-Interfacial Layers for High-Performance Zinc Metal Anodes," *Angewandte Chemie, International Edition* 63 (2024): 202409838.

193. S. Chen, Y. Xia, R. Zeng, et al., "Ordered Planar Plating/Stripping Enables Deep Cycling Zinc Metal Batteries," *Science Advances* 10 (2024): adn2265, https://doi.org/10.1126/sciadv.adn2265.

194. C. Yan, F. He, L. Feng, et al., "Interfacial Molecule Engineering Builds Tri-Functional Bilayer Silane Films with Hydrophobic Ion Channels for Highly Stable Zn Metal Anode," *Advanced Functional Materials* 35 (2025): 2503493, https://doi.org/10.1002/adfm.202503493.

195. B. Liu, S. He, F. Wei, et al., "Lipid Analogues Enhance the Lifespans of Reversible Zn-Based Aqueous Batteries via Optimal Interfacial Assembly," *Advanced Functional Materials* 35 (2025): 2502041, https://doi.org/10.1002/adfm.202502041.

196. Z. Wu, S. Yang, Z. Wei, et al., "Constructing Lipid-Like Biomimetic Structure via Electrolyte Designation for Stable Zinc-Ion Batteries," *ACS Nano* 19 (2025): 14085–14096, https://doi.org/10.1021/acsnano.4c18796.

197. D. Sha, C. Lu, R. Hu, Z. Bao, L. Pan, and Z. Sun, "Exploiting Bifunctional ZnTe for Zn Anode Protection and Conversion-type Cathode toward Compatible Aqueous Zn-ion Batteries," *Energy Storage Materials* 66 (2024): 103228, https://doi.org/10.1016/j.ensm.2024.103228.

198. V. P. Nguyen, M. Park, Y.-W. Byeon, et al., "Ultrathin yet Effective: 90 Nm ZnF 2 Layer for Stabilizing Zinc–Metal Anodes," *ACS Energy Letters* 10 (2025): 5503–5511, https://doi.org/10.1021/acsenergylett.5c02565.

199. Y. Tian, Y. An, Y. Yang, and B. Xu, "Robust Nitrogen/Selenium Engineered MXene/ZnSe Hierarchical Multifunctional Interfaces for Dendrite-free Zinc-metal Batteries," *Energy Storage Materials* 49 (2022): 122–134, https://doi.org/10.1016/j.ensm.2022.03.045.

200. L. Wang, L. Zhang, Y. Meng, et al., "Fluorinated Hybrid Interphases Enable Anti-corrosion and Uniform Zinc Deposition for Aqueous Zinc Metal Batteries," *Science China Materials* 66 (2023): 4595–4604, https://doi.org/10.1007/s40843-023-2598-0.

201. Z. Ge, L. Xu, Y. Xu, et al., "Multifunctional Fluorinated Carbon Dots Artificial Interface Layer Coupled with in-situ Generated Zn2+ Conductor Interlayer Enable Ultra-stable Zn Anode," *Nano Energy* 119 (2024): 109053, https://doi.org/10.1016/j.nanoen.2023.109053.

202. S. Huang, H. Fu, H. M. Kwon, et al., "Stereoisomerism of Multifunctional Electrolyte Additives for Initially Anodeless Aqueous Zinc Metal Batteries," *Nature Communications* 16 (2025): 6117, https://doi.org/10.1038/s41467-025-61382-0.

203. H. Fu, S. Huang, T. Wang, et al., "Synergistic Cationic Shielding and Anionic Chemistry of Potassium Hydrogen Phthalate for Ultrastable Zn—I 2 Full Batteries," *Advanced Materials* 37 (2024): 2411686, https://doi.org/10.1002/adma.202411686.

204. M. Wang, Z. Xu, C. He, et al., "Fundamentals, Advances and Perspectives in Designing Eutectic Electrolytes for Zinc-Ion Secondary Batteries," *ACS Nano* 19 (2025): 9709–9739, https://doi.org/10.1021/acsnano.4c18422.

205. K. Yang, H. Fu, Y. Duan, et al., "Poloxamer Pre-solvation Sheath Ion Encapsulation Strategy for Zinc Anode–electrolyte Interfaces," *ACS Energy Lett* 9 (2023): 209–217.

206. W. Fan, C. Zhu, X. Wang, et al., "All-natural Charge Gradient Interface for Sustainable Seawater Zinc Batteries," *Nature Communications* 16 (2025): 1273, https://doi.org/10.1038/s41467-025-56519-0.

207. Y. Li, X. Liu, M. Zhang, et al., "Optimization Strategy of Surface and Interface in Electrolyte Structure of Aqueous Zinc-Ion

Battery," *ACS Materials Letters* 6 (2024): 1938–1960, https://doi.org/10.1021/acsmaterialslett.4c00308.

208. J. Wei, P. Zhang, J. Sun, et al., "Advanced Electrolytes for High-performance Aqueous Zinc-ion Batteries," *Chemical Society Reviews* 53 (2024): 10335–10369, https://doi.org/10.1039/D4CS00584H.

209. M. Chen, Y. Wang, Q. Zhang, et al., "Double Eutectic Electrolytes with Optimized Inner-Outer Solvation Shell Engineering for Interphase-Stabilized Zinc-Metal Batteries," *Advanced Materials* (2025): 08315, https://doi.org/10.1002/adma.202508315.

210. Y. Zhu, J. Yin, X. Zheng, et al., "Concentrated Dual-cation Electrolyte Strategy for Aqueous Zinc-ion Batteries," *Energy & Environmental Science* 14 (2021): 4463–4473, https://doi.org/10.1039/D1EE01472B.

211. K. Wang, Y. Luo, H. Zhan, et al., "Ion Transport Modulations by Alkyl Chain Length Control of Quaternary Ammonium Additives Enabling Stable Cycling of Aqueous Zn Batteries," *Energy Storage Materials* 84 (2026): 104792, https://doi.org/10.1016/j.ensm.2025.104792.

212. D. Wang, Q. Li, Y. Zhao, et al., "Insight on Organic Molecules in Aqueous Zn-Ion Batteries with an Emphasis on the Zn Anode Regulation," *Advanced Energy Materials* 12 (2022): 2102707, https://doi.org/10.1002/aenm.202102707.

213. Y. Zhou, X. Ni, B. Hao, et al., "A Mini Review: How to Select Electrolyte Additives for Better Zn Anode Electrochemistry?," *Energy Storage Materials* 66 (2024): 103227, https://doi.org/10.1016/j.ensm.2024.103227.

214. L. Qin, J. Zhou, M. Sun, et al., "Comprehensive Review for Zinc Powder Anodes: Significance, Optimizing Design, and Industrial Feasibility in Zinc-ion Batteries," *Energy Storage Materials* 74 (2025): 103917, https://doi.org/10.1016/j.ensm.2024.103917.

215. X. Zhao, Y. Gao, Q. Cao, et al., "A High-Capacity Gradient Zn Powder Anode for Flexible Zn-Ion Batteries," *Advanced Energy Materials* 13 (2023): 2301741, https://doi.org/10.1002/aenm.202301741.

216. J. Huang, R. Feng, J. Wu, W. Lin, W. Du, and C. C. Li, "Structural Design Strategies of Zinc Powder Anode towards Rechargeable Zinc-based Batteries," *Energy Storage Materials* 74 (2025): 103934, https://doi.org/10.1016/j.ensm.2024.103934.

217. Q. Li, S. Tang, R. Luo, et al., "Regulating the Local Chemical Environment of Zn Powder Surface by Multi-site Anchoring Effect to Achieve Highly-stable Zn Anode," *Energy Storage Materials* 66 (2024): 103229, https://doi.org/10.1016/j.ensm.2024.103229.

218. H. Chen, W. Zhang, S. Yi, et al., "Zinc Iso-plating/Stripping: toward a Practical Zn Powder Anode with Ultra-long Life over 5600 h," *Energy & Environmental Science* 17 (2024): 3146–3156, https://doi.org/10.1039/D3EE04333A.

219. Q. Li, N. Li, and C. Zhi, "Zinc Powder Anodes for Rechargeable Aqueous Zinc-Based Batteries," *Nano Letters* 24 (2024): 4055–4063, https://doi.org/10.1021/acs.nanolett.4c00101.

220. B. Fu, G. Liu, Y. Zhang, et al., "Zn Powder-Based Anodes for Aqueous Zn Metal Batteries: Strategies, Structures, and Perspectives," *ACS Energy Letters* 9 (2024): 3292–3307, https://doi.org/10.1021/acsenergylett.4c00628.

221. X. Zheng, Z. Song, D. Zhang, et al., "Biomimetic Quasi-Skin-Capillary Structure Engineering of Ionic-Electronic Conducting Full-Chain Networks for Stable Zinc Powder Anodes," *Advanced Functional Materials* 35 (2024): 2413990, https://doi.org/10.1002/adfm.202413990.

222. Q. Hu, X. Wang, J. Cui, et al., "A Three-Tiered Golf Anode towards Ultralong-Life Zn−Mn Aqueous Batteries," *Angewandte Chemie, International Edition* 64 (2025): 202421217.

223. W. Tang, L. Zhang, Y. Liu, S. Wang, and J. Zhang, "A Dual-functional DMDAAC Electrode Enhancer with Hydrophobic Effect for Highly Stable Zn Powder Composite Anode," *Energy Storage Materials* 76 (2025): 104127, https://doi.org/10.1016/j.ensm.2025.104127.

224. H. Li, C. Guo, T. Zhang, et al., "Hierarchical Confinement Effect with Zincophilic and Spatial Traps Stabilized Zn-Based Aqueous Battery," *Nano Letters* 22 (2022): 4223–4231, https://doi.org/10.1021/acs.nanolett.2c01235.

225. C. Cao, K. Zhou, W. Du, et al., "Designing Soft Solid-like Viscoelastic Zinc Powder Anode toward High-Performance Aqueous Zinc-Ion Batteries," *Advanced Energy Materials* 13 (2023): 2301835, https://doi.org/10.1002/aenm.202301835.

226. Y. Zeng, P. X. Sun, Z. Pei, et al., "Nitrogen-Doped Carbon Fibers Embedded with Zincophilic Cu Nanoboxes for Stable Zn-Metal Anodes," *Advanced Materials* 34 (2022): 202200342.

227. J.-L. Yang, P. Yang, W. Yan, J.-W. Zhao, and H. J. Fan, "3D zincophilic Micro-scaffold Enables Stable Zn Deposition," *Energy Storage Materials* 51 (2022): 259–265, https://doi.org/10.1016/j.ensm.2022.06.050.

228. P. Xue, C. Guo, N. Wang, et al., "Synergistic Manipulation of Zn 2+ Ion Flux and Nucleation Induction Effect Enabled by 3D Hollow SiO 2 /TiO 2 /Carbon Fiber for Long-Lifespan and Dendrite-Free Zn–Metal Composite Anodes," *Advanced Functional Materials* 31 (2021): 2106417, https://doi.org/10.1002/adfm.202106417.

229. H. Yu, Y. Zeng, N. W. Li, D. Luan, L. Yu, and X. W. Lou, "Confining Sn Nanoparticles in Interconnected N-doped Hollow Carbon Spheres as Hierarchical Zincophilic Fibers for Dendrite-free Zn Metal Anodes," *Science Advances* 8 (2022): abm5766, https://doi.org/10.1126/sciadv.abm5766.

230. P. X. Sun, Y. Q. Zheng, X. Y. Zhang, H. Yu, Y. Guo, and L. Yu, "Spatial Confinement of Sn/TiO 2 Nanoparticles in Hollow Mesoporous Carbon Spheres Opal for Stable Zn Metal Anodes," *Advanced Energy Materials* 14 (2024): 2304138, https://doi.org/10.1002/aenm.202304138.

231. B. Li, Y. Zeng, W. Zhang, B. Lu, Q. Yang, and J. Zhou, "Separator Designs for Aqueous Zinc-ion Batteries," *Science Bulletin* 69 (2024): 688–703, https://doi.org/10.1016/j.scib.2024.01.011.

232. L. Li, S. Jia, Z. Cheng, and C. Zhang, *Chemsuschem* 16 (2023): 202202330.

233. Q. Nian, X. Yang, H. Hong, et al., "Advancements in Separator Materials for Aqueous Zinc Batteries," *Nanoscale Horizons* 10 (2025): 1932–1955, https://doi.org/10.1039/D5NH00172B.

234. J.-Q. Huang, W. G. Chong, and B. Zhang, "Tackling the Challenges of Aqueous Zn-ion Batteries via Functional Separator Design," *Journal of Power Sources* 594 (2024): 234036, https://doi.org/10.1016/j.jpowsour.2023.234036.

235. C. Li, Z. Sun, T. Yang, et al., "Directly Grown Vertical Graphene Carpets as Janus Separators toward Stabilized Zn Metal Anodes," *Advanced Materials* 32 (2020): 2003425, https://doi.org/10.1002/adma.202003425.

236. X. Zhang, J. Li, K. Qi, et al., "An Ion-Sieving Janus Separator toward Planar Electrodeposition for Deeply Rechargeable Zn-Metal Anodes," *Advanced Materials* 34 (2022): 202205175.

237. L. Hai, Y. Sun, M. Wu, et al., "SnS 2 (001)-Reinforced Ion/Molecular Sieving Separator Enables High-Performance Aqueous Zinc-Organic Batteries," *Advanced Functional Materials* 35 (2025): 2501468, https://doi.org/10.1002/adfm.202501468.

238. Y. Su, B. Liu, Q. Zhang, et al., "Printing-Scalable Ti 3 C 2 T X MXene-Decorated Janus Separator with Expedited Zn 2+ Flux toward Stabilized Zn Anodes," *Advanced Functional Materials* 32 (2022): 2204306, https://doi.org/10.1002/adfm.202204306.

239. S. Liu, Q. Han, C. He, et al., "Ion-Sieving Separator Functionalized by Natural Mineral Coating toward Ultrastable Zn Metal Anodes," *ACS Nano* 18 (2024): 25880–25892, https://doi.org/10.1021/acsnano.4c09678.

240. L. Wang, F. Wang, Z. Ding, et al., "Bilayer Separator Enabling Dendrite-free Zinc Anode with Ultralong Lifespan >5000 h," *Green Energy & Environment* 9 (2024): 771–776, https://doi.org/10.1016/j.gee.2022.09.013.

241. J. Zhou, Z. Zhang, W. Jiang, et al., "Ion-sieving Janus Separator Modified by Ti3C2Tx Toward Dendrite-free Zinc-ion Battery," *Journal of Alloys and Compounds* 950 (2023): 169836, https://doi.org/10.1016/j.jallcom.2023.169836.

242. Y. Sun, Q. Jian, T. Wang, et al., "A Janus Separator towards Dendrite-free and Stable Zinc Anodes for Long-duration Aqueous Zinc Ion Batteries," *Journal of Energy Chemistry* 81 (2023): 583–592, https://doi.org/10.1016/j.jechem.2023.03.007.

243. J. Yao, J. Li, C. Chen, et al., "Bifunctional Ion Rectification Layer Separators toward Superior Reversible Dendrite-Free Zinc Metal Anodes," *Advanced Functional Materials* 35 (2024): 2414117, https://doi.org/10.1002/adfm.202414117.

244. Y. Chen, C. Gao, J. Li, et al., "Organic/Inorganic Functional Janus Separator for High-performance Zinc Anode," *Journal of Energy Storage* 103 (2024): 114442, https://doi.org/10.1016/j.est.2024.114442.

245. H. Lee, J. Kang, H. W. Kang, et al., "A Hydrophilic Janus-faced Separator with Functionalized Nanocarbon for Stable Cycling of Aqueous Zn-metal Batteries," *Journal of Materials Chemistry A* 12 (2024): 3623–3632, https://doi.org/10.1039/D3TA06268F.

246. J. Mu, M. Yu, B. Zhao, et al., "Scalable, Flexible and Hierarchically Porous Janus Membrane Inducing Zn-Ion Flux Redistribution and Desolvation for Dendrite-free Zinc Anodes," *Chemical Engineering Journal* 506 (2025): 160365, https://doi.org/10.1016/j.cej.2025.160365.

247. Y. Shao, W. Lu, T. Zhang, et al., "A Self-Recognition Separator for Ion Management to Customize Selective Zn 2+ Channels toward Dendrite-Free Zinc Metal Anodes," *Carbon Energy* 7 (2025): 701, https://doi.org/10.1002/cey2.701.

248. Y. Chen, G. Zhou, X. Huang, et al., "Alleviating Salt Depletion at the Zinc Anode Interface by an Ion-releasing Separator to Achieve Ultra-stable Zinc Anode," *Energy Storage Materials* 78 (2025): 104247, https://doi.org/10.1016/j.ensm.2025.104247.

249. H. Tan, C. Wang, X. Li, et al., "Multiscale Ion-Sieving Separator toward Long-Cycling Aqueous Zinc-Based Batteries," *Small* (2025): 202510596.

250. Z. Wang, L. Dong, W. Huang, et al., "Simultaneously Regulating Uniform Zn2+ Flux and Electron Conduction by MOF/rGO Interlayers for High-Performance Zn Anodes," *Nano-Micro Letters* 13 (2021): 73, https://doi.org/10.1007/s40820-021-00594-7.

251. Z. Zheng, S. Guo, M. Yan, Y. Luo, and F. Cao, "A Functional Janus Ag Nanowires/Bacterial Cellulose Separator for High-Performance Dendrite-Free Zinc Anode under Harsh Conditions," *Advanced Materials* 35 (2023): 202304667.

252. T. Wu, H. Ma, M. Chen, X. Han, Q. Tian, and J. Chen, "Thin and Strong Janus Separator Based on Nanocellulose and Ti3C2Tx for Dendrite-free Aqueous Zinc-ion Batteries," *Journal of Energy Storage* 73 (2023): 108851, https://doi.org/10.1016/j.est.2023.108851.

253. J. Guo, Y. Wang, S. Li, et al., "Chitosan Hydrogel Polyelectrolyte-modified Cotton Pad as Dendrite-inhibiting Separators for Stable Zinc Anodes in Aqueous Zinc-ion Batteries," *Journal of Power Sources* 580 (2023): 233392, https://doi.org/10.1016/j.jpowsour.2023.233392.

254. S. Zheng, X. Yang, D. Chen, et al., "A Janus Separator Regulating Zinc Deposition Behavior Synergistically by Cellulose and ZrO2 Nanoparticles toward High-Performance Aqueous Zinc-Ion Batteries," *Small* 21 (2024): 202411463.

255. H. Bi, D. Tian, Z. Zhao, et al., "Multifunctional Janus Separator Engineering for Modulating Zinc Oriented Aspectant Growth and Iodine Conversion Kinetics toward Advanced Zinc-Iodine Batteries," *Advanced Functional Materials* 35 (2025): 2423115, https://doi.org/10.1002/adfm.202423115.

256. S. Li, C. Sun, M. Zhang, et al., "An Integrated Tandem-Structured Separator Enables Dual-Enhanced Stable Interfaces for Long-Cycle-Life and High-Areal-Capacity Aqueous Zinc–Iodine Batteries," *Angewandte Chemie, International Edition* 64 (2025): 202506849.

257. P. Xu, Y. Yu, B. Du, et al., "High Performance Janus Separator Based on Microstructurally Controllable Halloysite Nanotubes for Zinc-ion Batteries," *Journal of Energy Storage* 114 (2025): 115820, https://doi.org/10.1016/j.est.2025.115820.

258. Z. Cai, Z. Chen, L. Deng, T. Wei, and K. Sun, "Sandwich-structured Double-sided Hydrophobic Diaphragm for Long-life Zinc Ion Batteries," *Chemical Engineering Journal* 514 (2025): 163120, https://doi.org/10.1016/j.cej.2025.163120.

259. Y. Dong, W. Fan, X. Wang, et al., "Hydrophobicity Gradient in Ultra-thin Cellulose Separators for Durable Seawater-Based Zinc Batteries," *Advanced Functional Materials* (2025).

260. Z. Zhao, Y. Zhang, H. Zhang, et al., "Gradient Structured Separator Enables Stable Aqueous Zinc Metal Batteries," *Nano Letters* 25 (2025): 7483–7490, https://doi.org/10.1021/acs.nanolett.5c01125.

261. Y. Liang, D. Ma, N. Zhao, et al., "Novel Concept of Separator Design: Efficient Ions Transport Modulator Enabled by Dual-Interface Engineering toward Ultra-Stable Zn Metal Anodes," *Advanced Functional Materials* 32 (2022): 2112936, https://doi.org/10.1002/adfm.202112936.

262. L. Chang, D. Wang, Y. Ji, et al., "A Bifunctional Separator with Gradient Distribution of MCM-41 Zeolite for High-Performance Aqueous Zinc-ion Batteries," *Advanced Functional Materials* (2025): 17715.

263. P. Tian, Y. Gao, S. Huang, et al., "Constructing Gradient Separator to Stabilize Bi-Electrodes toward High-Performance Zn Metal Batteries," *Advanced Energy Materials* 14 (2024): 2401830, https://doi.org/10.1002/aenm.202401830.

264. W. Liu, S. Zhao, J. Lin, Y. Yang, Y. Chen, and G. Zeng, "Recent Advances in Cellulose-based Separators for Zinc Ion Batteries: a Review," *International Journal of Biological Macromolecules* 306 (2025): 141326, https://doi.org/10.1016/j.ijbiomac.2025.141326.

265. Y. Wang, H. Zhang, Y. Chen, et al., "Hydrogel Electrolytes for Temperature Robust Aqueous Zinc-Ion Batteries," *Advanced Energy Materials* 15 (2025): 03226, https://doi.org/10.1002/aenm.202503226.

266. G. Sun, Z. Cui, D. Zhao, et al., "Enhancing Zinc-Ion-Transport Kinetics in Solid-State Zinc Batteries via an Internal/Surface Dual Acceleration Strategy," *Nano Letters* 25 (2025): 10742–10750, https://doi.org/10.1021/acs.nanolett.5c01076.

267. S. Chen, Y. Ying, L. Ma, et al., "An Asymmetric Electrolyte to Simultaneously Meet Contradictory Requirements of Anode and Cathode," *Nature Communications* 14 (2023): 2925, https://doi.org/10.1038/s41467-023-38492-8.

268. D. Wang, D. Zhao, L. Chang, et al., "Interface Engineering of Electron-ion Dual Transmission Channels for Ultra-long Lifespan Quasi-solid Zinc-ion Batteries," *Energy Storage Materials* 74 (2025): 103903, https://doi.org/10.1016/j.ensm.2024.103903.

269. S. Zhao, S. Yang, X. Huang, et al., "A Janus-type Quasi-solid-state Electrolyte Enabling Dual-ion Relay for Long Lifespan of Nonaqueous Zinc Batteries," *Energy & Environmental Science* 18 (2025): 8618–8630, https://doi.org/10.1039/D5EE03224E.

270. G. Liu, S. Zhang, R. Wang, et al., "Inhibiting Proton Corrosion and Hydrogen Evolution Reaction on the Surface of Zinc Anodes by Hierarchical Structure Hydrogel to Realize Long-Life Aqueous Zinc Metal Batteries," *Advanced Energy Materials* (2025): 03823.

271. C. Li, W. Wang, J. Luo, et al., "High-Fluidity/High-Strength Dual-Layer Gel Electrolytes Enable Ultra-Flexible and Dendrite-Free Fiber-Shaped Aqueous Zinc Metal Battery," *Advanced Materials* 36 (2024): 2313772, https://doi.org/10.1002/adma.202313772.

272. H. Lu, D. Zhang, Q. Jin, et al., "Gradient Electrolyte Strategy Achieving Long-Life Zinc Anodes," *Advanced Materials* 35 (2023): 202300620.

273. X. Wang, Y. Ying, Y. Gong, et al., "Piezoelectric Gradient Electrolytes for Environmentally Adaptive and Stable Zinc Batteries," *Energy Storage Materials* 82 (2025): 104586, https://doi.org/10.1016/j.ensm.2025.104586.

274. K. Zhu, X. Niu, W. Xie, et al., "An Integrated Janus Hydrogel with Different Hydrophilicities and Gradient Pore Structures for High-performance Zinc-ion Batteries," *Energy & Environmental Science* 17 (2024): 4126–4136, https://doi.org/10.1039/D4EE01018C.

275. Q. Wang, J. Huang, L. Qi, et al., "A Bioinspired Gradient Hydrogel Electrolyte Network with Optimized Interfacial Chemistry toward Robust

Aqueous Zinc-Ion Batteries," *ACS Nano* 19 (2025): 26770–26781, https://doi.org/10.1021/acsnano.5c06914.

276. Q. Zhou, F. Zhang, Z. Tan, et al., "Gradient Hydrogel Electrolyte Enables High Ionic Conductivity and Robust Mechanical Properties for Dendrite-Free Aqueous Zinc-Ion Battery," *Advanced Materials* (2025): 202512775.

Biographies

Yuexin Liu received his Ph.D. degree from the Tongji University in 2024, and now he joined Zhejiang A&F University as an associate professor. His work focuses on the preparation of advanced electrode materials, separator, and hydrogel electrolytes in aqueous batteries.

Zhongqing Ma, Ph.D., is a professor and doctoral supervisor at Zhejiang A & F University, specializing in biomass thermochemical conversion. He focuses on the pyrolysis and gasification of biomass to produce high-quality biofuels and biochemicals. As a high-caliber researcher, he has been recognized as a Chinese Highly Cited Researcher by Elsevier (since 2024) and a Top 2% Scientist in the global list by Stanford University (since 2022). His innovative work contributes significantly to the field of renewable energy and biomass valorization.

Yong Hu obtained his Ph.D. degree in inorganic chemistry in 2006 at theUniversity of Science and Technology of China (USTC). He then worked as a research fellow at Nanyang Technological University (NTU). From 2008 to 2024, he worked as a full professor at the College of Chemistry and Life Science, Zhejiang Normal University. In 2025, he joined Zhejiang A&F University as a full professor at the College of Chemistry and Materials Engineering. His current research interests are focused on the design and synthesis of nanomaterials for energy and environmental applications.